ISSN 0972-9976

# International Journal of Tomography & Statistics


Volume 3 No. JJ05 June-July 2005

# International Journal of Tomography & Statistics (IJTS)

**ISSN 0972-9976**

## Editorial Board



International Journal of Tomography & Statistics (IJTS)

ISSN 0972-9976

# Contents

Volume 3 No. JJ05 June-July 2005

*International Journal of Tomography & Statistics (IJTS),*
*June-July 2005, Vol. 3, No. JJ05, 1-18*
*ISSN 0972-9976; Copyright © 2005 IJTS, ISDER*

# Table Detection in Scanned Document Images

**Yi Xiao and Qing-Hua Qin**

Department of Engineering,
Australian National University, Canberra, ACT 0200,
Australia
*Email: qinghua.qin@anu.edu.au*

## ABSTRACT

*Vertically and horizontally aligned text cells and/or ruling lines are the basic elements in a table image. This paper develops an algorithm based on Delaunay triangulation and Freeman chaincode to identify such table image through measuring the widths and orientations of the connected components of the image and locate the aligned text cell regions in the image. Experiments show that the proposed method can effectively detect general formatted tables.*

## KEY WORDS

Table detection, document image, Delaunay triangulation, chaincode

## 1. INTRODUCTION

Tables are an effective means for communicating information in documents. Identification of such tables is a challenging problem in document layout analysis. A table structure identifying algorithm is used to segment tables from the document pages and extract the information from these tables. Table detection is a crucial step for table structure identification.

Among the current document layout analysis systems, the specific problem of table detection has been neither addressed nor solved for the class of tables with variaty

of ruling lines or irregular table_cells (Lee *et al*., 2000). Most layout analysis methods (Jain and Yu, 1998; Mao *et al*., 2003) segment and classify document images into three basic categories: text, graphics, and pictures. Tables are usually classified as graphics or text.

Lee et al. (2000) presented a knowledge-based method for sophisticated geometric structure analysis of technical journal pages. Their knowledge base encodes geometric characteristics that are not only common in technical journals but also publication-specific in the form of rules. The method identifies tables by splitting or grouping segmented regions into composite layout components.

Jain and Yu (1998) grouped pixels into *Block Adjacency Graph* (BAG) nodes, while BAG nodes are grouped into connected components and horizontal and vertical lines, connected components are grouped into generalized text lines (GTLs), and GTLs are grouped into region blocks. For table identification, Jain and Yu first extract horizontal and vertical lines from non-text regions. They then test the lengths of the top and bottom lines, the mean and standard deviation of the orientations of both horizontal and vertical lines. Finally, they measure the average height and variation of the connected components in a table region. The methods of both Jain and Yu (1998) and Lee et al. (2000) have limitations for detecting unconnected tables.

Wang et al. (2004) recently presented a general formatted table structure understanding algorithm designed using optimization methods. The algorithm is probability-based, where the probabilities are estimated from geometric measurements made on the various entities in a large training set. With the algorithm, false alarms may, however, occur for flow charts, and tables with irregular text cells may be undetectable.

From the above review, we focus here on developing an algorithm based on Delaunay triangulation and Freeman chaincode for detecting general formatted tables in structured articles such as journals. With this algorithm, the limitations of ruling line connections and the number of characters in a text cell, occurred in the approaches mentioned above, has been removed. The proposed algorithm can, thus, effectively distinguish tables from drawings, flowcharts and mathematical expressions. It should be mentioned that tables are visually recognizable by a specific typography (alignment, fixed line space, character sizes, fields, cells, ruling lines) organized in a consistent manner. The computational geometric data structure-Delaunay triangulation (DT) (Okabe et al., 2000) is well suited for describing the specific typography of table structures in a document image. Xiao and Yan (2003) used DT for text block segmentation by statistically analysing the sizes and orientation of the triangles. With their method, table regions may be classified as non-text regions. In this paper, we further our analysis of the specific triangles that occupy tabular text regions and the margins between table cells.

## 2. METHOD

A non-text region ***C*** of the binary document image is specified by a set of connected components $\{cc_i\}$. $cc_i$ is characterized by its boundary $B(cc_i)$ and upper left and lower right bounding box coordinates $(x_u(cc_i), y_u(cc_i))$, $((x_l(cc_i), y_l(cc_i)))$, where $x_u < x_l$ and $y_u < y_l$. ***C*** is divided into a large connected component set and a small connected component set for table ruling line and table text detection.

### 2.1 Ruling Line Identification

- Large connected components and their local width distribution

We define ***L*** as

$$\boldsymbol{L} = \{cc_i \,|\, (x_u - x_l) > \Delta X \text{ or } (y_u - y_l) > \Delta Y\} \quad (1)$$

***L*** is the set of large connected components on the region ***C***. $\Delta X$ and $\Delta Y$ are the values which are set to be greater than the width and height of a character's bounding box.

The local width of a connected component is calculated by the length of the corresponding internal edge in the constrained Delaunay triangulation (CDT) (Chew, 1987) of a connected component's boundary (Fukushima, 1997; Xiao and Yan, 2004). An internal edge is a Delaunay edge not on the boundary. Figure 1 illustrates the internal edges in a connected component.

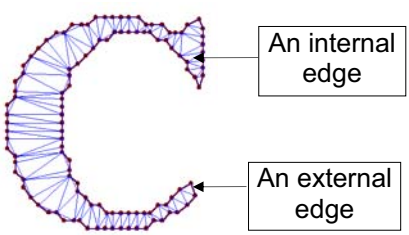


**Figure 1** The internal edges (thin line segments) and the external edges (broad line segments) in a character "C".

From the histogram of $h(w)$ we can obtain the local width distribution of connected components, where $w$ is the length of an internal edge in pixels.

Line-structured connected components are identified by the maximum local width ( $w_{\max}$ ). Here we have

$$w_{\max} = \max(w \mid h(w) \neq 0, w \in \{1, 2, ...m\}) \quad (2)$$

***L*** is a line structured connected component set if $w_{\max} < th_w$. Here $th_w$ is the width limitation of a line.

Figure 2 illustrates the local width distribution of the large connected components in non-text regions for five typical cases. In Figure 2, ruling lines and mathematical symbols have the smallest $w_{\max}$ . The halftone image in Figure 2 (c) has the largest $w_{\max}$ . All the line structured components have their $w_{\max}$ smaller than 110 (pixels).

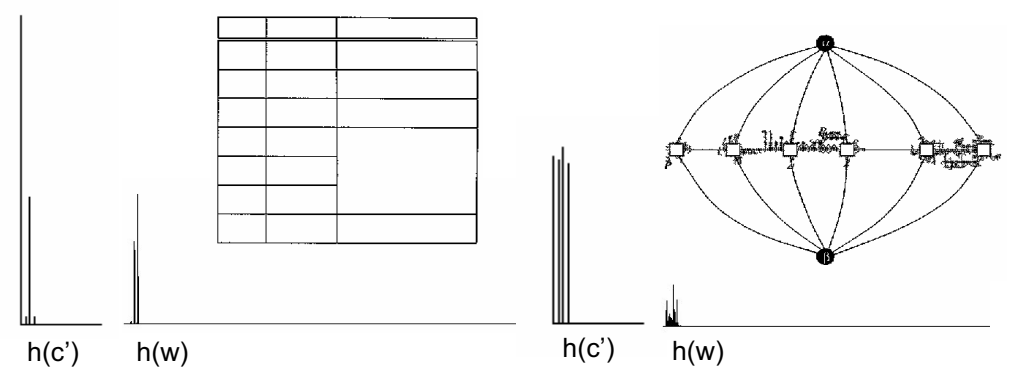


(a) In a table ( $w_{\max} = 51, w_{\min} = 16$ ) (b) In a drawing ( $w_{\max} = 179, w_{\min} = 11$ )

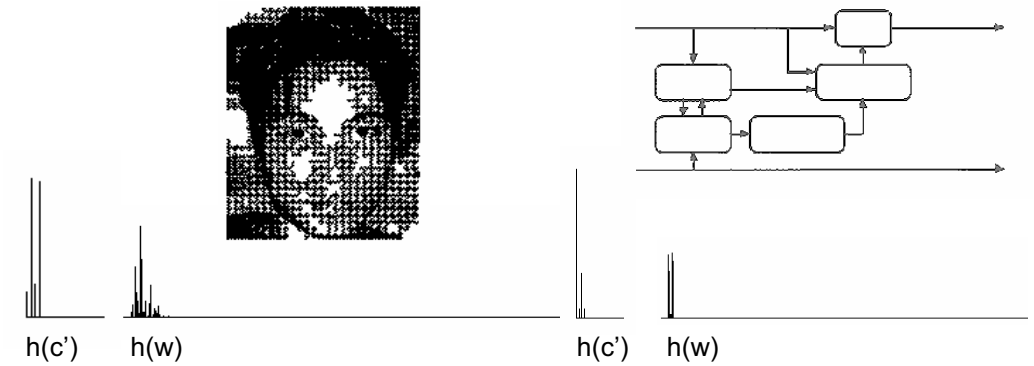


(c) In a halftone image( $w_{\max} = 591, w_{\min} = 11$ ) (d) In a flowchart ( $w_{\max} = 103, w_{\min} = 16$ )

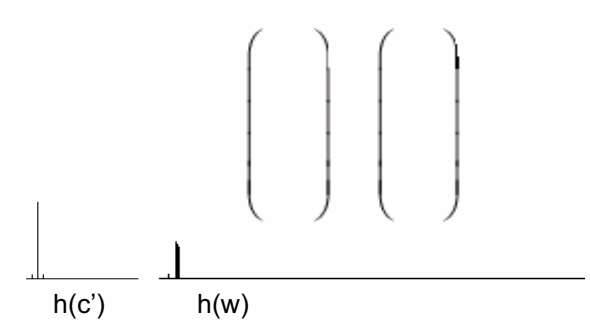


(e) In an equation ( $w_{\max} = 37, w_{\min} = 16$ )

**Figure 2** Local width and chaincode distributions ( $c_i^{'} = c_i \bmod 4$ ) of connected components.

- Line orientation measuring

A boundary is represented by an ordered sequence $B = \{p_i, (x_i, y_i)\}$, where *I* = 1, 2⋯n, $x_i$ and $y_i$ are integer multiples of *D* (the grid constant), and where $p_1 = p_n$. The boundary can also be expressed as a sequence of the chaincode

$F = \{c_i\}$ (Freeman *et al.*, 1970), where $c_i$ is a code for the direction from $p_{i-1}$ to $p_i$. There are eight possible directions coded from 0 to 7 as shown in Figure 3.

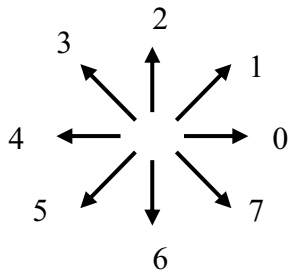


**Figure 3** Eight directions coded by chaincodes.

The chaincode distribution reveals the line orientation. For a vertical line, codes '2' and '6' dominate the sequence, whereas codes '0' and '4' dominate a horizontal line sequence. Table 1 lists the number of chaincodes for the images in Figure 2. From Figure 2 and Table 1 we can see that the table ruling lines, flowcharts and mathematical symbols have large numbers of even codes and small numbers of odd codes. The drawing in Figure 2 (b) has a nearly equivalent number of even and odd codes. The halftone image in Figure 2 (c) has a large number of odd codes and a small number of even codes. Furthermore, the mathematical symbols in Figure 2 (e) have a small number of codes '0' and '4' as they contain no horizontal lines.

**Table 1** Chaincode distributions

| Chaincode histogram / Image | h(0) | h(1) | h(2) | h(3) |
|---|---|---|---|---|
| Figure 2 (a) | 4355 | 132 | 1819 | 145 |
| Figure 2 (b) | 1972 | 9131 | 2088 | 1893 |
| Figure 2 (c) | 361 | 1919 | 481 | 1876 |
| Figure 2 (d) | 3474 | 246 | 1062 | 242 |
| Figure 2 (e) | 12 | 46 | 772 | 46 |

- Table ruling line identification

The table ruling line set is identified by measuring the local width and the chaincode distribution of the connected component as follows:

Let F' = $\{d_j\}$, where $d_j = c_i$ *module 4,* $c_i$ is a code in the corresponding chaincode sequences of ***L***. h(d) is the histogram of $d_j$. ***L*** is a table ruling line set if

1) $$w_{\max} < th_w \tag{3}$$

2) $$h(0) + h(2) > k_1 * (h(1) + h(3)) \tag{4}$$

3) $$h(2) < k_2 * h(0) \tag{5}$$

where equation (4) indicates both the vertical and horizontal lines are dominant; while equation (5) indicates only the horizontal lines are dominant. In our experiment, all the table ruling lines can be distinguished from other lines using equations (4) and (5) with $k_1 = 3, k_2 = 5$.

### 2.2 Tabular Text Identification

Given

$$\boldsymbol{T}=\boldsymbol{C}-\boldsymbol{L}, \tag{6}$$

where ***T*** represents the sparse text in the region, we construct a Delaunay triangulation on the centroids P of the $\{cc_i\}$ in ***T***. Let $\tau_i$ be a Delaunay triangle in the Delaunay triangulation over P. $\tau_i$ is charaterized by six parameters $e_i^l$, $e_i^m$, $e_i^s$, $\alpha_i^l$, $\alpha_i^m$ and $\alpha_i^s$, denoted as $\{e_i^l, e_i^m, e_i^s, \alpha_i^l, \alpha_i^m, \alpha_i^s\} \Rightarrow \tau_i$. Here $e_i^l$, $e_i^m$ and $e_i^s$ are the longest, second longest and shortest edges of $\tau_i$ respectively; $\alpha_i^l$, $\alpha_i^m$ and $\alpha_i^s$ are the acute angles between a horizontal line and $e_i^l$, $e_i^m$ and $e_i^s$ respectively.

- Triangle classification

Four types of triangles are defined:

Vertical triangle ($t_v$): A triangle $\tau_i$ with $\alpha_i^s < \alpha_{h1}$, $\alpha_i^m, \alpha_i^l > \alpha_{v1}$ ($\alpha_{h1} = 10^0, \alpha_{v1} = 50^0$).

Horizontal triangle ($t_h$): A triangle $\tau_i$ with $\alpha_i^s > \alpha_{v2}$, $\alpha_i^m, \alpha_i^l < \alpha_{h2}$ ($\alpha_{h2} = 40^0, \alpha_{v2} = 80^0$).

Text region triangle ($T_t$): Triangles in text cell regions.

Margin triangle($T_m$): Triangles in the margins between text cells in different columns.

In a tabular text region, $T_t$ and $T_m$ must be unemptied. Figure 4 shows the text region triangles ($T_t$) and margin triangles ($T_m$) in a table region. Triangles are clustered as $T_t$ and $T_m$ based on the orientations and connections of the triangles. The procedure is as follows:

$T_t$ searching:

i. Mark the vertical triangles that satisfy $e_i^l < h_t$ as text region triangles;

ii. For each non-text region triangle $\tau_i$, if it is adjacent to two text region triangles and has horizontal $\alpha_i^l$ or $\alpha_i^m$, mark the adjacent triangle as a text region triangle. The step continues until no more text region triangles are marked;

iii. Mark any single text region triangle as a non-text region triangle.

$T_m$ searching:

i. Mark the horizontal triangles with $2 * \Delta X < e_i^l < M_m$ as margin triangles;

ii. For each non-margin triangle $\tau_i$, if it is adjacent to a margin triangle and satisfies $\alpha_i^s > \alpha_{v2} - 20^0$, mark the triangle as a margin triangle. The step continues until no more margin triangles are marked;

iii. Mark any single margin triangle as a non-margin triangle.

| Method | Mesh | $\beta_1$ | $\beta_2$ | $\beta_D$ |
|---|---|---|---|---|
| BEM | $N = 10$ | 1.0374 | 0.4553 | 0.1905 |
| | 20 | 1.0727 | 0.4702 | 0.1952 |
| | 30 | 1.0811 | 0.4790 | 0.1990 |
| | 40 | 1.0820 | 0.4803 | 0.1998 |
| FEM | $M = 24$ | 0.9832 | 0.4304 | 0.1813 |
| | 48 | 1.0284 | 0.4442 | 0.1851 |
| | 72 | 1.0603 | 0.4559 | 0.1894 |
| | 96 | 1.0622 | 0.4572 | 0.1901 |

(a)

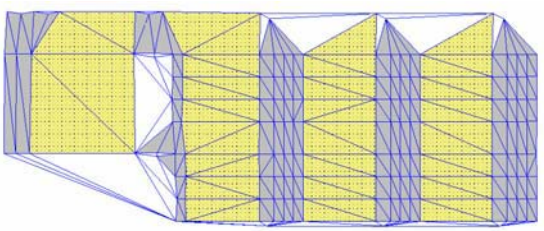

(b)

**Figure 4** Text region triangles and margin triangles in a table. (a) A table image; (b) Text region triangles and margin triangles for the image in (a), filled with different colours.

- Table text identification

Let $S_t$, $S_m$ and $S$ be the total areas of $T_t$, $T_m$ and all the triangles respectively. It should be mentioned that $S_t$ here represents the area of tabular text region and $S_m$ the area of margins between text cells. As an illustration $S_t$ stands for the total areas of the yellow triangles and $S_m$ total areas of the grey triangles in Figure 4. Figure 5 is a $S_t/S$-$S_m/S$ diagram of sparse text images. 140 typical sparse text images are used. These images include 68 table images, 49 equation images, 21 drawing images and 4 flowchart images. Most of the table images are within the regions of $S_t/S$>0.*14* and $S_m/S$>*0.1.*

We identify ***T*** as tabular text if $S_t / S > th_t$ and $S_m / S > th_m$. The setting of threshold values $th_t$ and $th_m$ are detailed in Section 3.

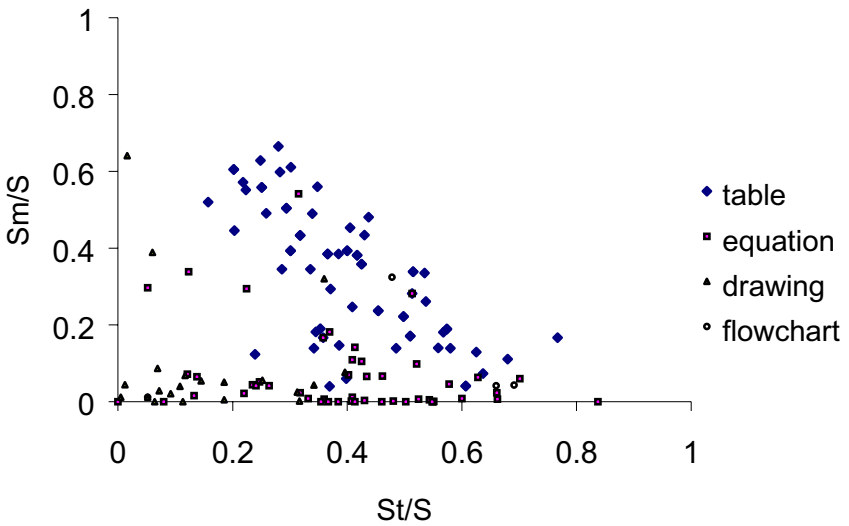


**Figure 5** $S_t/S$-$S_m/S$ plot for sparse text images.

As an equation or a drawing may have table-like arrangement, we need to apply the table ruling line test to distinguish such items from tables. On the other hand, misidentification may occur when a table is irregular. Examples are shown in Figure 6.

### 2.3 Table Identification

Figure 7 provides the overview of our table detection algorithm. The input is the connected component set ***C*** of a non-text block region. After ruling line analysis, halftone images, curved drawings, and equations with matrix are excluded from table image candidature. Table text analysis is applied further for table image identifying.

$$x = 0: \quad u = 0, \qquad x = a: \quad u = \bar{u}, \tag{4}$$
$$y = 0: \quad v = 0, \qquad y = b: \quad v = \bar{v}. \tag{5}$$

$$\begin{pmatrix} X''_u \\ Y''_u \end{pmatrix} = \begin{pmatrix} \cos\alpha & \sin\alpha \\ -\sin\alpha & \cos\alpha \end{pmatrix} \begin{pmatrix} X'_u \\ Y'_u \end{pmatrix},$$

(a) An equation with table-like structure. (b) An equation with table-like structure.

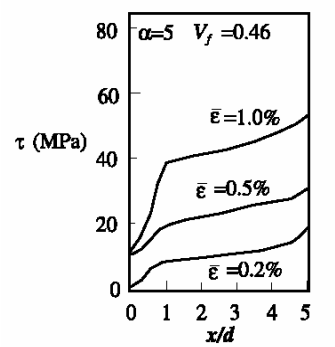


| Training Procedure | Classification Accuracy (%) Face Recognition | View Recognition | Training Time per view (sec) | Test Time per view (sec) |
|---|---|---|---|---|
| Random | 98.0 (max=100.0, min=94.3) | 80.8 (max=87.1, min=76.3) | 0.8 max | 0.79 max |
| Selected | 100.0 | 88.6 (max=89.3, min=87.4) | 0.8 max | 0.69 max |
| Selected | 100.0 | 99.8 (max=100.0, min = 99.7) | 1.6 max | 5.0 max |

(c) A drawing with table-like structure. (d) A table image classified as a non-table image

**Figure 6** Misclassification of images with sparse text.

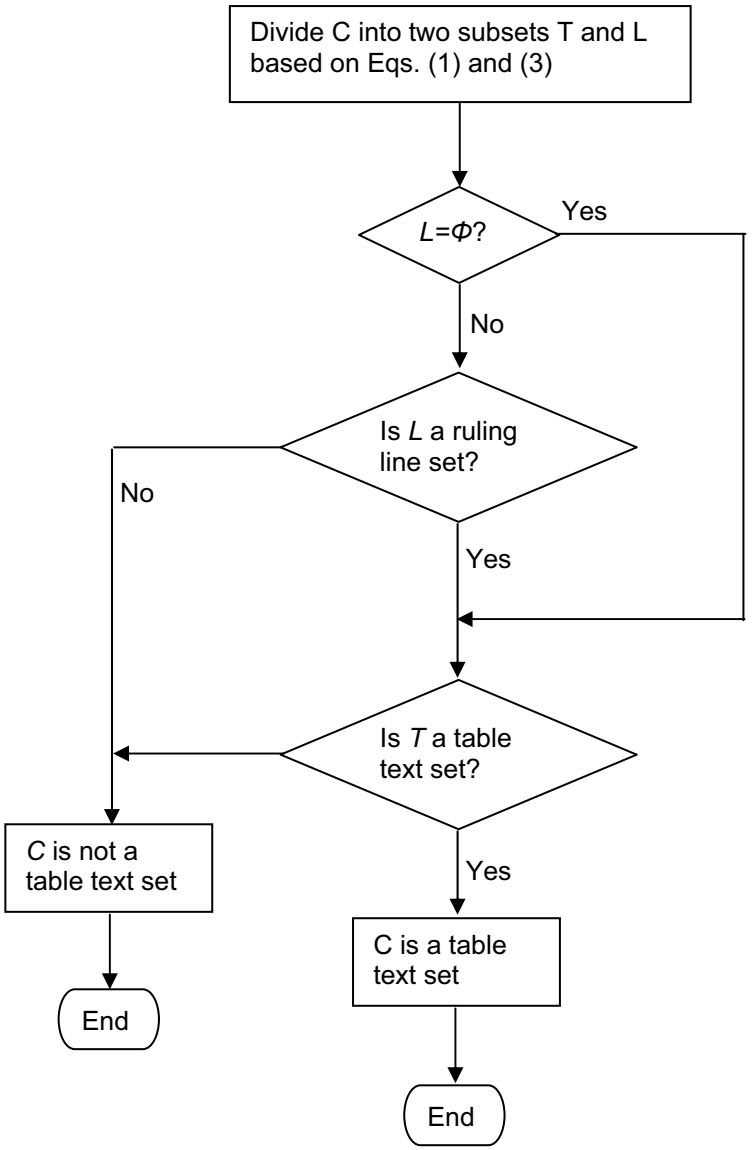


**Figure 7** The table detection algorithm

| System | Missed faces | Detect rate | False detects |
|---|---|---|---|
| 10) Nets 1,2 → AND(0) → threshold(2,3) → overlap elimination | 39 | 74.8% | 0 |
| 11) Nets 1,2 → threshold(2,2) → overlap elimination → AND(2) | 24 | 84.5% | 8 |
| 12) Nets 1,2 → threshold(2,2) → overlap → OR(2) → threshold(2,1) → overlap | 15 | 90.3% | 42 |
| Detector using a multi-layer network [21] | 36 | 76.8% | 5 |
| Detector using perceptron [21] | 28 | 81.9% | 13 |
| Support Vector Machine [14] | 39 | 74.2% | 20 |

(a)

| 日期/Date | 时间/Time | 议程/Conference Program | 地点/Venue |
|---|---|---|---|
| 12 月 14 日<br>星期二<br>December 14<br>Tuesday | 1:30 PM-10:00 PM | 报到、注册<br>Conference Registration | 宁波大学留学生公寓一楼大厅<br>Lobby,International Student Mansion, Ningbo University |
| | 6:00 PM | 晚餐/Dinner | 留学生公寓餐厅<br>Dining Room |
| | 7:00-9:00 PM | 大会组委会和学术委员会工作会议<br>Organizing Committee Meeting | 待定<br>To Be Informed |
| 12 月 15 日<br>星期三<br>December 15<br>Wednesday | 7:00-7:40 AM | 早餐/Breakfast | 留学生公寓餐厅<br>Dining Room |
| | 8:00-8:30 AM | **开幕式/Opening Ceremony**<br>**主席：王礼立，陈大年**<br>**Chairs: LL Wang and DN Chen** | **绣山工程大楼报告厅**<br>**Xiushan Auditorium** |
| | 8:30-9:50 AM | 大会报告 I<br>Keynote Presentations I | |
| | 9:50-10:20 AM | 拍照、休息<br>Photo & Coffee Break | |
| | 10:20-11:40 AM | 大会报告 II<br>Keynote Presentations II | |
| | 12:00AM-1:30PM | 午餐/Lunch | 留学生公寓餐厅<br>Dining Room |
| | 1:30-6:10AM | 分组报告 I<br>Session Presentations I | **报告厅**<br>**Conference Halls** |
| | 6:30 PM | **酒会/Conference Reception** | 留学生公寓咖啡吧<br>Coffee Bar |

(b)

| Algorithm | Represenation | Similarity measure |
|---|---|---|
| Excalibur Co. | Unknown | Unknown |
| MIT Media Lab 95 | PCA | $L_2$ |
| MIT Media Lab 96 | PCA-difference space | MAP Bayesian Statistic |
| Michigan St. U. | Fischer discriminant | $L_2$ |
| Rutgers U. | Greyscale projection | Weighted $L_1$ |
| U. of So. CA. | Dynamic Link Architecture (Gabor Jets) | Elastic graph matching |
| U. of MD 96 | Fischer discriminant | $L_2$ |
| U. of MD 97 | Fischer discriminant | Weighted $L_2$ |
| Baseline | PCA | $L_1$ |
| Baseline | Correlation | Angle |

(c)

| | Algorithm Ranking by Top Match<br>Gallery Size / Scored Probes | | | | | |
|---|---|---|---|---|---|---|
| Algorithm | 200/200<br>gallery 1 | 200/200<br>gallery 2 | 200/200<br>gallery 3 | 200/200<br>gallery 4 | 200/199<br>gallery 5 | 196/196<br>gallery 6 |
| Baseline PCA | 9 | 10 | 8 | 8 | 10 | 8 |
| Baseline correlation | 9 | 9 | 9 | 6 | 9 | 10 |
| Excalibur Corp. | 6 | 7 | 7 | 5 | 7 | 6 |
| MIT Sep96 | 4 | 2 | 1 | 1 | 3 | 3 |
| MIT Mar95 | 7 | 5 | 4 | 4 | 5 | 7 |
| Michigan State Univ. | 3 | 4 | 5 | 8 | 4 | 4 |
| Rutgers Univ. | 7 | 8 | 9 | 6 | 7 | 9 |
| UMD Sep96 | 4 | 6 | 6 | 10 | 5 | 5 |
| UMD Mar97 | 1 | 1 | 3 | 2 | 2 | 1 |
| USC | 2 | 3 | 2 | 2 | 1 | 1 |
| Average Score | 0.935 | 0.857 | 0.904 | 0.918 | 0.843 | 0.804 |

(d)

| | | Capable to handle with Head Variations | | | | Locate precise eye and eye corner locations |
|---|---|---|---|---|---|---|
| | Approach | Frontal view | Rotation in-depth | Out-the-plane Rotation | Different hairstyles | |
| **Lam et al. [2] [15] (1998 and 1998)** | Snake + Anthropological model | √ | × | Limited range | Moderate | √ |
| **Takacs et al. [3] (1997)** | Retinal fiber banks implemented via self-organizing feature map | √ | × | × | √ | √ |
| **Saber et al. [4] (1998)** | Colour information and face geometrical information | √ | Limited range | √ | √ | × |
| **Jeng et al. [5] (1998)** | Frontal face model + relative geometrical relation between facial features | √ | Limited range | √ | √ | × |
| **Feng et al. [13] (1998)** | Snake + Anthropological model + Variance projection function | √ | × | Limited range | × | √ |
| **The proposed method** | Multi cues | √ | √ | √ | √ | √ |

(e)

| Dimension | Connectivity | $\Delta t_{max}$ |
|---|---|---|
| 1-D | 2 | 1/3 |
| 2-D | 4 | 1/5 |
| | 8 | 1/7 |
| 3D | 6 | 1/7 |
| | 18 | 1/13 |
| | 26 | 3/47 |

(f)

**Figure 8** Detected table images.

## 3. EXPERIMENT AND DISCUSSION

Our algorithm has been tested on more than 900 non-text regions including halftones, drawings, flowcharts, equations and tables. The images were captured from journals from IEEE ALL Society Periodical Package, Stringer-Verlag and Science direct.

- Accuracy analysis

Based on the proposed algorithm, we have achieved a 94.4% accuracy rate of table detection for the 900 non-text block regions, while Jain and Yu (1998) achieved 89% and Wang et al. (2004) 91% accuracy rate using the methods described in their papers.

Figure 8 shows some of the detected table images. It includes tables with various ruling lines and text cells. With Jain and Yu's method, unconnected tables in Figure 8 (c) and Figure 8 (d) are failed to be identified and the tables with irregular table cells shown in Figure 8 (a) and Figure 8 (e) are misdetected with the method of Wang et al. (2004).

False alarms mainly occur in equation images, as some mathematical expressions have a similar geometrical structure to that of table images. An example is shown in Figure 6 (a). Misclassification occurs when the column space is narrower than the table line space. An example is shown in Figure 9.

| *Training* | *Classification Accuracy (%)* | | *Training Time* | *Test Time* |
|---|---|---|---|---|
| *Procedure* | *Face Recognition* | *View Recognition* | *per view (sec)* | *per view (sec)* |
| Random | 98.0 (max=100.0, min=94.3) | 80.8 (max=87.1, min=76.3) | 0.8 max | 0.79 max |
| Selected | 100.0 | 88.6 (max=89.3, min=87.4) | 0.8 max | 0.69 max |
| Selected | 100.0 | 99.8 (max=100.0, min = 99.7) | 1.6 max | 5.0 max |

**Figure 9** A table image misidentified as a non-table image.

- Processing time

Table 2 and 3 give the processing time for the current version of our C program for the images in Figures 2 and 8. Most of the processing time is used for triangle classification. The local width calculation of an image object may take longer time than other kinds of objects. When the number of characters increases, the time for $S_t/S$-$S_m/S$ computing may increase sharply.

**Table 2** Processing time for ruling line identification

| Image | Line orientation estimation (seconds) | Local width calculation (seconds) |
|---|---|---|
| Figure 2 (a) | 0.11 | 9.83 |
| Figure 2 (b) | 0.11 | 5.66 |
| Figure 2 (c) | 0.05 | 6.53 |
| Figure 2 (d) | 0.06 | 3.79 |
| Figure 2 (e) | <0.01 | 0.44 |

**Table 3** Processing time for table text identification

| Image | Delauany triangulation (seconds) | $S_t$-$S_m$ calculation (seconds) |
|---|---|---|
| Figure 8 (a) | 0.06 | 0.11 |
| Figure 8 (b) | 0.22 | 3.60 |
| Figure 8 (c) | 0.11 | 1.21 |
| Figure 8 (d) | 0.11 | 0.88 |
| Figure 8 (e) | 0.11 | 0.44 |
| Figure 8 (f) | 0.10 | 0.05 |

- Threshold selection

The threshold values are related to the specific typography of table structures in a document image. Table 4 lists the threshold values used for table detection. $\Delta X$ and $\Delta Y$ are obtained from the statistics of the image itself. They are the most frequent width and height respectively of the bounding boxes of the connected components, which indicate the width and height of a character used in the document image. $k_1$ and $k_2$ are determined by the knowledge of the table structure in a document image. $\alpha_{v1}$, $\alpha_{h1}$, $\alpha_{v2}$ and $\alpha_{h2}$ are tolerance thresholds for measuring the alignment of characters. $h_t$ and $M_m$ are the space tolerances between text cells.

**Table 4** Threshold values for table detection.

| $\Delta X$ | $\Delta Y$ | $T_w$ | $k_1$ | $K_2$ | $\alpha_{v1}$ | $\alpha_{h1}$ | $\alpha_{v2}$ | $\alpha_{h2}$ | $h_t$ | $M_m$ | $th_t$ | $th_m$ |
|---|---|---|---|---|---|---|---|---|---|---|---|---|
| ** | ** | ** | 3 | 5 | $10^0$ | $50^0$ | $40^0$ | $80^0$ | $15*\Delta Y$ | $10*\Delta X$ | 0.14 | 0.1 |

** indicates that the value is set based on the document image itself.

$th_t$ and $th_m$ are the sensitivity thresholds that affect the performance of table detection. Accuracy rate versus $th_t$ and $th_m$ are shown in Figure 10. From this figure we can see that the accuracy reaches highest when $th_t$ is around 0.14 and $th_m$ is around 0.1. When $th_t$ or $th_m$ is small, many equations and drawings may be misclassified as tables, and when $th_t$ or $th_m$ is large, tables may be misidentified as non-tables.

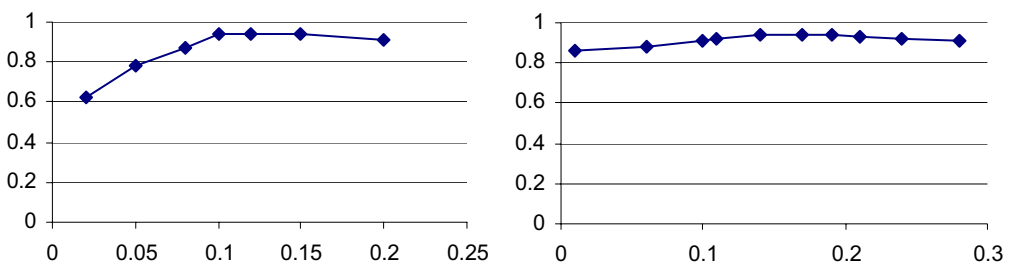


**Figure 10** The accuracy rate in terms of $th_t$ and $th_m$.

## 4. CONCLUSION

The Delaunay triangulation-based local width calculating and Freeman chaincode statistics can efficiently measure horizontal and vertical lines, and text cells in the table can be recognized by the clustering of different classified triangles. The proposed method is used for general formatted table detection. Experiments show that with this method, tables can be separated from other non-text regions such as halftones, equations and drawings, and any tables with wider column spacing are detectable. In particular, the limitations of ruling line connections and the number of characters in a text cell, occurred in the existing approaches mentioned above, has been removed in the proposed algorithm. Further work on table ruling line analysis can be carried out to improve the detection of tables with narrow column spacing.

## Acknowledgement

The support from Australian Research Council is fully acknowledged.

## REFERENCES

Chew, P., 1987, Constrained Delaunay Triangulation, *Proc. of the 3rd ACM Symp. on Comp. Geometry,* pp. 213-222.

Freeman, H., Lipkin B.S., and Rosenfeld A.(Eds), 1970, Boundary encoding and processing. *Picture Processing and Psychohistories*. Academic, New York, pp. 241-266.

Fukushima, S., 1997, Division-based analysis of symmetry and its application. IEEE Transactions on Pattern Analysis and Machine Intelligence, 19, 144-147.

Jain, A.K., and Yu, B., 1998, Document representation and its application to page decomposition. IEEE Transactions on Pattern Analysis and Machine Intelligence, 20, 294-308.

Lee, K., Choy, Y., and Chao, S., 2000, Geometric structure analysis of document images: A knowledge-based approach. IEEE Transactions on Pattern Analysis and Machine Intelligence, 22, 1224-1240.

Mao, S., Rosenfeld, A., and Kanungo, T., 2003, Document structure analysis algorithms: A literature survey. Proc of SPIE Conference on Electrical Image, 5010, 197-207.

Wang, Y.L., Phillips, I.T., and Haralick, R.M., 2004, Table structure understanding and its performance evaluation. Pattern Recognition, 37, 1479 –1497.

Xiao, Y., and Yan, H., 2003, Text region extraction in a document image based on the Delaunay tessellation. *Pattern Recognition*, 36, 799-809.

Xiao Y., and Yan, H., 2004, Location of title and author regions in document images based on the Delaunay triangulation. *Image and Vision Computing*, 22, 319-329.

Okabe, A., Boots, B., and Sugihara, K., 2000, Spatial tessellations-concepts and applications of Voronoi diagrams, Second Edition, *Wiley Series in Probability and Statistics*.

*International Journal of Tomography & Statistics (IJTS),*
*June-July 2005, Vol. 3, No. JJ05, 19-29*
*ISSN 0972-9976;* 

# MASS – *Modified Assignment* Algorithm in Facilities Layout Planning

**S. Bhattacharya[1], F. Smarandache[2], and M. Khoshnevisan[3]**
[1]Department of Business Administration
Alaska Pacific University, AK 99508, USA
E-mail: sbhattacharya@alaskapacific.edu

[2]Department of Mathematics
University of New Mexico, NM 87301, USA

[3]Department of Accounting, Finance and Economics
Griffith University, QLD 9726, Australia

**ABSTRACT**

*In this paper we have proposed a semi-heuristic optimization algorithm for designing optimal plant layouts in process-focused manufacturing/service facilities. Our proposed algorithm marries the well-known CRAFT (Computerized Relative Allocation of Facilities Technique) with the Hungarian assignment algorithm. Being a semi-heuristic search, MASS can be potentially more efficient in terms of CPU engagement time as it can converge on the global optimum faster than the traditional CRAFT, which is a pure heuristic. We also present a numerical illustration of our proposed algorithm.*

**KEY WORDS**

*CRAFT, facilities layout planning, Hungarian assignment algorithm.*

## INTRODUCTION

The fundamental integration phase in the design of productive systems is the layout of production facilities. A working definition of layout may be given as the arrangement of machinery and flow of materials from one facility to another, which

minimizes material-handling costs while considering any physical restrictions on such arrangement.

Usually this layout design is based either on considerations of machine-time cost and product availability; thus making the production system *product-focused*; or on considerations of quality and flexibility; thereby making the system *process-focused*. It is natural that while *product-focused* systems are better off with a 'line layout' dictated by available technologies and prevailing job designs, *process-focused* systems, which are more concerned with job organization, opt for a 'functional layout'. Of course, in reality the actual facility layout often lies somewhere in between a pure line layout and a pure functional layout format; governed by the specific demands of a particular production plant. Since our present paper concerns only functional layout design for process-focused systems, this is the only layout design we will discuss here.

The main goal to keep in mind is to minimize material handling costs - therefore the departments that incur the most interdepartmental movement should be located closest to one another. The main type of design layouts is *Block diagramming*, which refers to the movement of materials in existing or proposed facility. This information is usually provided with a *from/to* chart or a *load summary* chart, which gives the average number of unit loads moved between departments. A load-unit can be a single unit, a pallet of material, a bin of material, or a crate of material. The next step is to design the layout by calculating the composite movements between departments and rank them from most movement to least movement. Composite movement refers to the back-and-forth movement between each pair of departments. Finally, trial layouts are placed on a grid that graphically represents the relative distances between departments. This grid then becomes the objective of optimization when determining the optimal plant layout. We give a schematic representation of the basic operational considerations in a *process-focused* system as follows:

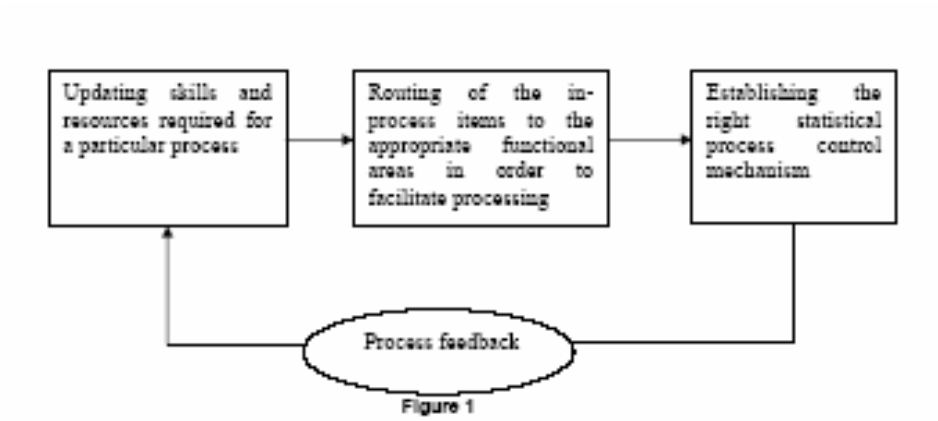


Figure 1

In designing the optimal functional layout, the fundamental question to be addressed is that of 'relative location of facilities'. The locations will depend on the need for one pair of facilities to be adjacent (or physically close) to each other relative to the need for all other pairs of facilities to be similarly adjacent (or physically close) to each other. Locations must be allocated based on the relative gains and losses for the alternatives and seek to minimize some indicative measure of the cost of having non-adjacent locations of facilities. Constraints of space prevents us from going into the details of the several criteria used to determine the gains or losses from the relative location of facilities and the available sequence analysis techniques for addressing the question; for which we advise the interested reader to look up *any* standard handbook of production/operations management.

## COMPUTERIZED RELATIVE ALLOCATION OF FACILITIES TECHNIQUE

Computerized Relative Allocation of Facilities Technique (CRAFT) (Buffa, Armour and Vollman, 1964) is a computerized heuristic algorithm that takes in *load matrix* of interdepartmental flow and transaction costs with a representation of a block layout as the inputs. The block layout could either be an existing layout or; for a new facility, any arbitrary initial layout. The algorithm then computes the departmental locations and returns an estimate of the total interaction costs for the initial layout. The governing algorithm is designed to compute the impact on a cost measure for two-way or three-way swapping in the location of the facilities. For each swap, the various interaction costs are computed afresh and the load matrix and the change in cost (increase or decrease) is noted and stored in the RAM. The algorithm proceeds this way through all possible combinations of swaps accommodated by the software. The basic procedure is repeated a number of times resulting in a more efficient block layout every time till such time when no further cost reduction is possible. The final block layout is then printed out to serve as the basis for a detailed layout template of the facilities at a later stage. Since its formulation, more powerful versions of CRAFT have been developed but these too follow the same, basic heuristic routine and therefore tend to be highly CPU-intensive (Khalil, 1973; Hicks and Cowan, 1976).

The basic computational disadvantage of a CRAFT-type technique is that one always has got to start with an arbitrary initial solution (Carrie, 1980). This means that there is no mathematical certainty of attaining the desired optimal solution after a given number of iterations. If the starting solution is quite close to the optimal solution by chance, then the final solution is attained only after a few iterations. However, as there is no guarantee that the starting solution will be close to the global optimum, the expected number of iterations required to arrive at the final solution tend to be quite large thereby straining computing resources (Driscoll and Sangi, 1988).

In this paper we propose and illustrate the Modified Assignment (MASS) algorithm as an extension to the traditional CRAFT, to enable faster convergence to the optimal solution. This we propose to do by marrying CRAFT technique with the

Hungarian assignment algorithm. As our proposed algorithm is semi-heuristic, it is likely to be less CPU-intensive than any traditional, purely heuristic CRAFT-type algorithm.

## *THE HUNGARIAN ASSIGNMENT ALGORITHM*

A general assignment problem may be framed as a special case of the *balanced transportation problem* with availability and demand constraints summing up to unity. Mathematically, it has the following *general linear programming* form:

$$\text{Minimize } \Sigma\Sigma\, C_{ij}X_{ij}$$
$$\text{Subject to } \Sigma X_{ij} = 1, \text{ for each i, j} = 1, 2 \ldots n$$

In terms of the classical assignment problem, $C_{ij}$ is the cost of assigning the $i^{th}$ job to the $j^{th}$ individual and $X_{ij}$ is the number of assignments of the $i^{th}$ job to the $j^{th}$ individual. In words, the problem may be stated as assigning each of n individuals to n jobs so that exactly one individual is assigned to each job in such a way as to minimize the total cost.

To ensure satisfaction of the basic requirements of the assignment problem, the basic feasible solutions of the corresponding balanced transportation problem must be integer valued. However, any such basic feasible solution will contain (2n – 1) variables out of which (n – 1) variables will be zero thereby introducing a high level of degeneracy in the solution making the usual solution technique of a transportation problem very inefficient.

This has resulted in mathematicians devising an alternative, more efficient algorithm for solving this class of problems, which has come to be commonly known as the *Hungarian assignment algorithm*. This algorithm is based on the following *optimality* theorem:

**Theorem**: *If a constant number is added to any row and/or column of the cost matrix of an assignment-type problem, then the resulting assignment-type problem has exactly the same set of optimal solutions as the original problem and vice versa.*

**Proof**: Let $A_i$ and $B_j$ (i, j = 1, 2 … n) be added to the ith row and/or jth column respectively of the cost matrix. Then the revised cost elements are $C_{ij}^{*} = C_{ij} + A_i + B_j$. The revised cost of assignment is $\Sigma\Sigma C_{ij}^{*}X_{ij} = \Sigma\Sigma\,(C_{ij} + A_i + B_j)\,X_{ij} = \Sigma\Sigma C_{ij}X_{ij} + \Sigma A_i\,\Sigma X_{ij} + \Sigma B_j \Sigma X_{ij}$. But by the imposed assignment constraint $\Sigma X_{ij} = 1$ (for i, j = 1, 2 … n), we have the revised cost as $\Sigma\Sigma C_{ij}X_{ij} + \Sigma A_i + \Sigma B_j$ i.e. the cost differs from the original by a constant. As the revised costs differ from the originals by a constant, which is independent of the decision variables, an optimal solution to one is also optimal solution to the other and vice versa.

The optimality theorem can be used in two different ways to solve the assignment problem. First, if in an assignment problem, some cost elements are negative, the problem may be converted into an equivalent assignment problem by adding a positive constant to each of the entries in the cost matrix so that they all become non-negative. Next, the important thing to look for is a feasible solution that has zero assignment cost after adding suitable constants to the rows and columns. Since it has been assumed that all entries are now non-negative, this assignment must be the globally optimal one (Mustafi, 1996).

Given a zero assignment, a straight line is drawn through it (a horizontal line in case of a row and a vertical line in case of a column), which prevents any other assignment in that particular row/column. The governing algorithm then seeks to find the minimum number of such straight lines, which would cover all the zero entries to avoid any redundancy. Let us say that *k* such lines are required to cover all the zeroes. Then the *necessary condition* for optimality is that number of zeroes assigned is equal to *k* and the *sufficient condition* for optimality is that *k* is equal to *n* for an *n x n* cost matrix.

## MASS (MODIFIED ASSIGNMENT) ALGORITHM

The basic idea of our proposed algorithm is to develop a systematic scheme to arrive at the initial input block layout to be fed into the CRAFT program so that the program does not have to start off from any initial (and possibly inefficient) solution. Thus, by subjecting the problem of finding an initial block layout to a mathematical scheme, we in effect reduce the purely heuristic algorithm of CRAFT to a semi-heuristic one. Our proposed MASS algorithm follows the following *sequential* steps:

**Step 1:** We formulate the load matrix such that each entry $l_{ij}$ represents the load carried from facility i to facility j.

**Step 2:** We insert $l_{ij} = M$, where M is a large positive number, into all the vacant cells of the load matrix signifying that no inter-facility load transportation is required or possible between the $i^{th}$ and $j^{th}$ vacant cells.

**Step 3:** We solve the problem on the lines of a standard assignment problem using the Hungarian assignment algorithm treating the load matrix as the cost matrix.

**Step 4:** We draft the initial block layout trying to keep the inter-facility distance $d_{ij}^*$ between the $i^{th}$ and $j^{th}$ *assigned* facilities to the minimum possible magnitude, subject to the available floor area and architectural design of the shop floor.

**Step 5:** We proceed using the CRAFT program to arrive at the optimal layout by iteratively improving upon the starting solution provided by the Hungarian assignment algorithm till the overall load function $L = \Sigma\Sigma\, l_{ij}d_{ij}^*$ subject to any

particular bounds imposed on the problem.

The Hungarian assignment algorithm will ensure that the initial block layout is at least very close to the global optimum if not globally optimal itself. Therefore the subsequent CRAFT procedure will converge on the global optimum much faster starting from this near-optimal initial input block layout and will be much less CPU-intensive than any traditional CRAFT-type algorithm. Thus MASS is not a stand-alone optimization tool but rather a rider on the traditional CRAFT that tries to ensure faster convergence to the optimal block layout for process-focused systems, by making the search semi-heuristic.

That MASS will be an improvement over traditional CRAFT in terms of computational efficiency is rather intuitive. At its worst the computational efficiency of MASS will be same as that of traditional CRAFT (in the rather unlikely scenario that the CRAFT heuristic chances upon the best possible layout in its very first iteration). In all other scenarios, MASS will give an initial solution to CRAFT which is much more likely to be closer to the global optimal than any random initial solution as under traditional CRAFT.

We provide a numerical illustration of the MASS algorithm in the Appendix by designing the optimal block layout of a small, single-storied, process-focused manufacturing plant with six different facilities and a rectangular shop floor design. The model can however be extended to cover bigger plants with a higher number of facilities. Also the MASS approach we have advocated here can even be extended to deal with the multi-floor version of CRAFT (Johnson, 1982) by constructing a separate assignment table for each floor subject to any predecessor-successor relationship among the facilities.

## APPENDIX: NUMERICAL ILLUSTRATION OF MASS

We consider a small, single-storied process-focused manufacturing plant with a rectangular shop floor plan having six different facilities. We mark these facilities as $F_I$, $F_{II}$, $F_{III}$, $F_{IV}$, $F_V$ and $F_{VI}$. The architectural design requires that there be an aisle of at least 2 meters width between two adjacent facilities and the total floor area of the plant is 64meters x 22meters. Based on the different types of jobs processed, the loads to be transported between the different facilities are supplied in the load matrix below:

**TABLE 1**

| | $F_I$ | $F_{II}$ | $F_{III}$ | $F_{IV}$ | $F_V$ | $F_{VI}$ |
|---|---|---|---|---|---|---|
| $F_I$ | – | 20 | – | – | – | 25 |
| $F_{II}$ | 10 | – | 15 | – | – | – |
| $F_{III}$ | – | – | – | 30 | – | – |
| $F_{IV}$ | – | – | 50 | – | – | 40 |
| $F_V$ | – | – | – | – | – | 10 |
| $F_{VI}$ | – | – | – | – | 15 | – |

We put in a very large positive value M in each of the vacant cells of the load matrix to signify that no inter-facility transfer of load is required or is permissible for these cells:

**TABLE 2**

| | $F_I$ | $F_{II}$ | $F_{III}$ | $F_{IV}$ | $F_V$ | $F_{VI}$ |
|---|---|---|---|---|---|---|
| $F_I$ | M | 20 | M | M | M | 25 |
| $F_{II}$ | 10 | M | 15 | M | M | M |
| $F_{III}$ | M | M | M | 30 | M | M |
| $F_{IV}$ | M | M | 50 | M | M | 40 |
| $F_V$ | M | M | M | M | M | 10 |
| $F_{VI}$ | M | M | M | M | 15 | M |

Next we apply the standard Hungarian assignment algorithm to obtain the initial solution:

**TABLE 3**

| | $F_I$ | $F_{II}$ | $F_{III}$ | $F_{IV}$ | $F_V$ | $F_{VI}$ |
|---|---|---|---|---|---|---|
| $F_I$ | *M-20* | *0* | *M-25* | *M-20* | *M-20* | *5* |
| $F_{II}$ | *0* | *M-10* | *0* | *M-10* | *M-10* | *M-10* |
| $F_{III}$ | M-30 | M-30 | M-35 | *0* | *M-30* | *M-30* |
| $F_{IV}$ | M-40 | M-40 | 5 | *M-40* | *M-40* | *0* |
| $F_V$ | M-10 | M-10 | M-15 | *M-10* | *M-10* | *0* |
| $F_{VI}$ | M-15 | M-15 | M-20 | *M-15* | *0* | *M-15* |

Above is the assignment table after first iteration. There are two rows and three columns that are covered i.e. $k = 5$. But as this is a 6x6 load matrix, the above solution is sub-optimal. So we make a second iteration:

**TABLE 4**

| | $F_I$ | $F_{II}$ | $F_{III}$ | $F_{IV}$ | $F_V$ | $F_{VI}$ |
|---|---|---|---|---|---|---|
| $F_I$ | *M-20* | *0* | *M-25* | *M-15* | *M-15* | *10* |
| $F_{II}$ | *0* | M-10 | *0* | *M-5* | M-5 | *M-5* |
| $F_{III}$ | *M-35* | M-35 | *M-40* | *0* | M-30 | *M-30* |
| $F_{IV}$ | *M-45* | M-45 | *0* | *M-40* | M-40 | *0* |
| $F_V$ | *M-15* | M-15 | *M-20* | *M-10* | M-10 | *0* |
| $F_{VI}$ | *M-20* | *M-20* | *M-25* | *M-15* | *0* | *M-15* |

Now columns $F_I$, $F_{III}$, $F_{IV}$, $F_{VI}$ and rows $F_I$ and $F_{VI}$ are covered i.e. k = 6. As this is a 6x6 load matrix the above solution is optimal.

The optimal assignment table (subject to the 2 meters of aisle between adjacent facilities) is shown below:

**TABLE 6**

| | $F_I$ | $F_{II}$ | $F_{III}$ | $F_{IV}$ | $F_V$ | $F_{VI}$ |
|---|---|---|---|---|---|---|
| $F_I$ | – | ' | – | – | – | – |
| $F_{II}$ | ' | – | – | – | – | – |
| $F_{III}$ | – | – | – | ' | – | – |
| $F_{IV}$ | – | – | ' | – | – | – |
| $F_V$ | – | – | – | – | – | ' |
| $F_{VI}$ | – | – | – | – | ' | – |

Initial layout of facilities as dictated by the Hungarian assignment algorithm:

**Figure 2**

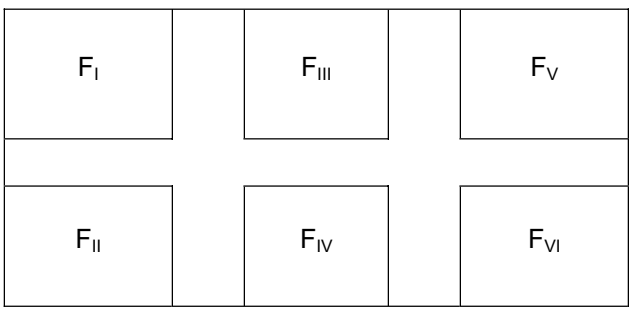


The above layout conforms to the rectangular floor plan of the plant and also places the assigned facilities adjacent to each other with an aisle of 2 meters width between them. Thus $F_I$ is adjacent to $F_{II}$, $F_{III}$ is adjacent to $F_{IV}$ and $F_V$ is adjacent to $F_{VI}$.

Based on the cost information provided in the load-matrix the total cost in terms of load-units for the above layout can be calculated as follows:

L = 2{(20 + 10) + (50 + 30) + (10 + 15)} + (44 x 25) + (22 x 40) + (22 x 15) = 2580.

By feeding the above optimal solution into the CRAFT program the final, the global optimum is found in a single iteration. The final, best layout as obtained by CRAFT is:

**Figure 3**

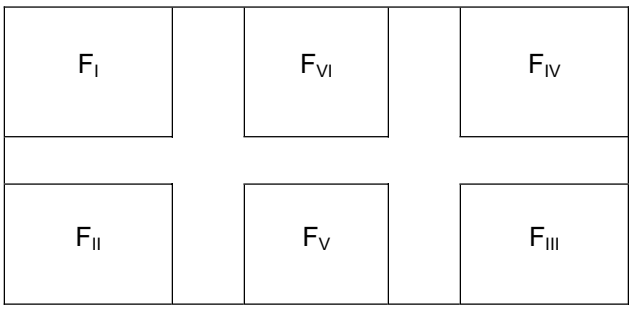


Based on the cost information provided in the load-matrix the total cost in terms of load-units for the optimal layout can be calculated as follows:

L* = 2{(10 + 20) + (15 + 10) + (5 + 30)} + (22 x 25) + (44 x 15) + (22 x 40) = 2360.

Therefore the final solution is an improvement of just 220 load-units over the initial solution! This shows that this initial solution fed into CRAFT is indeed near optimal and can thus ensure a faster convergence.

## REFERENCES

Buffa, Elwood S., Armour G. C. and Vollmann, T. E., 1964, *Allocating Facilities with CRAFT*, Harvard Business Review, 42(2), 136-158

Carrie, A. S., 1980, *Computer-Aided Layout Planning – The Way Ahead*, International Journal of Production Research, 18(3), 283-294

Driscoll, J. and Sangi, N. A., 1988, *An International Survey of Computer-aided Facilities Layout – The Development And Application Of Software*, Proc. of the IX$^{th}$ International Conference on Production Research, Anil Mital (Ed.), Elsevier Science Publishers, N.Y. U.S.A., 315-336

Hicks, P. E. and Cowan, T. E., 1976, *CRAFT-M for Layout Rearrangement*,

Industrial Engineering, 8(5), 30-35

Johnson, R. V., 1982, *SPACECRAFT for Multi-Floor Layout Planning*, Management Science, 28(4), 407-417

Khalil, T. M., 1973, *Facilities Relative Allocation Technique (FRAT)*, International Journal of Production Research, 2(2), 174-183

Mustafi, C. K., 1996, *Operations Research: Methods and Practice*, 3rd Ed., New Age International Ltd., New Delhi, India, 124-131

*International Journal of Tomography & Statistics (IJTS),*
*June-July 2005, Vol. 3, No. JJ05, 30-43*
*ISSN 0972-9976;* 

# Output Distributional Influence Function for Recursive Median Filters

**Sari Peltonen**

Institute of Signal Processing, Tampere University of Technology
P.O. Box 553, FIN-33101 Tampere, Finland
Email: sari.peltonen@tut.fi

## ABSTRACT

*In this paper we study robustness of recursive median filters (RMFs) by using a recently introduced method called output distributional influence function (ODIF). Unlike the traditionally used methods, such as the influence function and the change-of-variance function, the ODIF provides information about the robustness of finite length filters. So the ODIF is not only a good theoretical analysis tool but it can also be used in real filtering situations for selecting filters behaving as desired in the presence of contamination. The usefulness of the ODIF in the analysis of the robustness of the RMFs is demonstrated in illustrative examples and the robustness of the RMF is compared with the robustness of the standard median filter (SMF).*

## KEYWORDS

*Robustness, Recursive median filter, Influence function, Change-of-variance function, Output distributional influence function.*

## INTRODUCTION

Modern robust statistics began in 1960 with the papers by *Tukey* [1960] and *Anscombe* [1960]. The first theoretic approach to robust statistics was introduced by *Huber* [1964] where he used an asymptotic minimax framework. An extension of this basic idea is presented in his book *Huber* [1981]. *Hampel* [1968], [1974] originated a different theoretic approach based on influence functions (IFs) which especially after the book by *Hampel et al.* [1986] have become popular tools. A survey on robustness in signal processing can be found e.g. in *Kassam & Poor*

[1985].

There are different views on robustness. In this paper the robustness is seen in terms of the output distribution but, for example, in filter optimization robustness can also be seen as regarding the increase in error resulting from changing model conditions as in *Grigoryan and Dougherty* [1999].

The IF, introduced by Hampel under the name influence curve (IC), is a useful heuristic tool of robust statistics for studying the performance of estimators under noisy conditions.

**Definition 1.** The IF of estimator $T$ at underlying probability distribution $F$ is given by

$$\mathrm{IF}(y) = \lim_{\varepsilon \to 0^+} \frac{T\left((1-\varepsilon)F + \varepsilon \Delta_y\right) - T(F)}{\varepsilon}$$

for those $y$ where this limit exists.

In this definition $\Delta_y$ is the probability measure which puts mass 1 at the point $y$. The IF gives the effect that an infinitesimal contamination at point $y$ has on the estimator $T$ when divided by the mass of the contamination. So the IF gives asymptotic bias caused by the contamination and thus characterizes properties of the estimator as the number of observations approaches infinity.

We denote by $\Phi$ and $\phi$ the distribution and the density functions of the standard normal distribution. The influence functions for the mean and the median are shown in Fig. 1 where the underlying distribution $F = \Phi$. For the mean the gross error sensitivity, i.e., the worst influence which a small amount of contamination of fixed size can have on the value of the estimator, equals infinity and for the median it is finite and equals $\sqrt{\frac{\pi}{2}} \approx 1.253$. So for the mean single outlier can carry the estimate over all bounds but for the median an outlier has a fixed influence.

The IF gives only one aspect of robustness of an estimator, namely local robustness of the asymptotic value of the estimator. Another important aspect is the local robustness of the asymptotic variance. Asymptotic variance of estimator $T$ at $F$ denoted by $V(T,F)$ is defined to be the variance of $\sqrt{N}\left[T(F_N) - T(F)\right]$ as $N \to \infty$, where $F_N$ is the empirical distribution of sample $(X_1, X_2, \ldots, X_N)$. Local robustness of the asymptotic variance can be characterized by the change-of-variance function (CVF) defined as follows by *Hampel et al.* [1986].

**Definition 2.** The CVF of estimator $T$ at $F$ is defined as

$$\mathrm{CVF}(y) = \lim_{\varepsilon \to 0^+} \frac{V(T,(1-\varepsilon)F + \varepsilon\Delta_y) - V(T,F)}{\varepsilon}$$

for those $y$ where this limit exists.

If $F = \Phi$, the CVF of the mean is $y^2 - 1$, which is displayed in Fig. 2 by the solid line. In the same figure the CVF of the median at $F = \Phi$ is shown by the dashed line. It has a constant value $\pi \approx 3.142$ elsewhere but at zero, where the graph has a negative delta function. If the CVF is negative, the asymptotic variance of the estimator has decreased, and if positive, the asymptotic variance has increased. So for the mean, the asymptotic variance decreases if the contamination is in the interval $(-1,1)$. The further the contamination is from this interval the more the asymptotic variance is increased and a single outlier can carry the asymptotic variance over all bounds. For the median, contamination at the origin reduces the asymptotic variance significantly and the contamination anywhere else causes only a small constant increase to the asymptotic variance of the median. So the median is robust also in this sense of asymptotic variance.

## OUTPUT DISTRIBUTIONAL INFLUENCE FUNCTION

Since the IF is an asymptotic measure, it describes properties of infinite length filters which may differ from those of finite length filters used in the real world filtering applications. It would be more useful and more interesting to examine properties of these finite length filters rather than the asymptotic properties. In the case where the output distribution of a filter can be expressed in a closed form as a function of the distribution functions of the input samples we proposed in *Peltonen et al.* [2001] output distributional influence function (ODIF) for analyzing the robustness of the finite length filters.

We assume here that the input samples are independent and identically distributed (i.i.d.) random variables. First we need a way to denote the output distribution function of a filter when a fraction $\varepsilon$ of the input samples has different distribution than the rest of the samples. We denote by $H_{(1-\varepsilon)F+\varepsilon G_y}(\cdot)$ the output distribution $H_F(\cdot)$ of the filter where every occurrence of the common distribution function $F$ of the input samples is replaced by $(1-\varepsilon)F + \varepsilon G_y$ and $G_y$ can be any distribution function with mean $y$. As usual, we define $h_{(1-\varepsilon)F+\varepsilon G_y}(x) = \frac{\partial}{\partial x} H_{(1-\varepsilon)F+\varepsilon G_y}(x)$. We gave the following definition for the ODIF for the distribution function in *Peltonen et al.* [2001].

**Definition 3.** Let the output distribution function of a filter be $H_F(\cdot)$ where $F(\cdot)$ is the common distribution function of the input samples and let $G_y(\cdot)$ be a distribution function having mean $y$. Then the ODIF for the distribution function $\Omega(\cdot)$ is

$$\Omega(x, y) = \lim_{\varepsilon \to 0^+} \frac{H_{(1-\varepsilon)F+\varepsilon G_y}(x) - H_F(x)}{\varepsilon}$$

for those $x$ and $y$ where this limit exists.

If the output distribution function $H_F(\cdot)$ can be expressed as a simple function of the input distribution $F$ and thus does not contain any derivative of $F$, the ODIF for the distribution function $\Omega(\cdot)$ can be expressed as *Peltonen et al.* [2001]

$$\Omega(x, y) = \frac{h_F(x)}{f(x)}\Big(G_y(x) - F(x)\Big). \tag{1}$$

In *Peltonen et al.* [2001] we defined the ODIF in the same way as for the distribution function in Definition 3 also for the density function and moments. The ODIFs for the density function, expectation and variance were derived to be

$$\omega(x, y) = \frac{\partial}{\partial x}\Omega(x, y), \tag{2}$$

$$\omega_\mu(y) = \int_{-\infty}^{\infty} x\omega(x, y)dx \tag{3}$$

and

$$\omega_{\sigma^2}(y) = \int_{-\infty}^{\infty} x^2\omega(x, y)dx - 2\mu_{H_F}\omega_\mu(y), \tag{4}$$

where $\mu_{H_F}$ is the mean of the distribution $H_F$.

The ODIF for the expectation provides similar quantitative information and similar quantities can be derived from it as from the IF but now for finite length filters. Similar connection exists between the ODIF for the variance multiplied by the filter length and the CVF.

## ODIFS FOR STANDARD MEDIAN

In this paper we assume that the filter length $N$ is odd, i.e. $N = 2n+1$. In *Peltonen et al.* [2001] we derived the ODIFs for the standard median filter (SMF). The ODIFs for the distribution and density functions of the SMF of $N$ samples were obtained to be

$$\Omega(x,y) = \frac{N!}{(n!)^2} F(x)^n \left(1-F(x)\right)^n \left(G_y(x) - F(x)\right)$$

and

$$\omega(x,y) = \frac{N!}{(n!)^2} [nF(x)^{n-1}\left(1-F(x)\right)^{n-1}\left(1-2F(x)\right) f(x) \left(G_y(x) - F(x)\right)$$
$$+F(x)^n \left(1-F(x)\right)^n \left(g_y(x) - f(x)\right)].$$

When $F = \Phi$ and $G_y = \Delta_y$, the following forms were obtained for the ODIFs for the expectation and variance of the SMF of $N$ samples

$$\omega_\mu(y) = \frac{N!}{(n!)^2} [n \int_{-y}^{y} x\Phi(x)^{n+1}(1-\Phi(x))^{n-1}\phi(x)dx + y\Phi(y)^n \left(1-\Phi(y)\right)^n] \quad (5)$$

and

$$\omega_{\sigma^2}(y) = \frac{N!}{(n!)^2} [n \int_{-\infty}^{y} x^2\Phi(x)^{n+1}\left(1-\Phi(x)\right)^{n-1}\phi(x)dx$$

$$+n \int_{y}^{\infty} x^2\Phi(x)^{n-1}\left(1-\Phi(x)\right)^{n+1}\phi(x)dx + y^2\Phi(y)^n\left(1-\Phi(y)\right)^n$$

$$-(n+1)\int_{-\infty}^{\infty} x^2\Phi(x)^n\left(1-\Phi(x)\right)^n\phi(x)dx]. \quad (6)$$

Figs. 3 and 4 show the ODIFs for the expectation and variance of the SMFs of lengths 3, 5 and 15. These figures show the good robustness against outliers that the SMF has and how increase in filter length improves the robustness. Robustness of the SMF has been considered in more detail in *Peltonen et al.* [2001].

## ODIFS FOR RECURSIVE MEDIAN

Recursive extension of the SMF is the recursive median filter (RMF) defined by *Nodes and Gallagher* [1982] as

$$y(i) = \text{med}\{y(i-n), y(i-n+1), \ldots, y(i-1), x(i), \ldots, x(i+n)\}$$

where $x(i)$ and $y(i)$ are the input and output sequences, respectively. This means that some of the already filtered samples are used in the calculation of the output, which of course improves the noise removal capability of the RMF when compared to the SMF. Unfortunately this also means loss of details and highly correlated output samples for the RMF.

For the images we have a scanning window of some chosen shape (e.g. square, rectangle, plus or cross) inside of which the samples are numbered by some numbering scheme consistent with the scanning order. The image samples inside this window are often denoted as $X_1, X_2, \ldots, X_N$. Now the output of the SMF is $Y = \text{med}\{X_1, X_2, \ldots, X_N\}$ and of the RMF is $Y = \text{med}\{Y_1, Y_2, \ldots, Y_n, X_{n+1}, X_{n+2}, \ldots, X_N\}$. In the RMF $X_{n+1}$ in the image is replaced by Y and when the window moves to the next position in the scanning order the labeling of the samples inside the window is redone and filtering is repeated for this position. The most common scanning order is from top left row by row downwards. Below is an example of this case where the scanning window is $3 \times 3$ square. On the left hand side are the input samples inside this window for the SMF and on the right for the RMF:

$$\begin{array}{ccc} X_1 & X_2 & X_3 \\ X_4 & X_5 & X_6 \\ X_7 & X_8 & X_9 \end{array} \qquad \begin{array}{ccc} Y_1 & Y_2 & Y_3 \\ Y_4 & X_5 & X_6 \\ X_7 & X_8 & X_9 \end{array}$$

The center sample $X_5$ is the sample being filtered and in this scanning order one can notice that the already filtered samples of the RMF are on upper row and on left of the center sample. In the two-dimensional case the properties of the recursive filter depend on the scanning order that can also be some other than the one given above.

The output distribution of the RMF for i.i.d. input values is given by the following proposition in *Shmulevich et al.* [1999].

**Proposition 1.** Let the samples of the input sequence $x(i)$ of the RMF be i.i.d.

random variables having a common distribution function $F(\cdot)$. Then the output distribution function $H_F(x)$ of the RMF of $N$ samples is

$$H_F(x) = \left( 1 + \left( \frac{1-F(x)}{F(x)} \right)^n \cdot \frac{1-F(x)^{n+1}}{1-(1-F(x))^{n+1}} \right)^{-1}.$$

The density function of the RMF obtained by differentiation is

$$\begin{aligned} h_F(x) = f(x)\left(F(x)^{-1}-1\right)^n \left[\left(F(x)-1\right)F(x)\right]^{-1} [\left(1-F(x)\right)^n (n-(2n+1)F(x) \\ +(n+1)F(x)^2 + F(x)^{n+1} - F(x)^{n+2}) - n + F(x)^{n+1}\left((n+1)F(x)-1\right)] \\ \times [\left(1-F(x)\right)^{n+1} + \left(F(x)^{n+1}-1\right)\left(F(x)^{-1}-1\right)^n - 1]^{-2}. \end{aligned}$$

The ODIFs can be used for studying the robustness of the RMF as in *Peltonen* [2003]. In the following example we derive formula for the ODIFs for the expectation and variance of the RMF of length 3 when $F = \Phi$ and $G_y = \Delta_y$.

**Example 1.** Let us consider the RMF of length 3. The ODIF for the distribution function obtained by using Eq. (1) is

$$\Omega(x,y) = F(x)\frac{4-5F(x)+2F(x)^2-F(x)^3}{(1-F(x)+F(x)^2)^2}(G_y(x)-F(x))$$

and the ODIF for the density function obtained by using Eq. (2) is

$$\begin{aligned} \omega(x,y) = 2f(x)\frac{2-3F(x)-3F(x)^2+2F(x)^3}{(1-F(x)+F(x)^2)^3}(G_y(x)-F(x)) \\ +F(x)\frac{4-5F(x)+2F(x)^2-F(x)^3}{(1-F(x)+F(x)^2)^2}(g_y(x)-f(x)). \end{aligned}$$

When $F = \Phi$ and $G_y = \Delta_y$ we can derive by using Eq. (3) the ODIF for the expectation to be

$$\omega_{\mu}(y) = 2\int_{y}^{\infty} x\phi(x)\frac{2-3\Phi(x)-3\Phi(x)^2+2\Phi(x)^3}{(1-\Phi(x)+\Phi(x)^2)^3}dx$$
$$+y\Phi(y)\frac{4-5\Phi(y)+2\Phi(y)^2-\Phi(y)^3}{(1-\Phi(y)+\Phi(y)^2)^2}$$
$$+\int_{-\infty}^{\infty} x\Phi(x)\phi(x)(8-15\Phi(x)+5\Phi(x)^2-4\Phi(x)^3+3\Phi(x)^4-\Phi(x)^5)$$
$$\times(1-\Phi(x)+\Phi(x)^2)^{-3}dx.$$

When $\mathrm{F}=\Phi$ and $\mathrm{G}_{\mathrm{y}}=\Delta_{\mathrm{y}}$ for this filter $\mu_{\mathrm{H}_{\Phi}}=0$ and we obtain from Eq. (4) that the ODIF for the variance is

$$\omega_{\sigma^2}(y) = 2\int_{y}^{\infty} x^2\phi(x)\frac{2-3\Phi(x)-3\Phi(x)^2+2\Phi(x)^3}{(1-\Phi(x)+\Phi(x)^2)^3}dx$$
$$+y^2\Phi(y)\frac{4-5\Phi(y)+2\Phi(y)^2-\Phi(y)^3}{(1-\Phi(y)+\Phi(y)^2)^2}$$
$$+\int_{-\infty}^{\infty} x^2\Phi(x)\phi(x)(8-15\Phi(x)+5\Phi(x)^2-4\Phi(x)^3+3\Phi(x)^4-\Phi(x)^5)$$
$$\times(1-\Phi(x)+\Phi(x)^2)^{-3}dx.$$

In Fig. 5 are shown the ODIFs for the expectation of the RMF of Example 1 and of the RMFs of lengths 5 and 15 when $\mathrm{F}=\Phi$ and $\mathrm{G}_{\mathrm{y}}=\Delta_{\mathrm{y}}$. From this figure we can see that the supremum of the absolute value of the ODIF for the expectation of the RMF is limited and has higher value for smaller filter length. So the robustness against outliers can clearly be observed.

In Fig. 6 are shown the ODIFs for the variance multiplied by the filter length for the same three cases as in Fig. 5 for the expectation. From this figure we can see that in the variance sense the robustness against outliers gets very much better as the filter length increases.

In order to make comparisons easier the ODIFs for the expectation of the SMF and the RMF from Figs. 3 and 5 are presented again in Fig. 7 for filter lengths 3 and 15. We can see that the robustness against outliers is slightly better for the RMF than for the SMF of the same length. This can be understood for example by considering how the RMF actually uses also the signal values encountered before the current window position while the SMF uses strictly the values inside the filter window in the calculation of the output. Thus the true amount of samples used is different although the window lengths are equal.

In the case of variance in Fig. 8 the differences are even larger between the RMF and the SMF and the robustness of the RMF against outliers in the variance sense is significantly better than that of the SMF. This results from the correlatedness of the RMF outputs and their tighter concentration around the mean value, which increases heavily as the filter length increases.

Robustness against small fluctuations in the observations at some point can be measured by considering the slope of the ODIF for the expectation in that point. In the context of IFs this type of robustness is measured by local-shift sensitivity. From Fig. 7 we can observe that near the center of symmetry (origin) the slopes of the graphs for the RMFs have higher values than the corresponding graphs for the SMFs have and in this sense the SMF has better robustness. This type of robustness however is much less important than robustness against outliers.

## CONCLUSIONS

Recently derived output distribution of the RMFs by *Shmulevich et al.* [1999] has made it possible to study more thoroughly statistical properties of the RMFs than what has been possible in the past. In this paper we examined the robustness of the RMFs by using the ODIF which is a recently introduced tool for determining the robustness of finite length filters. Comparisons between the robustness properties of the SMF and the RMF were also made.

## REFERENCES

Anscombe, F. J., 1960, *Rejection of Outliers*, Technometrics, 2, 123–147.

Grigoryan, A. M., and Dougherty, E. R., 1999, *Design and Analysis of Robust Binary Filters in the Context of a Prior Distribution for the States of Nature*, J. Math. Imag. Vis., 11, 3, 239–254.

Hampel, F. R., 1968, *Contribution to the Theory of Robust Estimation*, Ph.D. Thesis, University of California, Berkeley.

Hampel, F. R., 1974, *The Influence Curve and Its Role in Robust Estimation*, J. Amer. Statist. Assoc., 69, 346, 383–393.

Hampel, F. R., Rousseeuw, P. J., Ronchetti, E. M., and Stahel, W. A., 1986, *Robust Statistics: The Approach Based on Influence Functions*, Wiley, New York.

Huber, P. J., 1964, *Robust Estimation of a Location Parameter*, Ann. Math. Statist., 35, 1, 73–101.

Huber, P. J., 1981, *Robust Statistics*, Wiley, New York.

Kassam, S. A., and Poor, H. V., 1985, *Robust Techniques for Signal Processing: A Survey*, Proc. IEEE, 73, 3, 433–481.

Nodes, T. A., and Gallagher, N. C., 1982, *Median Filters: Some Modifications and Their Properties*, IEEE Trans. on Acoustics, Speech, and Signal Processing, 30, 5, 739–746.

Peltonen, S., Kuosmanen, P., and Astola, J., 2001, *Output Distributional Influence Function*, IEEE Trans. on Signal Processing, 49, 9, 1953–1960.

Peltonen, S., 2003, *Output Distributional Influence Function for Recursive Median Filters*, Proc. of 2003 IEEE - Eurasip Workshop on Nonlinear Signal and Image Processing, NSIP 2003, Grado-Trieste, Italy, 8-11 June.

Shmulevich, I., Yli-Harja, O., Egiazarian, K., and Astola, J., 1999, *Output Distributions of Recursive Stack Filters*, IEEE Signal Processing Letters, 6, 7, 175–178.

Tukey, J. W., 1960, *A Survey of Sampling from Contaminated Distributions*, in Contributions to Probability and Statistics, I. Olkin, Ed., Stanford University Press, Stanford, CA, 448–485.

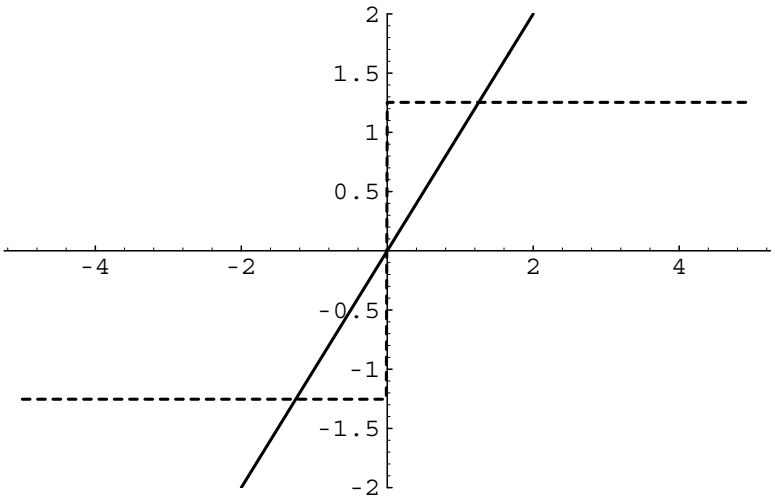


**Figure 1**. The IFs of the mean (–) and the median (- -) at $F = \Phi$ .

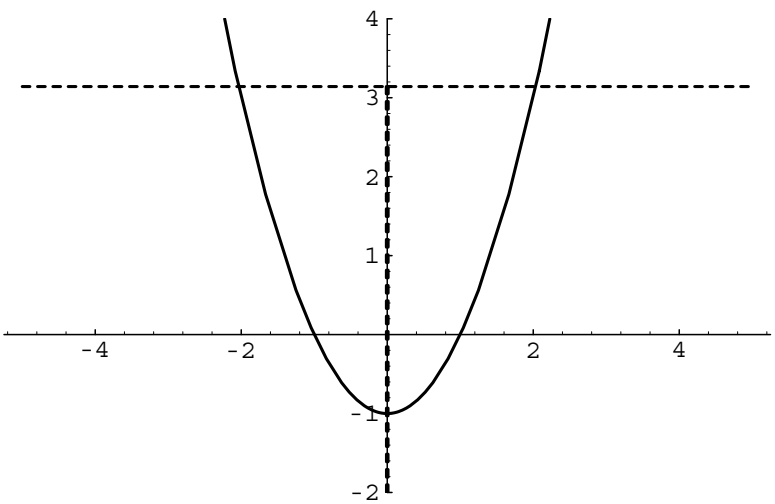


**Figure 2**. The CVFs of the mean (–) and the median (- -) at $F = \Phi$ .

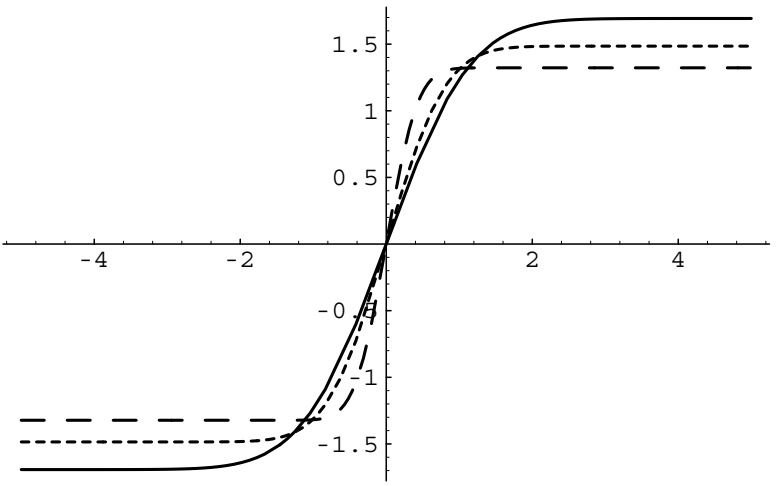


**Figure 3.** The ODIFs for the expectation of the SMFs of lengths 3 (solid line), 5 (short dashes) and 15 (long dashes) at $F = \Phi$ and $G_y = \Delta_y$.

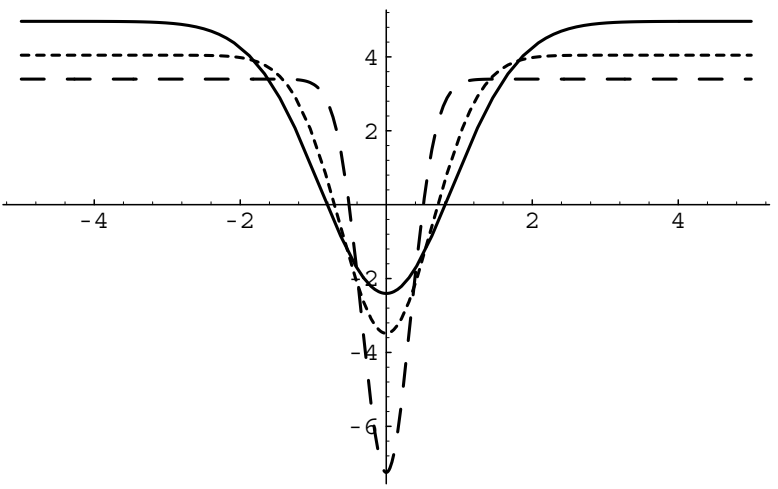


**Figure 4**. The ODIFs for the variance of the SMFs of lengths 3 (solid line), 5 (short dashes) and 15 (long dashes) multiplied by the filter length $N$ at $F = \Phi$ and $G_y = \Delta_y$.

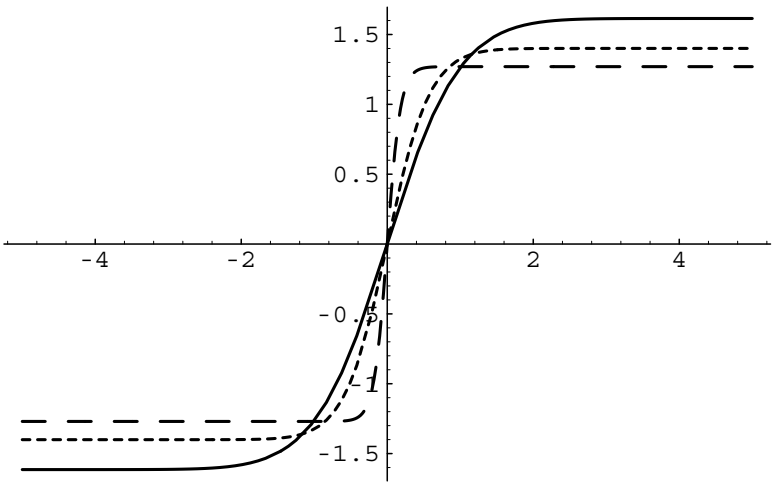


**Figure 5**. The ODIFs for the expectation of the RMFs of lengths 3 (solid line), 5 (short dashes) and 15 (long dashes) at $\mathrm{F} = \Phi$ and $\mathrm{G_y} = \Delta_\mathrm{y}$.

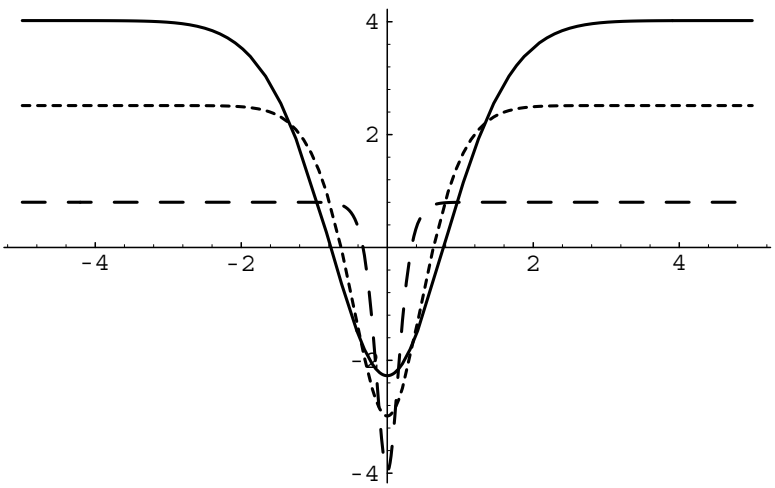


**Figure 6**. The ODIFs for the variance of the RMFs of lengths 3 (solid line), 5 (short dashes) and 15 (long dashes) multiplied by the filter length $\mathrm{N}$ at $\mathrm{F} = \Phi$ and $\mathrm{G_y} = \Delta_\mathrm{y}$.

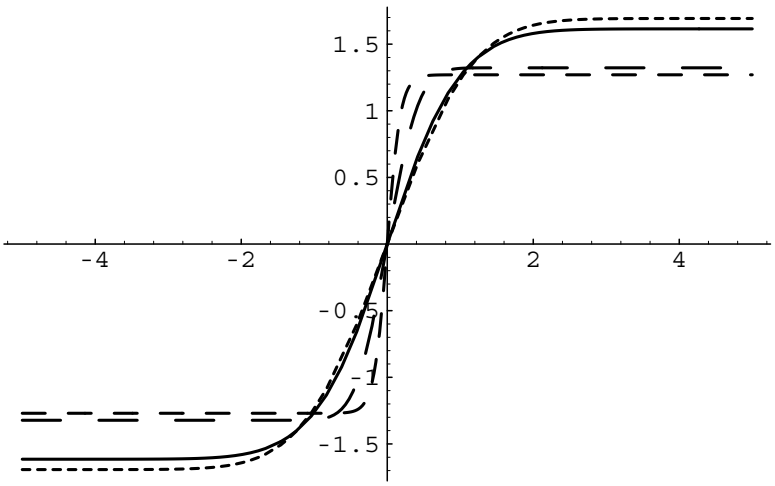


**Figure 7**. The ODIFs for the expectation of the RMFs of lengths 3 (solid line) and 15 (medium dashes) and of the SMFs of lengths 3 (small dashes) and 15 (long dashes) at $\mathrm{F} = \Phi$ and $\mathrm{G}_{\mathrm{y}} = \Delta_{\mathrm{y}}$.

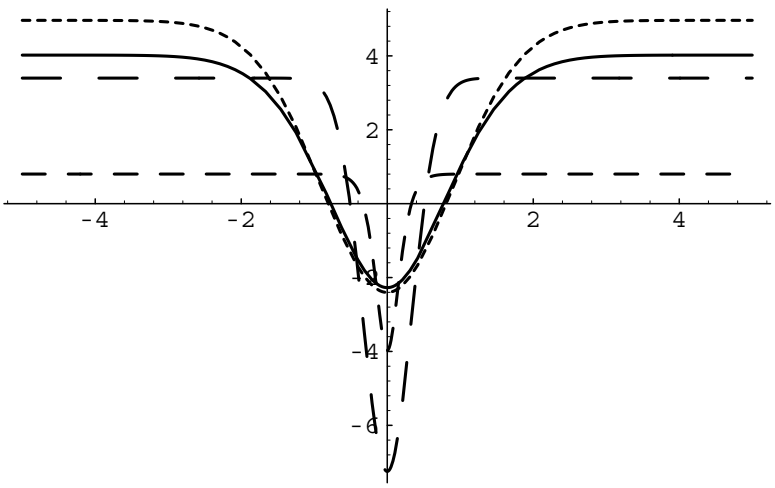


**Figure 8**. The ODIFs for the variance of the RMFs of lengths 3 (solid line) and 15 (medium dashes) and of the SMFs of lengths 3 (small dashes) and 15 (long dashes) multiplied by the filter length $\mathrm{N}$ at $\mathrm{F} = \Phi$ and $\mathrm{G}_{\mathrm{y}} = \Delta_{\mathrm{y}}$.

*International Journal of Tomography & Statistics (IJTS),*
*June-July 2005, Vol. 3, No. JJ05, 44-80*
*ISSN 0972-9976;* 

# Fourier Trigonometric Compression in Magnetic Resonance Imaging

**R.K.S. Rathore[1], R.K. Gupta[2], R. Kalyan Raman[3], Divya K.S. Rathore[4]**

[1]Department of Mathematics,
Indian Institute of Technology, Kanpur-208016, India
Email:rksr@iitk.ac.in

[2]Department of Radiology, SGPGIMS, Lucknow, India,

[3]TCS, Chennai, India

[4]Venera Technologies, Noida, India

## ABSTRACT

*MRI scanners produce Fourier coefficients of the magnetic moment field due to spinning protons from the water molecules present in the cross section under consideration. MRI images are reconstructed from the associated partial sums of Fourier series of two variables. As the basic measurements that give rise to such images consist of the Fourier data it is natural to consider MRI compressions based on trigonometric series. In the present paper, besides characterizing cross-sections belonging to certain Besov spaces by a sequence of trigonometric polynomials obtained from their Fourier Series, we also obtain theoretical storage bounds for a proposed compression algorithm. Compressed images are analyzed from the point of view of artefacts and subsequent use in the tissue parameter calculations.*

## KEY WORDS

MRI, Fourier reconstruction, Besov spaces, modulii of smoothness, Hardy's inequality, direct and inverse theorems, Image compression, storage bounds

## INTRODUCTION

A study of Besov Spaces $B_q^{\alpha,k}(L_p(I))$ has been made in the context of compression of wavelet decompositions by R.A.DeVore, B.Jawerth and V.A.Popov [4]. They characterized functions having certain prescribed degree of

approximation by dyadic splines. The interpolation spaces between a pair of Besov Spaces have also been studied by R.A.DeVore and V.A.Popov [5]. In 1992, R.A.DeVore, B.Jawerth and B.J.Lucier [3] have proposed a compression algorithm based on wavelet decomposition. They associate to each set of pixel values a function f given by

(0.1) $$f = \sum_{k \geq 0,\, j=(j_1, j_2)} c_{j,k} \phi_{j,k} ,$$

where $c_{j,k}$'s are the wavelet coefficients of f. $\phi_{j,k}$'s are generated from a single function $\phi$ by their dyadic dilates and translates given by,

(0.2) $$\phi_{j,k}(x) = \phi(2^k x - j) .$$

After obtaining a wavelet-based decomposition of the form (0.1), the compression algorithm quantizes the transform coefficients to obtain quantized coefficients $\tilde{c}_{j,k}$ and the compressed function takes the form,

(0.3) $$\tilde{f} = \sum_{k \geq 0,\, j=(j_1, j_2)} \tilde{c}_{j,k} \phi_{j,k} .$$

Their theory relates the smoothness of images in certain smoothness classes called Besov Spaces [5], which are defined as follows:

Definition (1.4.4) (Besov Spaces):

Fix $\alpha > 0$ and an integer $k > 0$. Define the k-th forward difference with a prameter $h \in \Re^+$ by

$$\Delta_h^0 f(x) := f(x)$$

and, for j = 1,…..,k,

$$\Delta_h^j f(x) := \Delta_h^{j-1} f(x+h) - \Delta_h^{j-1} f(x) .$$

For $1 \leq p < \infty$, the k-th modulus of smoothness in $L_p(I)$ is defined as

$$\omega_k(f,t)_p = \sup_{|h| \leq t} \left( \int_{I_{rh}} |\Delta_h^k f(x)|^p dx \right)^{\frac{1}{p}} ,$$

and, for $p = \infty$,

$$\omega_k(f,t) := \sup_{|h| \leq t} (|\Delta_h^k f(x)|) ,$$

where $I_{rh} = \{x \in I : x+rh \in I\}$. $\Delta_h^k f(x)$ is defined iff $x \in I_{rh}$. The Besov space, $B_q^{\alpha,k}(L_p(I))$ norm is defined as

$$\|f\|_{B_q^{\alpha,k}(L_p(I))} = \|f\|_p + \left( \int_0^\infty \left[ t^{-\alpha} \omega_k(f,t)_p \right]^q \frac{dt}{t} \right)^{\frac{1}{q}}$$

for $1 \le p \le \infty$, $0 < q < \infty$, and, for $q = \infty$,

$$\| f \|_{B_q^{\alpha,k}(L_p(I))} := \| f \|_p + \sup_{t>0} [t^{-\alpha} \omega_k(f,t)_p]$$

By definition, $f \in B_q^{\alpha,k}(L_p(I))$ if $||f||_{B_q^{\alpha,k}(L_p(I))} < \infty$.

The error function in $L_p(I)$ is given by,

(1.4.5) $$a_N(f)_p = \inf_{\tilde{f} \text{ has} \le N \text{ coefficients}} \left\| f - \tilde{f} \right\|_{L_p(I)}.$$

For certain choices of $\varphi$, DeVore, Jawerth and Popov [4] have shown that,

(1.4.6) $$a_N(f)_p = O(N^{-\alpha/2}) \Leftrightarrow f \in B_q^{\alpha,k}(L_q(I))$$

where, $\alpha/2 + 1/p = 1/q$.

They have proposed a compression algorithm based on the wavelet decomposition of f. The quantization strategy to obtain $\tilde{c}_{j,k}$'s is that they satisfy,

(1.4.7) $$\left\| \left( c_{j,k} - \tilde{c}_{j,k} \right) \phi_{j,k} \right\|_{L_p(I)} \le N^{-1/q}.$$

Here N, the quantization parameter, is a chosen positive integer, and it determines the amount of compression. The number $\boldsymbol{N}$, of nonzero coefficients $\tilde{c}_{j,k}$'s is shown to satisfy,

(1.4.8) $$\boldsymbol{N} \le C_1 N \|f\|^q_{B_q^\alpha(L_q(I))}.$$

The paper is organized as follows. The first section contains preliminaries including the definition of Besov Spaces. These spaces are identified with weighted sequence spaces $l_q^\alpha(X)$ (defined more precisely in section two). The norm equivalence is obtained in section two. In section three, we prove a Hardy type inequality and some lemmas including bound on Fourier coefficients by

integral modulus of smoothness. These lemmas are used in our main theorem and subsequent storage bounds.

Direct and inverse theorems, which relate MR images in Besov spaces and their degree of approximation by partial sums of Fourier series, are presented in section four.

Compression algorithms based on Fourier and Poission approximation process and theoretical storage bounds for MR images are obtained in section five. Section six deals with the compression of the raw data and the paper ends with section seven where the numerical experiments and results are discussed.

We have tried to keep the presentation accessible and self contained, by including proofs, as far as possible.

## 1. BESOV SPACES

We use the following notations throughout this paper. Let I = $[0,2\pi]^2$ and f(x), $(x_1,x_2)' = x \in I$, be the analog intensity distribution function of the underlying cross section viewed as a mapping from I to the interval [0,1],

$$f : [0,2\pi]^2 \rightarrow [0,1].$$

The function f(x) is of two variables, with. Let $n = (n_1,n_2)' \in Z_2^+$ and $h = (h_1, h_2)' \in \Re^2$. The operations addition and dot product are given by, $x + h = (x_1+h_1, x_2+h_2)$, $x.h = x_1h_1 + x_2h_2$, $x.n = x_1n_1+x_2n_2$, for $t > 0$, $|h| < t \Rightarrow |h_1| < t$, $|h_2| < t$ and for any positive integer k, $kh = (kh_1, kh_2)$.

For a fixed $\alpha > 0$ and an integer $k > 0$. The k-th forward difference with a parameter $h=(h_1, h_2)' \in I$ is given by: $\Delta_h^0 f(x) := f(x)$, and,

$$\Delta_h^j f(x) := \Delta_h^{j-1} f(x+h) - \Delta_h^{j-1} f(x), \; j = 1,\ldots..,k, \; x = (x_1,x_2)' \in I.$$

For $1 \leq p < \infty$, the k-th modulus of smoothness in $L_p(I)$ is defined as

$$\omega_k(f,t)_p = \sup_{|h|\leq t} \left( \int_I |\Delta_h^k f(x)|^p dx \right)^{1/p} \tag{1.1}$$

and, for $p = \infty$,

(1.2) $$\omega_k(f,t) = \sup_{|h|\le t}(|\Delta_h^k f(x)|)$$

The Besov space $B_q^{\alpha,k}(L_p(I))$ (cf., R.A.DeVore, et al. [4]) norm is defined as

(1.3) $$\| f \|_{B_q^{\alpha,k}(L_p(I))} := \| f \|_p + \left( \int_0^{2\pi} \left[ t^{-\alpha} \omega_k(f,t)_p \right]^q \frac{dt}{t} \right)^{1/q}$$

for $1 \le p \le \infty$, $1 \le q < \infty$ and for $q = \infty$,

(1.4) $$||f||_{B_q^{\alpha,k}(L_p(I))} := ||f||_p + \sup_{t>0}[t^{-\alpha}\omega_k(f,t)_p]$$

where $f \in B_q^{\alpha,k}(L_p(I))$ iff $||f||_{B_q^{\alpha,k}(L_p(I))} < \infty$.

The limits of integral, in the right hand side of (1.3) go from 0 to $\infty$ in the definition used in [4]. Since we are dealing with $2\pi$ periodic functions we let the limits run from 0 to $2\pi$. Although Besov spaces are defined for $0 < q < 1$, we restrict ourselves to the normed spaces, i.e. $q \ge 1$. We note that when $q = \infty$, we require $\omega_k(f,t)_p$ to decay at least as fast as $O(t^\alpha)$ as $t \to 0$, whereas when $q < \infty$, $\omega_k(f,t)_p$ should decay at a slightly faster rate. As $\omega_{k+1}(f,t)_p \le 2\omega_k(f,t)_p$,

(1.5) $$f \in B_q^{\alpha,k}(L_p(I)) \Rightarrow f \in B_q^{\alpha,k+1}(L_p(I)).$$

It follows by induction that for any $k' > k$, f will be in $B_q^{\alpha,k'}(L_p(I))$ if f is in $B_q^{\alpha,k}(L_p(I))$. If both k and k′ are strictly greater than $\alpha$, then $B_q^{\alpha,k}(L_p(I))$ is equivalent to $B_q^{\alpha,k'}(L_p(I))$. This result is presented in the form of a theorem.

**Theorem 1.1:** If $k' > k > \alpha$ then, $||.||_{B_q^{\alpha,k}(L_p(I))} \sim ||.||_{B_q^{\alpha,k'}(L_p(I))}$.

To prove this theorem we need three lemmas, which are as follows.

**Lemma 1.1:** The k-th differences $\Delta_h^k f(x)$ of a function of two variable f satisfy

$$\Delta_{2h}^k f(x) = \sum_{\upsilon=0}^{k} \binom{k}{\upsilon} \Delta_h^k f(x + \upsilon h).$$

**Proof:** For the case of a one variable function the above identity is available (see Timan [71]). Here we prove the above identity for two variables by using induction on k.

For k =1,

$$\begin{aligned}\Delta_{2h}^{k} f(x) &= f(x_1+2h_1, x_2+2h_2) - f(x_1, x_2) \\ &= f(x_1+2h_1, x_2+2h_2) - f(x_1+h_1, x_2+h_2) + f(x_1+h_1, x_2+h_2) - f(x_1, x_2) \\ &= \Delta_h^k f(x+h) + \Delta_h^k f(x)\end{aligned}$$

The identity is true for k=1, let us assume that it is true for k-1 and we prove for k.

$$\begin{aligned}&\Delta_{2h}^{k} f(x) \\ &= \Delta_{2h}^{k-1} f(x+2h) - \Delta_{2h}^{k-1} f(x) \\ &= \sum_{\upsilon=0}^{k-1} \binom{k-1}{\upsilon} \left[\Delta_h^{k-1} f(x+2h+\upsilon h) - \Delta_h^{k-1} f(x+\upsilon h)\right] \\ &= \sum_{\upsilon=0}^{k-1} \binom{k-1}{\upsilon} \left[\Delta_h^{k-1} f(x+2h+\upsilon h) - \Delta_h^{k-1} f(x+h+\upsilon h) + \Delta_h^{k-1} f(x+h+\upsilon h) - \Delta_h^{k-1} f(x+\upsilon h)\right] \\ &= \sum_{\upsilon=0}^{k-1} \binom{k-1}{\upsilon} \left[\Delta_h^{k} f(x+h+\upsilon h) + \Delta_h^{k} f(x+\upsilon h)\right] \\ &= \sum_{\upsilon=1}^{k-1} \binom{k-1}{\upsilon-1} \left[\Delta_h^{k} f(x+\upsilon h)\right] + \Delta_h^{k} f(x+kh) + \Delta_h^{k} f(x) + \sum_{\upsilon=1}^{k-1} \binom{k-1}{\upsilon} \left[\Delta_h^{k} f(x+\upsilon h)\right] \\ &= \sum_{\upsilon=1}^{k-1} \binom{k}{\upsilon} \left[\Delta_h^{k} f(x+\upsilon h)\right] + \Delta_h^{k} f(x+kh) + \Delta_h^{k} f(x), \text{ as } \binom{k-1}{\upsilon-1} + \binom{k-1}{\upsilon} = \binom{k}{\upsilon} \\ &= \sum_{\upsilon=0}^{k} \binom{k}{\upsilon} \left[\Delta_h^{k} f(x+\upsilon h)\right]\end{aligned}$$

**Lemma 1.2:** Let $1 \leq p \leq \infty$, and $f \in L_p(I)$ then,

$$\omega_k(f,t)_p \leq M_k t^k \left\{ \| f \|_p + \int_t^{\pi/k} \frac{\omega_{k+1}(f,u)_p}{u^{k+1}} du \right\},$$

where the constant $M_k$ does not depend on f.

**Proof:** For the case of functions of one variable and p = ∞, the proof is available (Timan, [10, p.108]). For functions of two variables and for $1 \le p < \infty$, the proof is similar. We just give the outline:

$$\left\|\Delta_{2h}^k f(x) - 2^k \Delta_h^k f(x)\right\|_p = \left\|\sum_{\upsilon=0}^{k}\binom{k}{\upsilon}\left\{\Delta_h^k f(x+\upsilon h) - \Delta_h^k f(x)\right\}\right\|_p \quad \text{[By Lemma 1.1]}$$

Hence, $$\left\|\Delta_{2h}^k f(x) - 2^k \Delta_h^k f(x)\right\|_p \le \sum_{\upsilon=1}^{k}\binom{k}{\upsilon}\left\{\sum_{\mu=0}^{\upsilon-1}\left\|\Delta_h^{k+1} f(x+\mu h)\right\|_p \le k2^{k-1}\omega_{k+1}(f,h)\right\}$$

Consider, $\varepsilon = (\varepsilon_1, \varepsilon_2)$, putting here, successively $h=2^m\varepsilon$ (m=0,1,……,k-1) and taking $0 \le \varepsilon_1, \varepsilon_2 \le t$. We obtain system of inequalities of the form

$$\left\|\Delta_{2^{m+1}\varepsilon}^k f(x) - 2^k \Delta_{2^m\varepsilon}^k f(x)\right\|_{L_p[0,2\pi-2kh]} \le k2^{k-1}\omega_{k+1}(f, 2^m\varepsilon)_p .$$

Multiply both sides by $2^{-(m+1)k}$ and summing for m=0,1,…,r-1 and using the fact that $\omega_{k+1}(f,u)_p$ is non-decreasing with u, we get

$$\left\|2^{-rk}\Delta_{2^r\varepsilon}^k f(x) - \Delta_\varepsilon^k f(x)\right\|_p \le k^2 t^k \int_t^{2^r t} \frac{\omega_{k+1}(f,u)_p}{u^{k+1}} du ,$$

which implies that

$$\left\|\Delta_\varepsilon^k f(x)\right\|_p \le 2^{-(r-1)k}\left\|f\right\|_p + k^2 t^k \int_t^{2^r t} \frac{\omega_{k+1}(f,u)_p}{u^{k+1}} du . \tag{1.6}$$

Proceeding as in above with f(x) replaced by $\phi(x) = f(2\pi - x)$, i.e. $\phi(x_1, x_2) = f(2\pi - x_1, 2\pi - x_2)$, we obtain

$$\left\|\Delta_\varepsilon^k \phi(x)\right\|_p \le 2^{-(r-1)k}\left\|f\right\|_p + k^2 t^k \int_t^{2^r t} \frac{\omega_{k+1}(f,u)_p}{u^{k+1}} du , \tag{1.7}$$

$$\left(\int_0^{2\pi}\left|\Delta_\varepsilon^k f(x)\right|^p dx\right)^{1/p} \le \left(\int_0^{\pi}\left|\Delta_\varepsilon^k f(x)\right|^p dx\right)^{1/p} + \left(\int_\pi^{2\pi}\left|\Delta_\varepsilon^k f(x)\right|^p dx\right)^{1/p} \tag{1.8}$$

$$= J_1 + J_2 , \text{ say.}$$

We have,

(1.9) $J_2 = \left( \int_{\pi}^{2\pi} \left| \Delta_{\varepsilon}^{k} f(x) \right|^{p} dx \right)^{1/p} = \left( \int_{0}^{\pi} \left| \Delta_{\varepsilon}^{k} f(2\pi - y) \right|^{p} dy \right)^{1/p} = \left( \int_{0}^{\pi} \left| \Delta_{\varepsilon}^{k} \phi(y) \right|^{p} dy \right)^{1/p}$

Hence from (1.6), (1.7), (1.8) and (1.9) it follows that

(1.10) $\left\| \Delta_{\varepsilon}^{k} f(x) \right\|_{p} \le 2.2^{-(r-1)k} \left\| f \right\|_{p} + 2.k^{2} t^{k} \int_{t}^{2^{r} t} \frac{\omega_{k+1}(f,u)_{p}}{u^{k+1}} du$ Now by using the following lemma, Hardy's inequality (Butzer and Berens [2, p.199]), in conjunction with the lemma 1.2 we will complete a proof of theorem 1.1.

We choose integer r=r(t) such that $2\pi / 4 \le 2^{r} tk \le 2\pi / 2$ this gives by (1.10) that

(1.11) $\left\| \Delta_{\varepsilon}^{k} f(x) \right\|_{L_p[0,2\pi - k\varepsilon]} \le M_k t^{k} \left\{ \left\| f \right\|_{p} + \int_{t}^{\pi/k} \frac{\omega_{k+1}(f,u)_{p}}{u^{k+1}} du \right\}$ .

Since $\varepsilon \le t$ is arbitrary the result follows from (1.11).

Now by using the following Hardy's inequality (Butzer and Berens [2, p.199]), in conjunction with the lemma 1.2 we will complete a proof of theorem 1.1.

**Hardy's inequality:** Let $\alpha > 0$, $1 \le q \le \infty$. If $\psi(s)$ is a non-negative measurable function on $(0,\infty)$ (measurable with respect to the measure ds/s), then

(1.12) $\left\{ \int_{0}^{\infty} \left( t^{-\alpha} \int_{0}^{t} \psi(s) \frac{ds}{s} \right)^{q} \frac{dt}{t} \right\}^{1/q} \le \frac{1}{\alpha} \left\{ \int_{0}^{\infty} \left( s^{-\alpha} \psi(s) \right)^{q} \frac{ds}{s} \right\}^{1/q}$, and,

(1.13) $\left\{ \int_{0}^{\infty} \left( t^{\alpha} \int_{t}^{\infty} \psi(s) \frac{ds}{s} \right)^{q} \frac{dt}{t} \right\}^{1/q} \le \frac{1}{\alpha} \left\{ \int_{0}^{\infty} \left( s^{\alpha} \psi(s) \right)^{q} \frac{ds}{s} \right\}^{1/q}$ .

Proof of Theorem 1.1: $\omega_{k+1}(f,t)_{p} \le 2\omega_{k}(f,t)$

$\Rightarrow$ $\| f \|_{B_q^{\alpha,k+1}(L_p(I))} \le C \| f \|_{B_q^{\alpha,k}(L_p(I))}$

Conversely, by Lemma 1.2,

$$\left( \int_{0}^{2\pi} \left( t^{-\alpha} \omega_{k}(f,t)_{p} \right)^{q} \frac{dt}{t} \right)^{1/q} \le \left( \int_{0}^{2\pi} \left[ t^{-\alpha} \left( M_k t^{k} \left\{ \left\| f \right\|_{p} + \int_{t}^{2\pi/2k} \frac{\omega_{k+1}(f,u)_{p}}{u^{k+1}} du \right\} \right) \right]^{q} \frac{dt}{t} \right)^{1/q}$$

(1.14) $$\le M_k 2^{\frac{q-1}{q}} \left( \|f\|_p^q \int_0^{2\pi} t^{(k-\alpha)q-1} dt + M_k \int_0^{2\pi} \left[ t^{k-\alpha} \int_t^{2\pi} \frac{\omega_{k+1}(f,u)}{u^k} \frac{du}{u} \right]^q \frac{dt}{t} \right)^{1/q}$$

$$\le M_{k,\alpha} \|f\|_p + M_k I_1 \text{, where } I_1 = \left( \int_0^{2\pi} \left[ t^{k-\alpha} \int_t^{2\pi} \frac{\omega_{k+1}(f,u)}{u^k} \frac{du}{u} \right]^q \frac{dt}{t} \right)^{1/q} .$$

Taking $\psi(s) = \begin{cases} s^{-k} \omega_{k+1}(f,s)_p , & 0 \le s \le 2\pi \\ 0 & , s > 2\pi \end{cases}$, by the Hardy's inequality,

$$I_1 = \left( \int_0^{\infty} \left[ t^{k-\alpha} \int_t^{\infty} \psi(s) \frac{ds}{s} \right]^q \frac{dt}{t} \right)^{1/q} \le C_{\alpha,k} \left( \int_0^{\infty} \left( s^{k-\alpha} \psi(s) \right)^q \frac{ds}{s} \right)^{1/q} \quad [By\ Lemma\ 2.1.3]$$

where the constant $C_{\alpha,k}$ depends only on $\alpha$ and k. Hence

(1.15) $$I_1 \le C_{\alpha,k} \left( \int_0^{2\pi} \left( s^{-\alpha} \omega_{k+1}(f,s)_p \right)^q \frac{ds}{s} \right)^{1/q} .$$

Substituting (1.15) in (1.14), $\| f \|_{B_q^{\alpha,k1}(L_p(I))} \le C_1 \| f \|_{B_q^{\alpha,k+1}(L_p(I))}$. Hence the proof.

In the next section we define certain sequence norm and will show its equivalence with this Besov space norm.

## 2. EQUIVALENT NORMS

In the present section we identify Besov Space $B_q^{\alpha}(L_p(I))$ norm with a weighted sequence space $l_q^{\alpha}$ norm by proving their norm equivalence.

If a = $\{a_n\}$ is a sequence whose component functions are in the quasi normed space X, the $l_q^{\alpha}(X)$ norms, for $1 \le q < \infty$, is defined as:

(2.1) $$\|a\|_{l_q^{\alpha}(X)} := \left( \sum_{n=1}^{\infty} \left[ n^{\alpha} \|a_n\|_X \right]^q \frac{1}{n} \right)^{1/q} ,$$

with the usual change to a supremum norm when $q = \infty$. When $\{a_n\}$ is a sequence of real numbers, we replace $\|a_n\|_X$ by $|a_n|$ in (2.1) and denote the resulting norm by $\|(a_n)\|_{l_q^{\alpha}}$.

**Theorem 2.1:** For f ∈ $L_p(I)$, f ∈ $B_q^{\alpha,r}(L_p(I))$ iff $\{\omega_r(f,2\pi/n)_p\}_n \in l_q^\alpha$.

Proof: Let $\{\omega_r(f,2\pi/n)_p\}_n \in l_q^\alpha$. Then, $\sum_{n=1}^{\infty}\left[n^\alpha \omega_r(f,2\pi/n)_p\right]^q (1/n) < \infty$.

$$\int_0^{2\pi}\left[t^{-\alpha}\omega_r(f,t)_p\right]^q \frac{dt}{t} = \sum_{k=1}^{\infty}\int_{2\pi/k+1}^{2\pi/k}\left[t^{-\alpha}\omega_r(f,t)_p\right]^q \frac{dt}{t}, \quad [\omega_r \text{ non decreasing}]$$

$$\le \frac{1}{(2\pi)^{\alpha q}}\sum_{k=1}^{\infty}(k+1)^{\alpha q}\,\omega_r\left(f,\frac{2\pi}{k}\right)_p^q \frac{1}{k}, \quad \because \int_{2\pi/k+1}^{2\pi/k}\frac{dt}{t} \le \frac{2\pi}{(k+1)k}\frac{(k+1)}{2\pi} = \frac{1}{k}$$

$$\le C_{\alpha,q}\sum_{k=1}^{\infty}\left[k^\alpha \omega_r(f,2\pi/k)_p\right]^q (1/k) < \infty \quad \text{[by hypothesis].}$$

It follows that f ∈ $B_q^\alpha(L_p(I))$. Conversely, let f ∈ $B_q^\alpha(L_p(I))$,

$$\infty > \int_0^{2\pi}\left[t^{-\alpha}\omega_r(f,t)_p\right]^q \frac{dt}{t} = \sum_{n=1}^{\infty}\int_{2\pi/n+1}^{2\pi/n}\left[t^{-\alpha}\omega_r(f,t)_p\right]^q \frac{dt}{t}$$

$$\ge \sum_{n=1}^{\infty}[n^\alpha \omega_r(f,2\pi/(n+1))_p]^q\, n/[n(n+1)] \ge \frac{1}{2^{\alpha q}}\sum_{n=1}^{\infty}[(n+1)^\alpha \omega_r(f,2\pi/(n+1))_p]^q/(n+1)$$

Therefore, $\{\omega_r(f,2\pi/n)_p\}_n \in l_q^\alpha$, completing the proof.

In the next section we shall prove some lemmas which will be used along with this norm equivalence to characterize Magnetic Resonance Images in Besov spaces.

## 3. A HARDY TYPE INEQUALITY AND BOUND ON FOURIER COEFFICIENTS:

In this section we shall obtain a bound for Fourier coefficients in terms of modulus of smoothness and in what follows, we shall prove a Hardy type inequality which will be used in proving the inverse theorem in the next section.

**Lemma 3.1:** Let c > 1, p > 1 and $S_n = a_1 + a_2 + \cdots + a_n$, where $a_j \ge 0$ then

$$\sum_{n=1}^{\infty} n^{-c}\, S_n^p \;\le\; K_{p,c}\sum_{n=1}^{\infty} n^{-c}(n\,a_n)^p, \quad (K_{p,c} = [p/(c-1)]^p).$$

Proof: Let $S_0 = 0$. Define $\phi_n = n^{-c} + (n+1)^{-c} + \ldots\ldots$ then $\phi_n < k\, n^{1-c}$. This follows from the fact that $n^{-c} + (n+1)^{-c} + \ldots\ldots < \int_n^{\infty} \frac{dx}{x^c} = \frac{n^{1-c}}{c-1}$ we take $k = \frac{1}{c-1}$.

$$\sum_1^m n^{-c} S_n^p = \sum_1^m (\phi_n - \phi_{n+1}) S_n^p = \sum_1^m \phi_n S_n^p - \sum_1^m \phi_{n+1} S_n^p = \sum_1^m \phi_n S_n^p - \sum_2^{m+1} \phi_n S_{n-1}^p$$

$$\le \phi_1 S_1^p + \sum_2^m \phi_n \left(S_n^p - S_{n-1}^p\right) \le \phi_1 \left(S_1^p - S_0^p\right) + \sum_2^m \phi_n \left(S_n^p - S_{n-1}^p\right)$$

$$\le \sum_1^m \phi_n \left(S_n^p - S_{n-1}^p\right) \le \mathrm{k} \sum_1^{\mathrm{m}} \mathrm{n}^{1-\mathrm{c}} \left(\mathrm{S}_{\mathrm{n}}^{\mathrm{p}} - \mathrm{S}_{\mathrm{n-1}}^{\mathrm{p}}\right) \le k \sum_1^m n^{1-c} (S_n - S_{n-1}) p S_n^{p-1}$$

$$\le k_{p,c} \sum_1^m n^{1-c} S_n^{p-1} a_n, \quad \text{where } k_{p,c} = \frac{p}{c-1}$$

$$\le k_{p,c} \sum_1^m n^{-c/p} n^{-c/p'} S_n^{p-1} (n a_n), \text{ where } \frac{1}{\mathrm{p}} + \frac{1}{\mathrm{p}'} = 1$$

$$= k_{p,c} \sum_1^m n^{-c/p} (n a_n) n^{-c/p'} S_n^{p/p'}.$$

$$\sum_1^m n^{-c} S_n^p \le k_{p,c} \left( \sum_1^m n^{-c} (n a_n)^p \right)^{1/p} \left( \sum_1^m n^{-c} S_n^p \right)^{1/p'} \quad \text{[by Holders inequality]}$$

$$\Rightarrow \left( \sum_1^m n^{-c} S_n^p \right)^{1/p} \le k_{p,c} \left( \sum_1^m n^{-c} (n a_n)^p \right)^{1/p}, \text{ i.e., } \sum_1^m n^{-c} S_n^p \le K_{p,c} \sum_1^m n^{-c} (n a_n)^p .$$

**Corollary 3.1**: If c > 1, q >1, $S_n = \sum_{i=1}^n \sum_{j=1}^n a_{ij}$, where $a_{ij} \ge 0$, there is a constant $K_{q,c}^1$, depending only on q and c, such that $\sum_{n=1}^{\infty} n^{-c} S_n^q \le K_{q,c}^1 \sum_{n=1}^{\infty} n^{-c} \left(n^2 a_{nn}\right)^q$.

Proof: As $S_n = P_1^n + \cdots + P_n^n$, where $\mathrm{P_j^n} = \sum_{k=1}^n a_{kj}$, we have

$$\sum_{n=1}^{\infty} n^{-c} S_n^q \le K_{q,c} \sum_{n=1}^{\infty} n^{-c} \left(nP_n^n\right)^q, \text{ [ applying lemma 3.1 ]}$$

$$= \mathrm{K_{q,c}} \sum_{n=1}^{\infty} n^{-c} T_n^q, \qquad \text{[ where } \mathrm{T_n} = \sum_{\mathrm{k=1}}^{\mathrm{n}} \mathrm{na_{kn}} \text{ ]}$$

$$\le \mathrm{K^1_{q,c}} \sum_{n=1}^{\infty} n^{-c} (n^2 a_{nn})^q.$$

The following lemma bounds the Fourier coefficients.

**Lemma 3.2:** If $f \in L_p(I)$, $1 \le p \le \infty$, $k \in Z^+$, and $n = (n_1, n_2)' \ne 0$,

$$\left|\hat{\mathrm{f}}(\mathrm{n})\right| \le \mathrm{C_k}\, \omega_{\mathrm{k}}\left(\mathrm{f}, \mathrm{t}\right)_{\mathrm{p}},$$

where, $t = \pi/[2(|n_1| + |n_2|)] > 0$. The constant $C_k$ is independent of f.

Proof: Let us consider, $I = [0,2\pi]^2$, $h = (h_1, h_2) \in I$, $n = (n_1, n_2) \in Z_2^+$, $x = (x_1, x_2) \in I$, $dx = dx_1 dx_2$, and the dot product $n.x = n_1x_1 + n_2x_2$. We have,

$$\left(\Delta_h^k f\right)^{\wedge}(n) = (4\pi^2)^{-1} \int_I \left(\Delta_h^{k-1} f(x+h) - \Delta_h^{k-1} f(x)\right) e^{-in.x}\, dx$$

$$= (4\pi^2)^{-1} e^{in.h} \int_I \Delta_h^{k-1} f(x) e^{-in.x}\, dx - (4\pi^2)^{-1} \int_I \Delta_h^{k-1} f(x) e^{-in.x}\, dx$$

$$= (4\pi^2)^{-1} \left(e^{in.h} - 1\right) \int_I \Delta_h^{k-1} f(x) e^{-in.x}\, dx \quad = (4\pi^2)^{-1} \left(e^{in.h} - 1\right)^k \int_I f(x) e^{-in.x}\, dx$$

$$\Rightarrow \left[e^{in\cdot h/2}\left(e^{in\cdot h/2} - e^{-in\cdot h/2}\right)\right]^k \left|\hat{f}(n)\right| \le (4\pi^2)^{-1} \int_I \left|\Delta_h^k f(x)\right| dx$$

$$\Rightarrow \left|2\sin\frac{n.h}{2}\right|^k \left|\hat{f}(n)\right| \le (4\pi^2)^{-1} \left(4\pi^2\right)^{1/p'} \left(\int_I \left|\Delta_h^k f(x)\right|^p dx\right)^{1/p}, \text{ ( by, Holder's inequality).}$$

Let $t = \pi/[2(|n_1| + |n_2|)]$, and $h = (h_1, h_2)' = \left(t\,\mathrm{sgn}(n_1), t\,\mathrm{sgn}(n_2)\right)'$.

$$\Rightarrow \left|2^k\right| \left|\hat{f}(n)\right| \le C_p\, \omega_k(f,t), \text{ where } C_p = 1/\left(4\pi^2\right)^{1/p} \Rightarrow \quad \left|\hat{\mathrm{f}}(\mathrm{n})\right| \le \mathrm{C_{p,k}}\, \omega_{\mathrm{k}}\left(\mathrm{f}, \mathrm{t}\right),$$

where, $C_{p,k} = 1/[2^k \left(4\pi^2\right)^{1/p}]$. Hence the proof.

In the next section we shall present the direct and inverse theorem.

## 4. SOME DIRECT AND INVERSE THEOREMS

Here, in the direct theorem we treat the cases $1 < p < \infty$ and $p = 1, \infty$ separately. For the case $1< p < \infty$ we use the partial sums of Fourier series, and for $p =1, \infty$, the Steklov approximations are used to establish the results. Inverse results are obtained for the trigonometric polynomials of best approximation. To prove our main theorem, certain results about the trigonometric polynomials of best approximation for functions of two variables are required, and these are available in the literature. Here we just state the results. These results are based on partial modulus of smoothness (Timan [10]).

For functions of two variables the partial modulii of smoothness are defined as follows.

Definition 4.1. (Partial Modulus of Smoothness)

$$\hat{\omega}_k(f;u,0) = \sup_y \sup_{|t|\le u} \left| \sum_{\upsilon=0}^{k} (-1)^{k-\upsilon} \binom{k}{\upsilon} f(x+\upsilon t, y) \right|,$$

$$\hat{\omega}_k(f;0,v) = \sup_x \sup_{|t|\le v} \left| \sum_{\upsilon=0}^{k} (-1)^{k-\upsilon} \binom{k}{\upsilon} f(x, y+\upsilon t) \right|,$$

and for $1 \le p < \infty$,

$$\hat{\omega}_k(f;u,0)_p^p = \sup_{|t|\le u} \int_I \left| \sum_{\upsilon=0}^{k} (-1)^{k-\upsilon} \binom{k}{\upsilon} f(x_1+\upsilon t, x_2) \right|^p dx,$$

$$\hat{\omega}_k(f;0,v)_p^p = \sup_{|t|\le v} \int_I \left| \sum_{\upsilon=0}^{k} (-1)^{k-\upsilon} \binom{k}{\upsilon} f(x_1+\upsilon t, x_2) \right|^p dx.$$

Definition 4.2. (Total Modulus of Smoothness)

$$\hat{\omega}_k(f;u,v) = \sup_{|h_1|<u} \sup_{|h_2|\le v} \left| \sum_{\upsilon=0}^{k} (-1)^{k-\upsilon} \binom{k}{\upsilon} f(x_1+\upsilon h_1, x_2+\upsilon h_2) \right|,$$

$$\hat{\omega}_k(f;u,v)_p^p = \sup_{|h_1|<u} \sup_{|h_2|\le v} \int_I \left| \sum_{\upsilon=0}^{k} (-1)^{k-\upsilon} \binom{k}{\upsilon} f(x_1+\upsilon h_1, x_2+\upsilon h_2) \right| dx, \ (1 \le p < \infty).$$

Definition 4.3. (Mixed Modulus of Smoothness)

$$\hat{\omega}_{k,l}(f;u,v) = \sup_{|h_1|<u}\sup_{|h_2|\le v}\left|\Delta^k_{h_1}\Delta^l_{h_2} f(x_1,x_2)\right|$$

$$= \sup_{|h_1|<u}\sup_{|h_2|\le v}\left|\sum_{\upsilon=0}^{k}\sum_{\mu=0}^{l}(-1)^{k+l-\upsilon-\mu}\binom{k}{\upsilon}\binom{l}{\mu} f(x_1+\upsilon h_1, x_2+\upsilon h_2)\right|$$

and, for $1 \le p < \infty$,

$$\hat{\omega}_{k,l}(f;u,v)_p^p = \sup_{|h_1|<u}\sup_{|h_2|\le v}\int_I\left|\sum_{\upsilon=0}^{k}\sum_{\mu=0}^{l}(-1)^{k+l-\upsilon-\mu}\binom{k}{\upsilon}\binom{l}{\mu} f(x_1+\upsilon h_1, x_2+\upsilon h_2)\right| dx .$$

The relation between moduli of smoothness is as follows (Timan [10]).

$$\max\{\hat{\omega}_k(f;u,0), \hat{\omega}_k(f;0,v)\} \le \hat{\omega}_k(f;u,v) \le \sum_{\upsilon=0}^{k}\binom{k}{\upsilon}\hat{\omega}_{k-\upsilon,\upsilon}(f;u,v) . \tag{4.1}$$

For the case when u = v = t, we have $\hat{\omega}_k(f;u,v)=\omega_k(f;t)$, where $\omega_k(f;t)$ for functions of two variable is defined by equations (1.1) and (1.2). Let $E_n^*(f)_p = \|f - T_n\|_p$ where the function f is of two variables, and $T_n(x)$ is the trigonometric polynomial of best approximation, or order n,n in the corresponding variables $x_1$,$x_2$.

**Theorem 4.1:** Consider the function f(x) with $x = (x_1, x_2)'$, defined throughout the whole space of the variables $x_1$ and $x_2$ and having period $2\pi$ in each of these variables. If $1 \le p \le \infty$, and if $f \in L_p(I)$, then for any integers $k_1$, $k_2$, $n \ge 0$, with $k = (k_1, k_2)$ we have

$$E_n^*(f)_p \le C_k \left(\hat{\omega}_{k_1}(f,1/(n+1),0)_p + \hat{\omega}_{k_2}(f,0,1/(n+1))_p\right),$$

where $C_k$ is a constant depending only on k, and $\omega_k(f; t_1,t_2)_p$ is the corresponding integral partial modulus of smoothness.

From the above theorem and (4.1) it is clear that, for $1 \le p \le \infty$,

$$E_n^*(f)_p \le C_k\, \omega_k(f,t)_p , \tag{4.2}$$

where $t = 1/(n+1)$ and $k = k_1 = k_2$. The $\omega_k(f ; t)$ in the right hand side of (4.2) is the modulus of smoothness for functions of two variables, as defined in (1.1). Next we state a theorem which relates approximation by partial sums of Fourier series and the best approximation in case of $1 < q < \infty$.

**Theorem 4.2:** If $1 < q < \infty$ and if the function f(x), $x = (x_1, x_2)$, periodic in both the variables of period $2\pi$ belongs to $L_q$ on I, then for any $n \geq 0$,

$$\left\{ \int_I \left| f(x) - S_n^*(f;x) \right|^q dx \right\}^{1/q} \leq C_q \, E_n^*(f)_q ,$$

where $C_q$ is a constant depending only on q and $S_n^*(f;x)$ is the partial sum of order n,n of the Fourier Series of $f(x_1,x_2)$.

Proof: Let $T_n(x)$ be the trigonometric polynomial of best approximation, of order (n, n) in the corresponding variables $(x_1, x_2)$. Using that $S_n^*$ are uniformly bounded operators on $L_q(I)$ for $1 < q < \infty$, for a constant $C_q$ depending only on q, we have,

$$\| f - S_n^*(f) \|_q = \| f - T_n + T_n - S_n^*(f) \|_q \leq \left(1 + \| S_n^* \|_q\right) \| f - T_n \|_q \leq C_q E_n^*(f)_q .$$

Next we state a converse theorem for best approximations by trigonometric polynomials.

**Theorem 4.3:** If for a certain q ($1 \leq q \leq \infty$) the function f(x) belongs to the class $L_q$ over the square I, and $E_{n_1,n_2}^*(f)$ ($n_1$, $n_2$ = 0, 1, 2 ……) is the sequence of best approximation by trigonometric polynomials $T_{n_1 n_2}(x)$, of order $n_1,n_2$ in the corresponding variables $x_1$ and $x_2$, then whatever the integers $k_1,k_2$ may be, the inequality

$$\hat{\omega}_{k_1,k_2}\left(f, 1/n, 1/n\right)_q \leq \frac{C_{k_1,k_2}}{n^{k_1+k_2}} \sum_{\upsilon_1=0}^{n} \sum_{\upsilon_2=0}^{n} (\upsilon_1+1)^{k_1-1} (\upsilon_2+1)^{k_2-1} E_{\upsilon_1\upsilon_2}^*(f)_q$$

remains valid, where $C_{k_1,k_2}$ is a constant depending only on $k_1$, $k_2$ and $\hat{\omega}_{k_1,k_2}\left(f, 1/n, 1/n\right)_q$ is the corresponding mixed modulus of smoothness.

**Theorem 4.4:** If $f \in B_q^{\alpha,k}(L_p(I))$ for a certain p ($1 < p < \infty$), q ($1 \leq q < \infty$) and k and $\alpha$ such that $0 < \alpha < k$, then $\left\{E_n(f)_p\right\}_n \in l_q^{\alpha}$, where $E_n(f)_p = \| f - S_n(f) \|_p$ and $S_n(f)$ is the partial sum of order (n, n) in the corresponding variables $(x_1,x_2)$ of the Fourier series for the function f.

Proof: $\sum_{n=1}^{\infty} \left[ n^{\alpha} E_n(f)_p \right]^q \frac{1}{n} \leq C_q \sum_{n=1}^{\infty} \left[ n^{\alpha} E_n^*(f)_p \right]^q (1/n)$ [ by theorem 4.2]

$$\leq C_{q,k} \sum_{n=1}^{\infty} \left[ n^{\alpha} \omega_k \left( f, 1/n \right)_p \right]^q (1/n) \qquad [\text{by } (4.2)]$$

$< \infty$ [by theorem 2.1]

$\Rightarrow \left\{ E_n (f)_p \right\}_n \in l_q^{\alpha}$. Hence the proof.

For the case p = 1, ∞, we make use of Steklov approximations.

Definition 4.4. ($W^{m,p}(I)$ Space): Let $1 \leq p \leq \infty$, $W^{m,p}(I)$ is space of all functions for which $||f||_{m,p} < \infty$, where the norm is given by,

$$\| f \|_{m,p} = \| f \|_{L_p(I)} + \| f^{(m)} \|_{L_p(I)} .$$

**Steklov Approximations**

The m-th Steklov approximations $\{f_{\eta,m}\}$, ($\eta > 0$, m = 1,2…) is defined as

$$f_{\eta,m}(x) = \left( \frac{\eta}{m} \right)^{-m} \int_0^{\frac{\eta}{m}} \cdots \int_0^{\frac{\eta}{m}} \left\{ f(x) - (-1)^m \Delta^m_{\sum_{i=1}^{m} \eta_i} f(x) \right\} d\eta_i \cdots d\eta_m .$$

For $1 \leq p \leq \infty$, for every $f \in L_p(I)$, $\{f_{\eta,m}\} \in W^{m,p}(I)$ and we have the following:

**Theorem 4.5:** For every $f \in L_p(I)$ $1 \leq p \leq \infty$ and $\eta > 0$,

$$\left\| f - f_{\eta,m} \right\|_p \leq \omega_m (f, \eta)_p .$$

Proof: $f_{\eta,m}(x) - f(x) = \left( \frac{\eta}{m} \right)^{-m} \int_0^{\frac{\eta}{m}} \cdots \int_0^{\frac{\eta}{m}} \left\{ (-1)^{m+1} \Delta^m_{\sum_{i=1}^{m} \eta_i} f(x) \right\} d\eta_i \cdots d\eta_m .$

Using Generalized Minkowski's inequality we have,

$$\left\| f_{\eta,m} - f \right\|_p \leq \left( \frac{\eta}{m} \right)^{-m} \left( \frac{\eta}{m} \right)^{m} \left\| \Delta^m_{\sum_{i=1}^{m} \eta_i} f(x) \right\|_p$$

$$\leq \sup_{|h|<\eta} \left\| \Delta_h^m f(x) \right\|_p$$

$$= \omega_m(f,\eta)_p \ .$$

**Theorem 4.6:** If $f \in B_q^{\alpha,k}(L_p(I))$ for a certain p ($1 \leq p \leq \infty$), q ($1 \leq q < \infty$) and for any k and $\alpha$ such that $0 < \alpha < k$, then $\left\{ e_n(f)_p \right\}_n \in l_q^\alpha$, where $e_n(f)_p = \| f - f_n \|_p$ and $f_n$'s correspond to $f_{\eta,k}$, the k-th Steklov approximation of the function f, for $\eta = k/n$.

Proof: The proof of theorem 4.6 is similar to that of theorem 4.4 and uses theorem 4.5.

An inverse theorem for the best approximation by trigonometric polynomials is obtained next:

**Theorem 4.7:** If $f \in L_p(I)$, $1 \leq p \leq \infty$, and $\left\{ E_n^*(f)_p \right\}_n \in l_q^\alpha$, where $E_n^*(f)_p = \left\| f - T_n \right\|_p$ where $T_n(x)$ with $x = (x_1, x_2)'$ is the trigonometric polynomial best approximation of f of order (n, n) in the variables $(x_1, x_2)$, then for all k and $\alpha$ such that $0 < \alpha < k$, $f \in B_q^{\alpha,k}(L_p(I))$.

Proof: By theorem 2.1, the result would follow if $\sum_{n=1}^{\infty} \left[ n^\alpha \omega_k(f, 1/n)_p \right]^q (1/n) < \infty$.

Consider, $\hat{\omega}_k$ and $\hat{\omega}_{k,\upsilon}$ the total and mixed modulus of smoothness respectively (cf: definitions 4.2 and 4.3). For n > 0, we have,

$$\omega_k\left(f; \frac{1}{n}\right) = \hat{\omega}_k(f; 1/n, 1/n) \leq \sum_{\upsilon=0}^{k} \binom{k}{\upsilon} \hat{\omega}_{k-\upsilon,\upsilon}(f; 1/n, 1/n)$$

$$\leq \sum_{\upsilon=0}^{k} \binom{k}{\upsilon} \frac{C_k}{n^k} \sum_{\upsilon_1=0}^{n} \sum_{\upsilon_2=0}^{n} (\upsilon_1+1)^{k-\upsilon-1} (\upsilon_2+1)^{\upsilon-1} E^*_{\upsilon_1\upsilon_2}(f)$$

[by theorem 4.3]

$$\leq \sum_{\upsilon=0}^{k} \binom{k}{\upsilon} (C_k / n^k) \sum_{\upsilon_1=0}^{n} \sum_{\upsilon_2=0}^{n} n^{k-2} E^*_{\upsilon_1\upsilon_2}(f)$$

$$\leq 2^k k (C_k / n^k) \sum_{\upsilon_1=0}^{n} \sum_{\upsilon_2=0}^{n} n^{k-2} E^*_{\upsilon_1\upsilon_2}(f) \ ,$$

where $E^*_{\upsilon_1\upsilon_2}(f)$ is the best approximation of orders $\upsilon_1, \upsilon_2$ in variables $x_1, x_2$ of f(x).

Therefore, we have

$$\sum_{n=1}^{\infty}\left[n^{\alpha}\omega_k(f,1/n)_p\right]^q(1/n) \le \sum_{n=1}^{\infty}[n^{\alpha}(C_k/n^k)\sum_{\upsilon_1=1}^{n}\sum_{\upsilon_2=1}^{n}n^{k-2}E^*_{\upsilon_1\upsilon_2}(f)_p]^q(1/n)$$

$$\le C_k\sum_{n=1}^{\infty}n^{\alpha q-kq-1}S_n^q\,,\ [S_n=\sum_{i=1}^{n}\sum_{j=1}^{n}a_{ij}\,,\ a_{ij}=n^{k-2}E^*_{ij}(f)_p]$$

$$\le C_k\sum_{n=1}^{\infty}n^{-(1+(k-\alpha)q)}S_n^q$$

$[(1 + (k-\alpha)q ) > 1 \because q > 0 \text{ and } 0 < \alpha < k]$

Applying the corollary of lemma 3.1 we get,

$$\sum_{n=1}^{\infty}\left[n^{\alpha}\omega_k(f,1/n)_p\right]^q(1/n) \le C_{q,k}\sum_{n=1}^{\infty}n^{-(1+(k-\alpha)q)}(n^2a_{nn})^q$$

$$\le C_{q,k}\sum_{n=1}^{\infty}\left[n^{\alpha}E^*_n(f)_p\right]^q n^{-1}n^{-kq}n^{kq}$$

$$\le C_{q,k}\sum_{n=1}^{\infty}\left[n^{\alpha}E^*_n(f)_p\right]^q\frac{1}{n}<\infty\,,\quad \text{[by hypothesis].}$$

Here the constant $C_{q,k}$ depends only on q and k and is independent of the function f. $\Rightarrow f \in B_q^{\alpha,k}(L_p(I))$ and hence the proof.

In the next section we propose a compression algorithm for MR images and obtain storage bounds for the same.

## 5. COMPRESSION ALGORITHM AND STORAGE BOUNDS

Let the given MRI image be

$$f(x,y) = \sum_{j,k}c_{j,k}e^{i(jx+ky)}. \tag{5.1}$$

We apply an invertible transformation on the Fourier coefficient's to get a new function $\tilde{f}$. This transformation could be based on a known convolving function or otherwise, so that

(5.2) $$\tilde{f}(x,y) = \sum_{j,k} \tilde{c}_{j,k} e^{i(jx+ky)},$$

with $|\tilde{c}_{j,k}| \le |c_{j,k}|$ holding. The next step in the compression algorithm is to modify $\tilde{c}_{j,k}$'s to $c^*_{j,k}$'s such that only non zero $c^*_{j,k}$'s are to be retained. Normally the zero coefficients occur in clusters so that the storage indexing is a minimal.The Compression Ratio (C.R) is given by

(5.3) $$C.R = \frac{\text{Uncompressed image size} - \text{Compressed image size}}{\text{Uncompressed image size}}.$$

A higher compression ratio in the method is obtained indeed because of the number of vanishing $c^*_{j,k}$'s . The compressed image data file contains a header. Patient information and certain parameters are stored in the header. We store the zero frequency term in the header and all other frequency terms are stored by using the following algorithm consisting of four steps.

**Algorithm 5.1 :**

**Step 1 :** Calculate $c_{j,k}$'s from the pixel data $p_{j,k}$'s using FFT.

**Step 2 :** Calculat $\tilde{c}_{j,k}$'s from $c_{j,k}$'s for the chosen convolving function.

**Step 3 :** Choose a positive integer **N** and numbers $1 < p < \infty$, $\alpha > 0$. Choose q such that $\alpha q > 2$ and quantized coefficients $c^*_{j,k}$ that satisfy

(i) $|\tilde{c}_{j,k} - c^*_{j,k}|^q \le \frac{1}{N}$,

(ii) $|\tilde{c}_{j,k}| \le |c_{j,k}|$, and,

(iii) $\tilde{c}_{j,k} = 0$ if $|\tilde{c}_{j,k}| \le \frac{1}{N}$.

**Step 4 :** Store non zero $c^*_{j,k}$'s using a variable length coding procedure (cf: 1.2).

Now we give a bound on storage space required for the above algorithm, here the $\tilde{c}_{j,k}$'s are the Fourier coefficients of the pixel data and $\tilde{f}$ is the approximation of f by partial sums of Fourier series. With $n = (n_1, n_2)'$, we define

$$\hat{f}_s^m(|n|) = \max\left\{ \left|\hat{f}(n_1,n_2)\right| \quad \ni \ |n_1| + |n_2| = n \right\}.$$

From the definition it is clear that,

$$\sum_{n_1\in Z}\sum_{n_2\in Z}\left|\hat{f}(n_1,n_2)\right| \le \sum_{|n|=1}^{\infty} 4|n|\,\hat{f}_s^m(|n|) + \hat{f}_s^m(0), \tag{5.4}$$

where $\hat{f}_s^m(0)$ is the maximum of the set containing one element, $\hat{f}(0)$. It is stored in the header. We do not include the zero frequency information, in our compression estimates. A small storage space is usually reserved for the header information. By lemma 3.2, we have,

$$\left|\hat{f}_s^m(|n|)\right| \le C_k\,\omega_k(f;1/|n|) \ . \tag{5.5}$$

The above relation is used in obtaining storage bounds for the algorithm 5.1

**Theorem 5.1** (Storage bound)**:** If $f \in B_q^{\alpha,k}(L_p(I))$, $1 < p < \infty$, $0 < q \le \infty$, $0 < \alpha < k$ and $\alpha q > 2$, the number $\eta$ of non-zero coefficients $c_{j,k}^*$'s in algorithm 5.1, satisfies: $\eta \le C_k N |f|^q_{B_q^{\alpha,k}(L_p(I))}$, where $|f|_{B_q^{\alpha,k}(L_p(I))} = \left(\int_0^{2\pi}[t^{-\alpha}\omega_k(f,t)_p]^q t^{-1}dt\right)^{1/q}$.

Proof: Let N be the quantization parameter in the algorithm 5.1 and $\eta$ is the number of non-zero coefficients. Let the zero frequency information $\hat{f}(0)$, be stored in the header as per our compression procedure. We have

$$\frac{\eta}{N} \le \sum_{c_{j,k}^*\neq 0}\left|c_{j,k}^*\right|^q \le \sum_{j,k}\left|c_{j,k}\right|^q \le \sum_{n_1\in Z}\sum_{n_2\in Z}\left|\hat{f}(n_1,n_2)\right|^q$$

$$[\because \left|c_{j,k}^*\right| \le \left|c_{j,k}\right|, \text{ by algorithm } 5.1,\ c_{j,k} = \hat{f}(j,k)\,]$$

$$\le \sum_{|n|=1}^{\infty} 4|n|\,|\hat{f}_s^m(|n|)|^q \quad [\text{by (5.4). For } |n| = 0, \text{storage is in the header}]$$

$$\le C\sum_{|n|=1}^{\infty} 4|n|\,[\omega_k(f;1/|n|)]^q \qquad [\text{by (5.5)}]$$

$$\le C\sum_{|n|=1}^{\infty} |n|^{\alpha q-1}\,[\omega_k(f;1/|n|)]^q \quad [\because \alpha q > 2 \Rightarrow \alpha q - 1 > 1]$$

$$\le C\sum_{|n|=1}^{\infty}[|n|^{\alpha}\ \omega_k(f;1/|n|)]^q\,(1/|n| \le C\,|f|^q_{B_q^{\alpha,k}(L_p(I))}$$

$$\Rightarrow \qquad \eta \le C_k N \left|f\right|^q_{B_q^{\alpha,k}(L_p(I))}.$$

**Poisson Approximation Process**

Poisson's approximation (see Zygmund [11]) for the image is achieved by multiplying the Fourier coefficients $\hat{f}(m,n)$ by $r^{|m|+|n|}$, (0 < r < 1). This convolution induces smoothness in the image. The lower the value of r the higher the smoothness. The value of r is taken to be near 1 to avoid blurring. Algorithm 5.1 is applied for image compression with coefficients $\tilde{c}_{j,k}$ as the Poisson coefficients, i.e. $\tilde{c}_{m,n} = \hat{f}(m,n)\, r^{|m|+|n|}$ with the image represented as

(5.6) $$\tilde{f}(x,y) = \sum_{j,k} \tilde{c}_{j,k}\, e^{i(jx+ky)}.$$

Now the quantized coefficients $c^*_{j,k}$ 's are chosen as per algorithm 5.1

$$\left|\tilde{c}_{j,k} - c^*_{j,k}\right|^q \le N^{-1},\ |\, r^{|j|+|k|}\tilde{c}_{j,k}\,|^q = \left|c^*_{j,k}\right|^q \le N^{-1} \Rightarrow c^*_{j,k} = 0.$$

The compressed image is represented as,

(5.7) $$f^*(x,y) = \sum_{j,k} c^*_{j,k}\, e^{i(jx+ky)}.$$

**Theorem 5.2 (Storage bound for Poisson approximation process):** If $\tilde{f} \in B_q^{\alpha,k}(L_p(I))$ for $1 < p < \infty$, $0 < q \le \infty$, $0 < \alpha < k$, $0 < r < 1$, and $\alpha q > 2$, then $\eta$ the number of non zero coefficients $c^*_{j,k}$'s in the above algorithm satisfies

$$\eta \le C_k N r^q \left|\tilde{f}\right|^q_{B_q^{\alpha,k}(L_p(I))}, \text{ where } \left|\tilde{f}\right|_{B_q^{\alpha,k}(L_p(I))} = \left(\int_0^{2\pi}\left[t^{-\alpha}\omega_k(\tilde{f},t)_p\right]^q t^{-1}dt\right)^{1/q}.$$

Proof: Let N be the quantization parameter as in the algorithm 5.1 and $\eta$ the number of non zero coefficients. We have

$$\frac{\eta}{N} \le \sum_{c^*_{j,k} \ne 0} \left|c^*_{j,k}\right|^q \le \sum_{j,k} \left|c_{j,k}\right|^q \sum_{n_1 \in Z} \sum_{n_2 \in Z} \left|r^{|n|}\hat{f}(n_1,n_2)\right|^q \quad \text{[by algorithm 2.5.4, } \left|c^*_{j,k}\right| \le \left|c_{j,k}\right|,$$

$c_{j,k} = \hat{f}(j,k)$ & $\hat{f}(0,0)$ is stored in header]

$$\Rightarrow \eta \leq C_k N r^q \left|f\right|^q_{B_q^{\alpha,k}(L_p(I))}.$$

$$\leq \sum_{|n|=1}^{\infty} 4 |n| r^{|n|} \hat{f}_s^m (|n|)|^q \qquad \text{[By (2.5.3)]}$$

$$\leq C r^q \sum_{|n|=1}^{\infty} 4 |n| \omega_k \left(f; 1/|n|\right)^q \qquad \text{[By (2.5.4) and } 0 < r < 1]$$

$$\leq C_1 r^q \sum_{|n|=1}^{\infty} |n|^{\alpha q-1} \omega_k \left(f; \frac{1}{|n|}\right)^q \qquad [\because \alpha q > 2 \Rightarrow \alpha q - 1 > 1]$$

$$\leq C_1 r^q \sum_{|n|=1}^{\infty} \left[|n|^{\alpha} \omega_k \left(f; \frac{1}{|n|}\right)\right]^q \frac{1}{|n|} \leq C_k r^q \left|f\right|^q_{B_q^{\alpha,k}(L_p(I))}$$

## 6. COMPRESSION OF RAW DATA

The usual MRI image is the magnitude image reconstruction from the complex signal data. However, MRI offers various other reconstructions e.g., real, imaginary and phase images and each gives information of specific significance for medical diagnosis. For example, the phase images (see Stark and Bradley [9]) help determine if a blood vessel is patent or if it is filled with clotted blood instead. The presence of flowing blood is suggested if a blood vessel in a phase image has a pattern of stripes distinct from tissues that are known to be stationary. They also provide information about the flow of Cerebro Spinal Fluid (CSF) (See Partain et al. [6]). Real images are advantageous for certain techniques notably inversion recovery (See Partain et al. [7]). The information present in real, imaginary and phase images thus complement the MR signals present in the modulus images. One can reconstruct all these from the raw data.

The raw data contains frequency information, with the magnitude decaying as the frequency increases. The maximum magnitude of the raw data in the exterior of concentric circles about zero frequency decays (see Graph (6.1), for a typical MRI). The decay is faster if the image under investigation is more smooth. This decay property gives rise to compression of raw data. In Graph 6.1 Frequency circles in the x-axis refers to the radius of the concentric circles considered with center as the zero frequency term. Instead of storing the raw data in the matrix form, they can be stored in concentric circles and a variable length coding based on the a priori information obtained from graph 6.1 can be used so that the preceding zero entries corresponding to each circle need not be stored.

## 7. EXPERIMENTAL RESULTS

Algorithm 5.1 has been implemented on the test image set 1 consisting of 256x256 magnitude reconstructions of four different cross sections. The required Fourier coefficients are computed using FFT routines, due to Cooley and Tuckey (see Brigham, [1]). Images after certain compression and decompression of test images are shown in Images 7.1-7.3. Performances of algorithm 5.1 are plotted in Graphs 7.1-7.4. Computation of tissue parameters using a certain test image set is done following the method proposed in Rao et al. [8]. First the computations of the tissue parameters are done on the uncompressed images and they are compared with the parameter images computed from compressed images at various levels of compression. Along with the computed images (Images 7.4-7.7), maps of points where the computations are not carried out are given. The effect of compression in tissue parameter computations is listed in Table 7.1. The test images used in these experiments are normalized to take two bytes per pixel. To estimate the amount of distortion induced because of compression and decompression, we use two kinds of error measures, they are defined as follows. The amount of compression obtained is measured, by percentage compression (P.C) given by

Percentage Compression (P.C) = Compression Ratio (C.R) X 100.

The following quantities are used for measuring the error in decompression,

$$\text{Relative } l_1 \text{ Error } (rl_1) = \frac{\sum_{\text{all pixels}} | f(i) - \tilde{f}(i) |}{\sum_{\text{all pixels}} | f(i) |},$$

$$\text{Relative } l_2 \text{ Error } (rl_2) = \frac{\left( \sum_{\text{all pixels}} | f(i) - \tilde{f}(i) |^2 \right)^{\frac{1}{2}}}{\left( \sum_{\text{all pixels}} | f(i) |^2 \right)^{\frac{1}{2}}},$$

$$\text{Average } l_1 \text{ Error } (al_1) = \frac{\sum_{\text{all pixels}} | f(i) - \tilde{f}(i) |}{\text{Total no. of pixels}},$$

$$\text{Average } l_2 \text{ Error } (al_2) = \frac{\left( \sum_{\text{all pixels}} | f(i) - \tilde{f}(i) |^2 \right)^{\frac{1}{2}}}{\text{Total no. of pixels}}.$$

In the above expressions f is the uncompressed image and $\tilde{f}$ is the decompressed image. For the compression of $T_1$, $T_2$ and spin density weighted images, we store them in a set of three images corresponding to one cross section. The total size of the set is used for calculating the percentage compression.

The decompressed images at 55,60 and 65% compression levels are shown in Images 7.1-7.3. The graphs of Percentage compression vs relative error are presented in Graphs 7.1-7.4. From the images and graphs we observe that there is no visual deterioration of images up to 60% compression. After that the image architechture deteriorates slightly. Apart from test images performance of algorithm 5.1 has been tested on images corresponding to several other cross sections and the results obtained are similar. Upto 60% compression is suggested for the images under consideration.

In some specific cases of diagnosis, computed $T_1$,$T_2$ and density images are used. Three images from a certain test image set which corresponded to the same cross-sections from which these parameters can be calulated in retrospect were compressed and stored as a set. Images 7.4-7.7 and the corresponding error table shows that upto 57% compression the $l_1$-relative error after decompression is less than 5%. At around 67% compression we note from Table 7.1 that the relative $l_1$-error goes upto 15%.

Images 7.8-7.9 are reconstructed using compressed raw data. Reconstructed images with compressed raw data are compared with the ones obtained reconstructed from raw data without compression. From the following images and the error graph (Graph 7.5) we note that the distortion is not perceivable by human eye up to 65% compression. Above that level, slight deterioration is observed. The test raw data permits 65% compression through algorithm 5.1 without a visual loss of information.

## REFERENCES

[1] Brigham, E.O.: *The Fast Fourier Transform*, Englewood Cliffs, NJ: Prentice Hall, 1974.

[2] Butzer, P.L. and Berens, H.: *Semi-Groups of operators and approximation*, Springer-Verlag, New York, 1967.

[3] DeVore, R.A., Jawerth, B. and Lucier, B.: Image compression through wavelet transform coding, *IEEE Trans. Inform. Theory*, vol.38, pp. 719-746, 1992.

[4] DeVore, R.A., Jawerth, B. and Popov, V.A.: Compression of wavelet decompositions, *Amer. J. Math.*, vol.114, pp. 737-785, 1992.

[5] DeVore, R.A. and Popov, V.A.: Interpolation of Besov Spaces, *Trans. Amer. Math. Soc.*, vol.305, pp. 397-414, 1988.

[6] Partain C.L., Price, R.R., Patton, J.A., Kulkarni, M.V. and James, A.E. Jr.: *Magnetic Resonance Imaging*, vol. I, Clinical Principles, W.B.Saunders Company, Harcourt Brace Jovanovich, Inc., Philadelphia, 1988.

[7] Partain C.L., Price, R.R., Patton, J.A., Kulkarni, M.V. and James, A.E. Jr.: *Magnetic Resonance Imaging*, vol. II, Physical Principles and Instrumentation, W.B.Saunders Company, Harcourt Brace Jovanovich, Inc., Philadelphia, 1988.

[8] Rao, S.B., Gupta, R.K., Kaliprasad, V.S.N., Mahesh, Kalyanaraman, R., Reddy, P.V.K., and Rathore, R.K.S.: Tissue Parameters Estimation in MR Imaging, *5th National Symposium on Magnetic Resonance*, IIP Dehradun, India, Feb. 23-26, 1999.

[9] Stark, D.D. and Bradley, W.G.: *Magnetic Resonance Imaging*, Mosby-year Book, St.Louis, Missouri, 1992.

[10] Timan, A.F.: *Theory of approximation of functions of a real variable*, Hindustan Publishing Corporation, Delhi, India, 1966.

[11] Zygmund, A.: *Trigonometric Series*, vol. I, Cambridge University Press, London-New York, 1968.

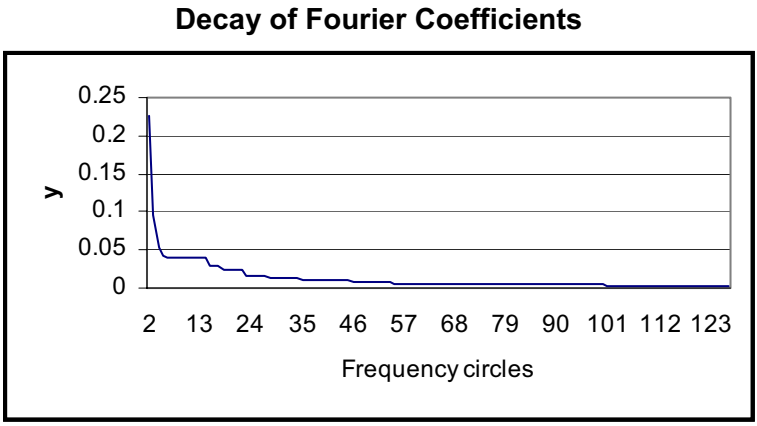


y– Maximum magnitude of the raw data in the exterior of frequency circle.

**Graph 6.1**

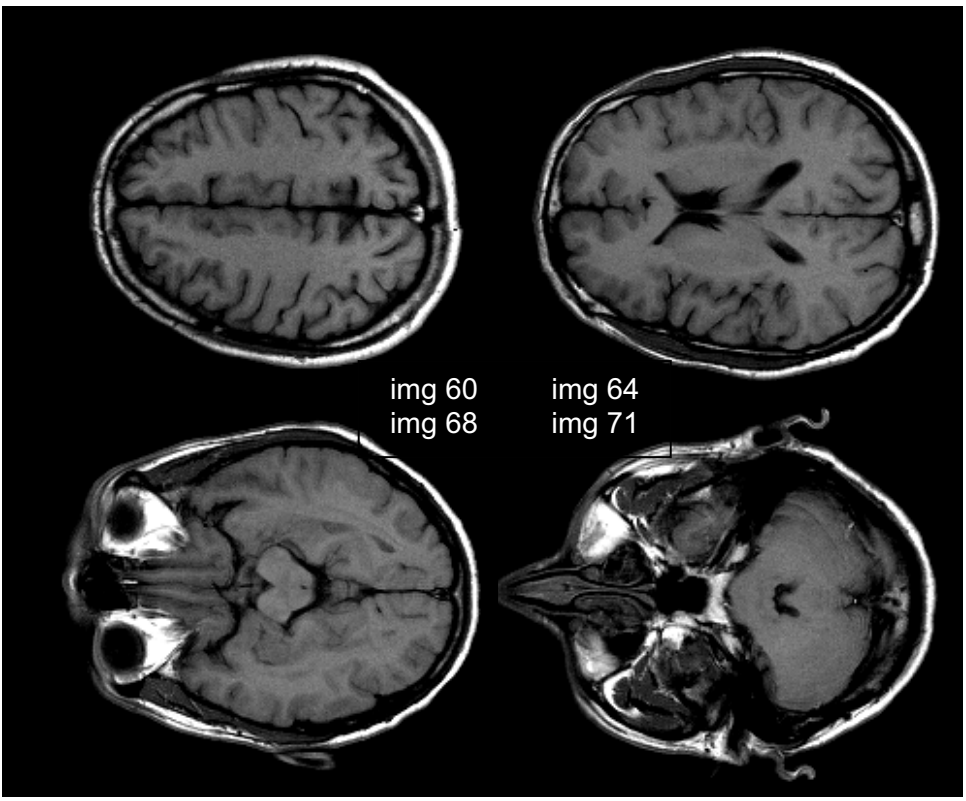


**Image 7.0**

**55 % Compression using Algorithm 5.1**

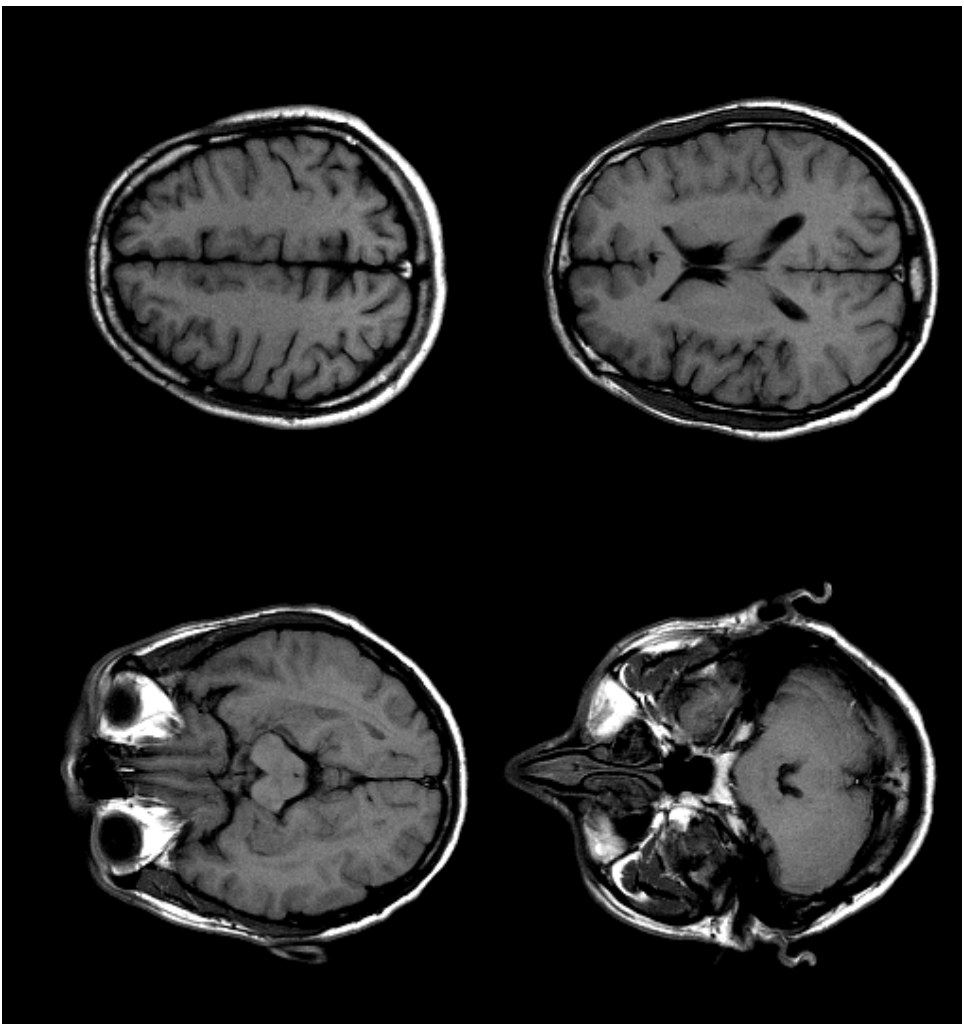

**Image 7.1**

**60 % Compression using Algorithm 5.1**

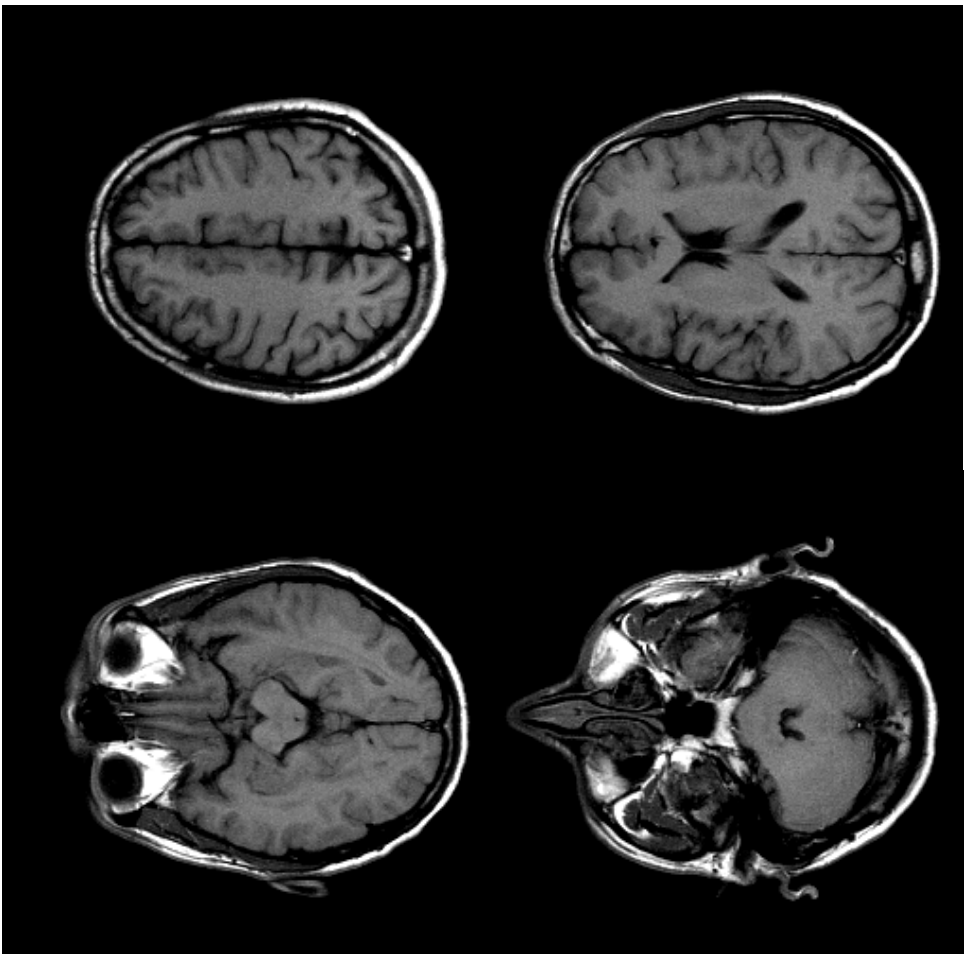

**Image 7.2**

**65 % Compression using Algorithm 5.1**

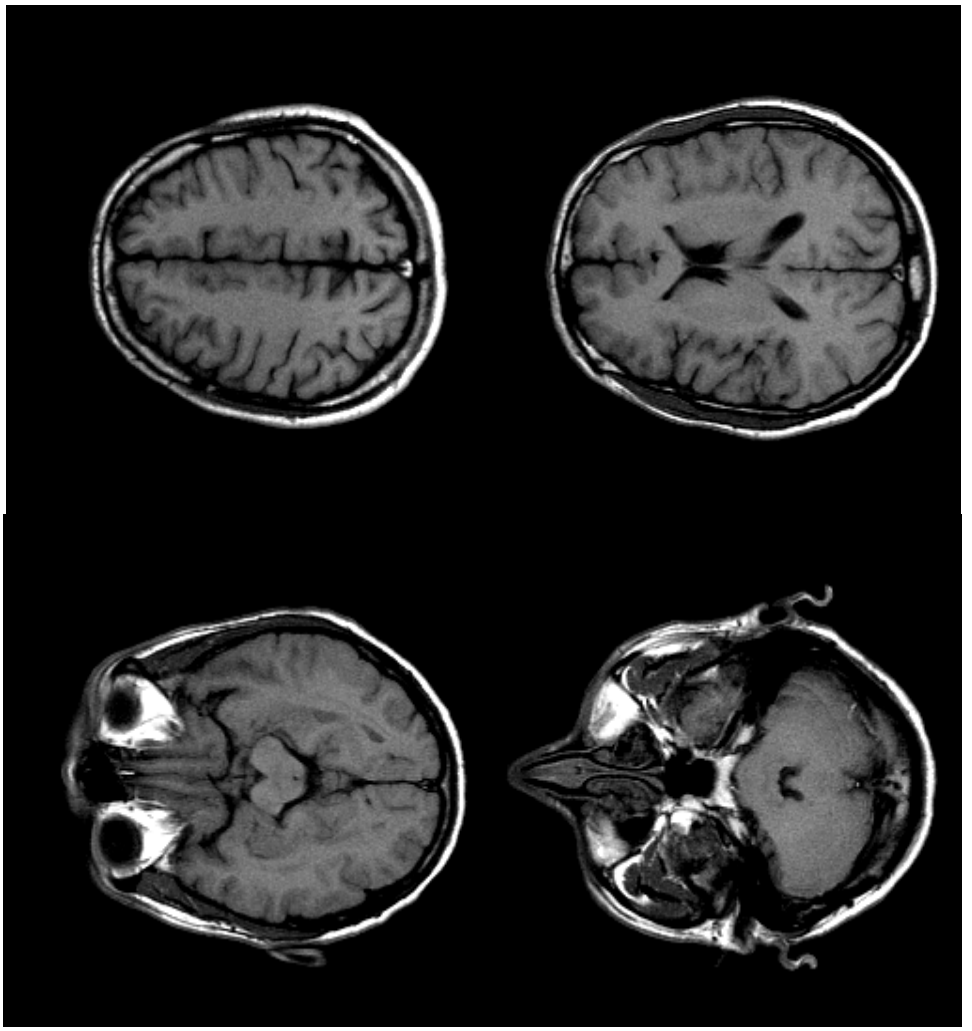

**Image 7.3**

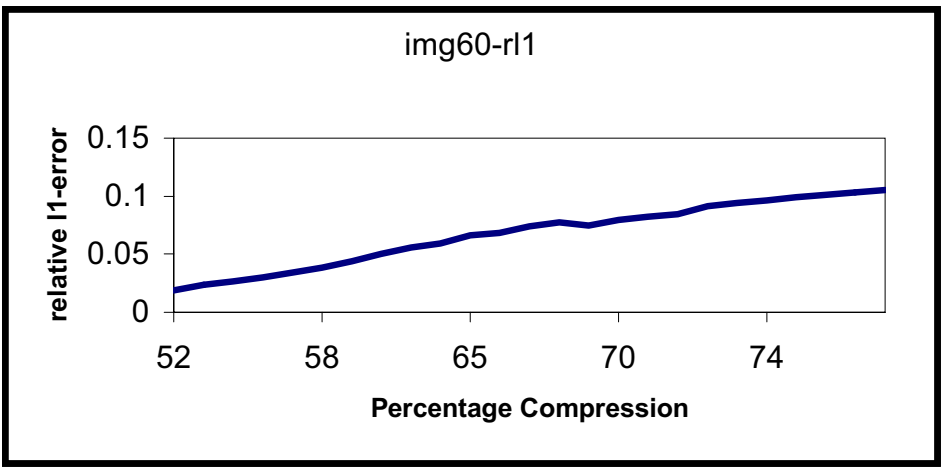


Percentage Compression vs. Relative Error

**Graph 7.1**

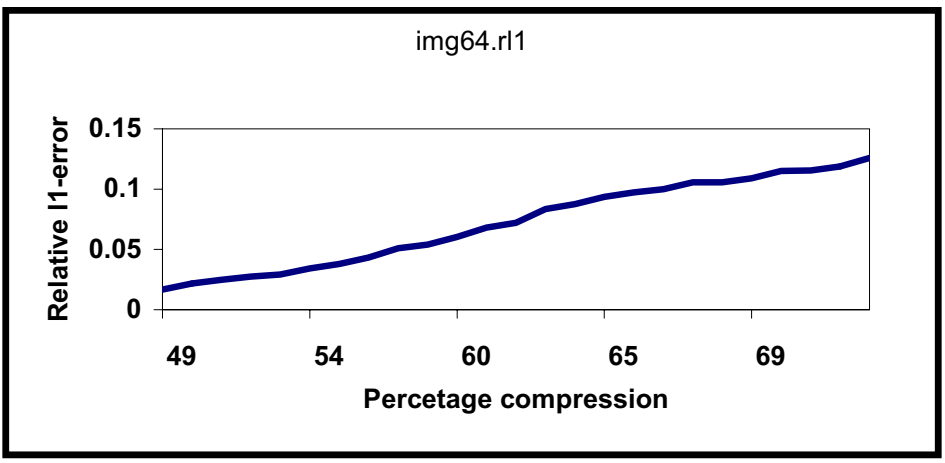


**Graph 7.2**

Percentage Compression vs. Relative Error

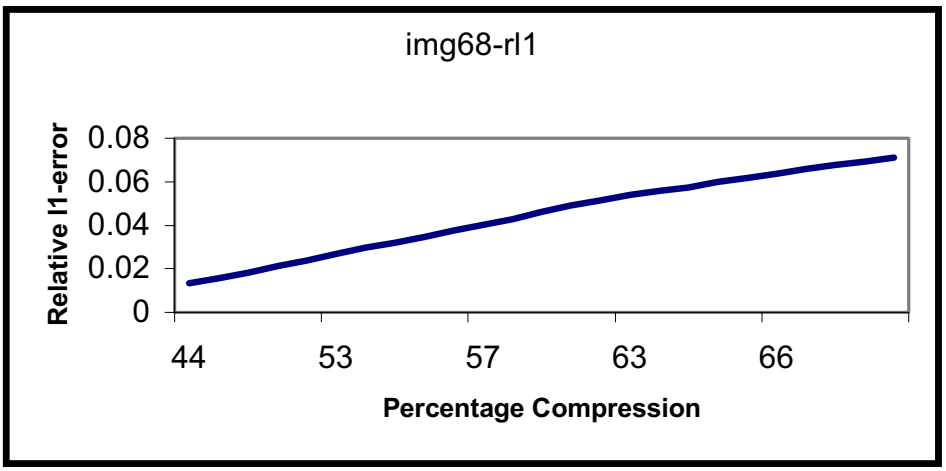


**Graph 7.3**

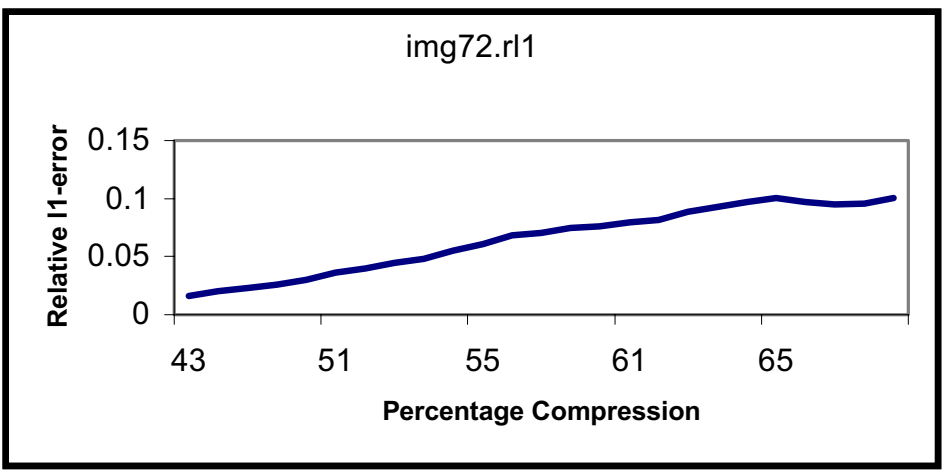


**Graph 7.4**

T1, T2 and Spin Density Computed from Uncompressed Images

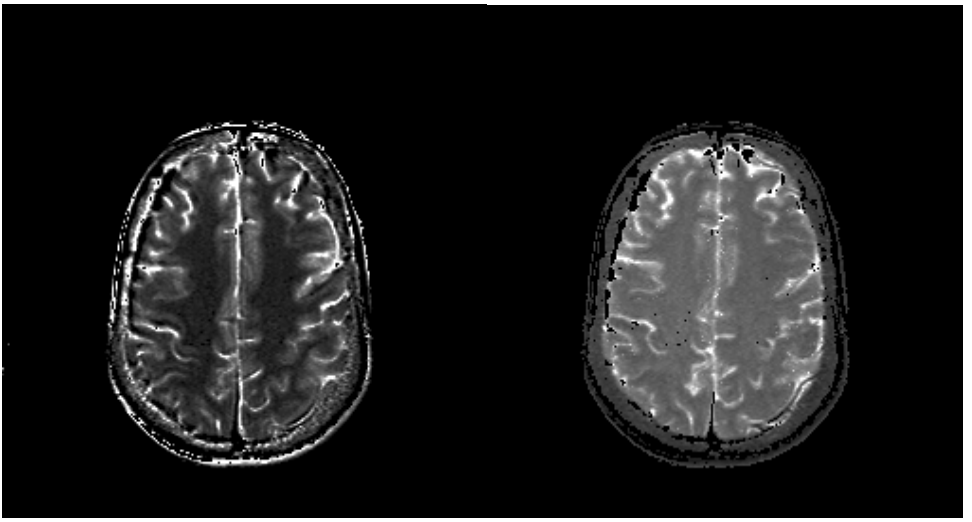

T1 T2

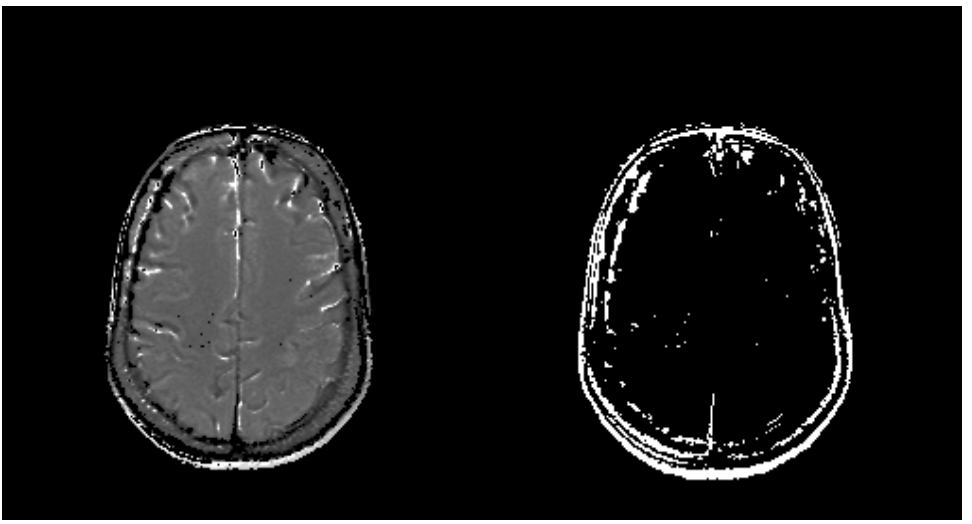

Spin Density Points not Computated

**Image 7.4**

From 47.38 % Compressed Image Set

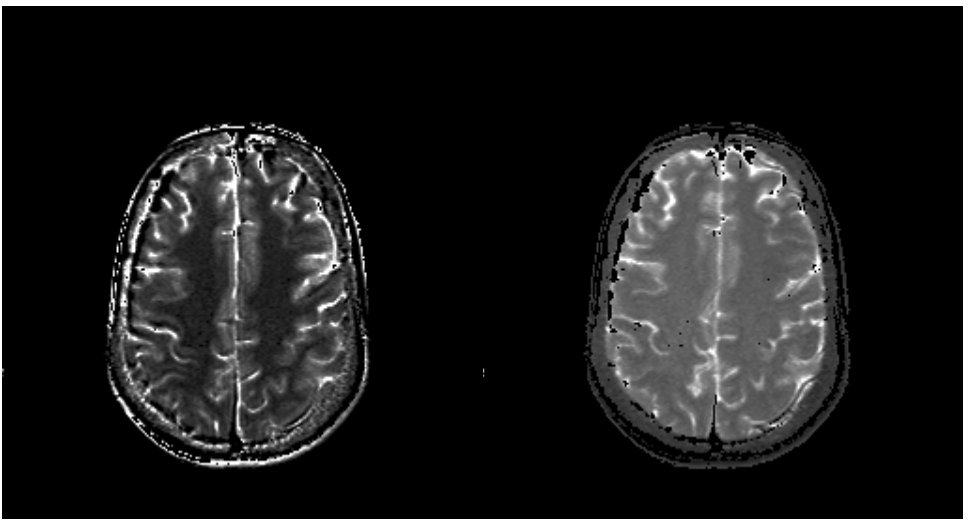

T1 T2

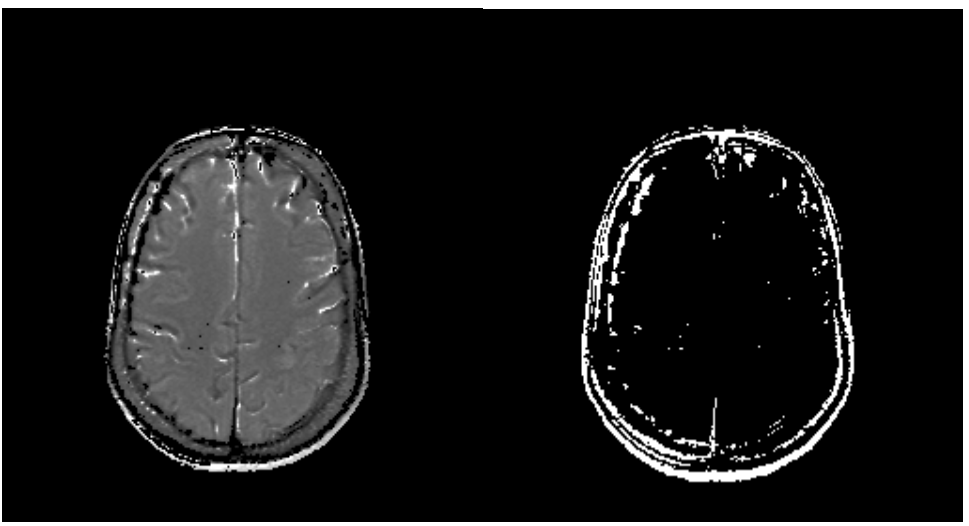

Spin Density Points not Computated

**Image 7.5**

Computed from 57.68 % Compressed Image set

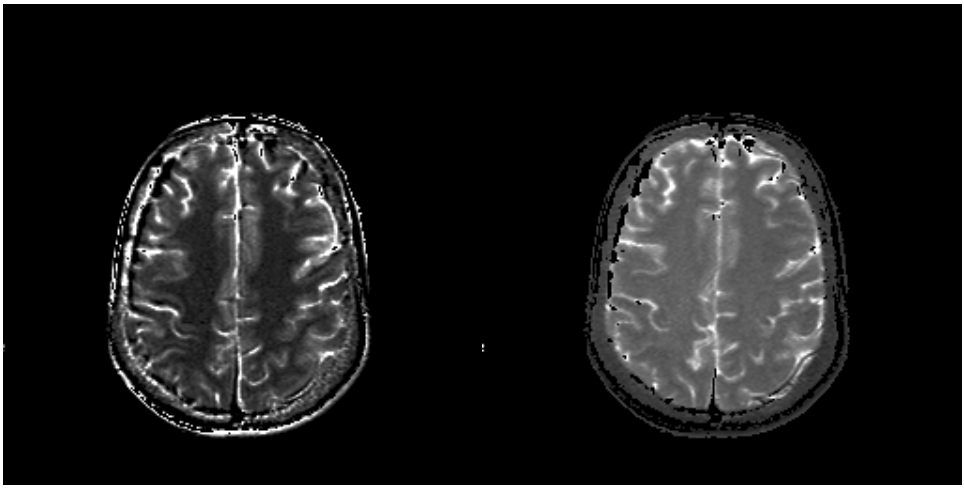

T1 T2

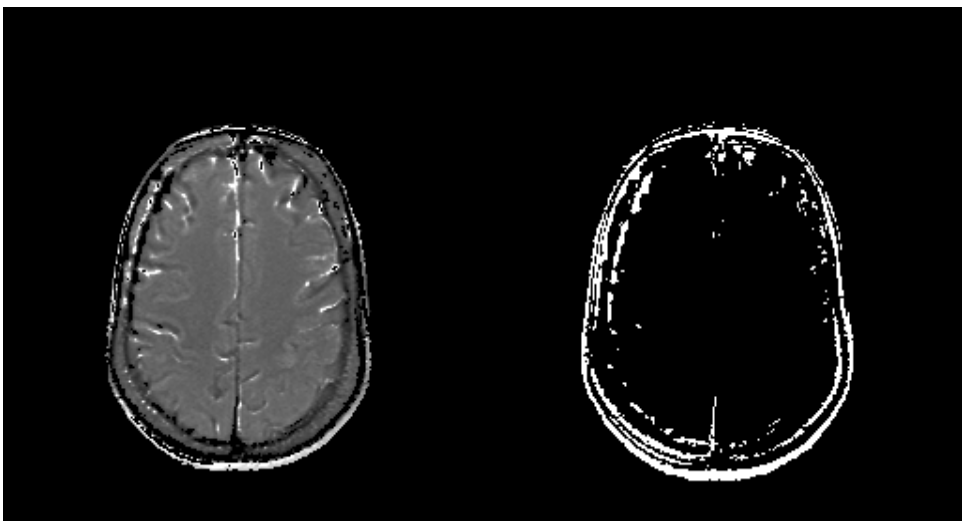

Spin Density Points not Computated

**Image 7.6**

**Computed from 66.75 % Compressed image set**

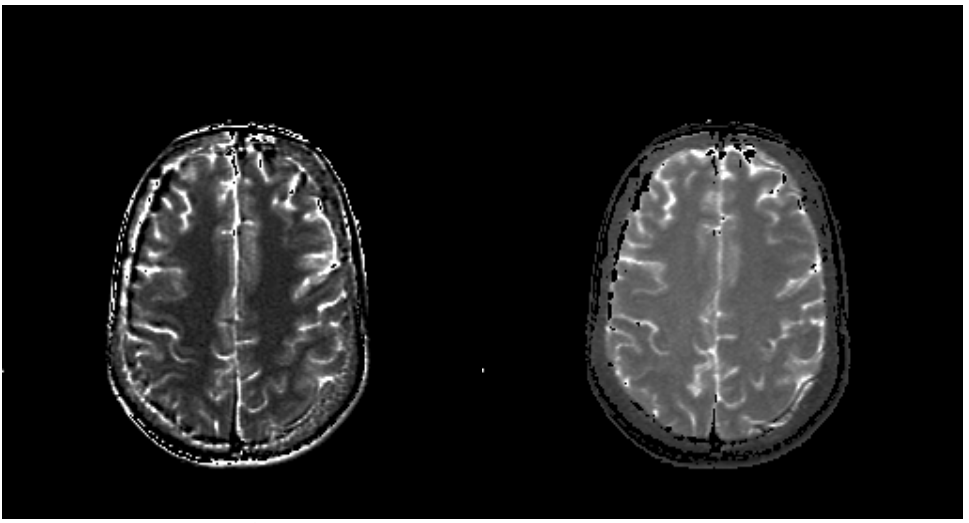

T1 T2

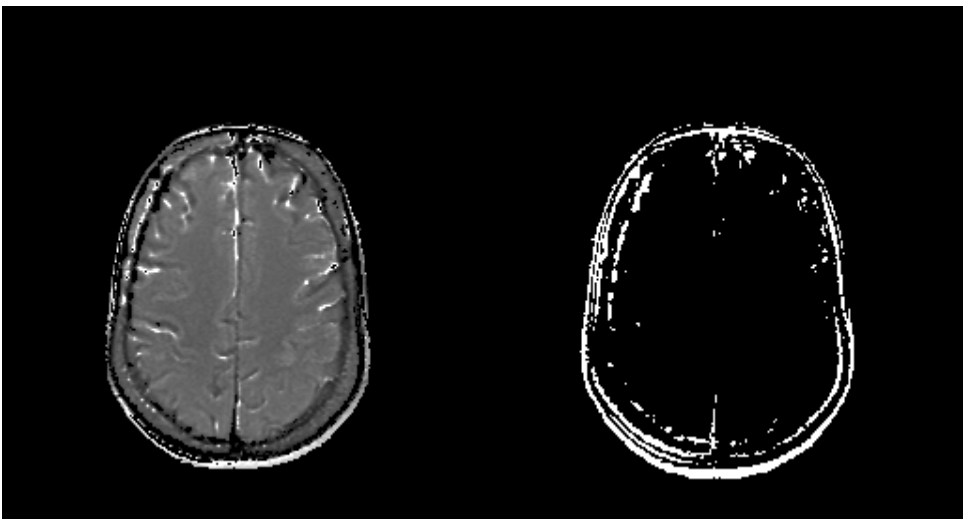

Spin Density Points not Computated

**Image 7.7**

**Compression of Raw Data**

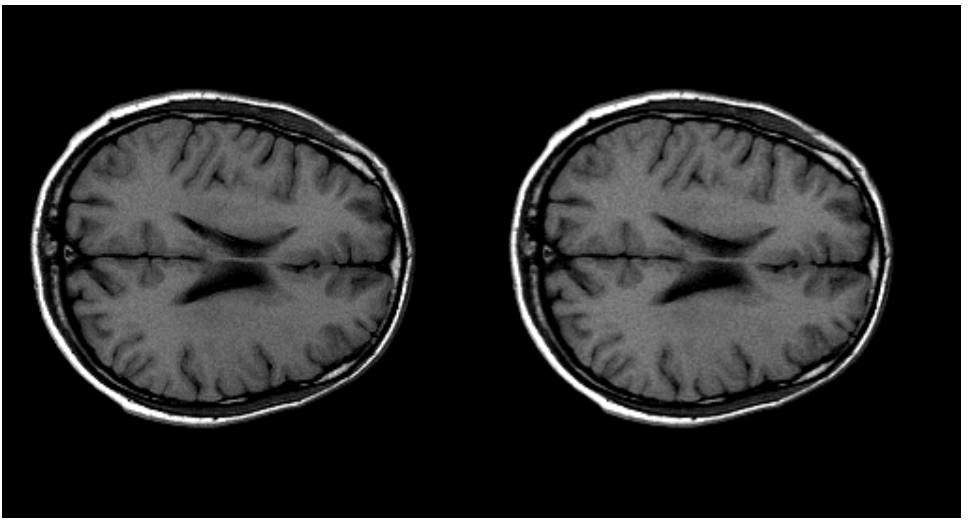

Raw data uncompressed Raw data 65 % compressed

**Image 7.8**

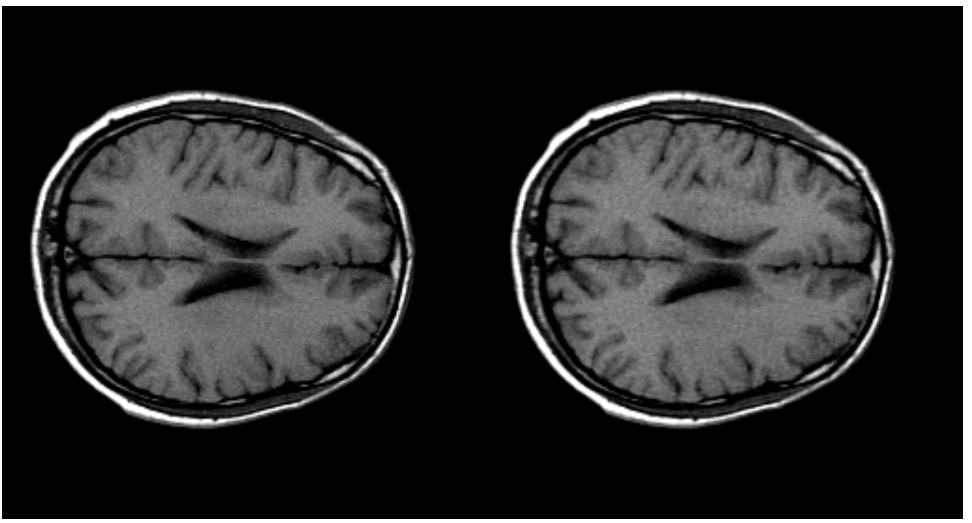

Raw data 70 % compressed Raw data 75 % compressed

**Image 7.9**

## Effect of Compression in the Computation of Tissue Parameters

Relative errors obtained are with respect to the parameters computed from uncompressed images. In the following table, P.C stands for percentage compression, $rl_1$ and $rl_2$ stands for relative $l_1$ error and relative $l_2$ error.

| P.C | T1 | | T2 | | P.D | |
|---|---|---|---|---|---|---|
| | $rl_1$ | $rl_2$ | $rl_1$ | $rl_2$ | $rl_1$ | $rl_2$ |
| 47.38 | 0.023001 | 0.108814 | 0.038972 | 0.082052 | 0.017739 | 0.110434 |
| 57.68 | 0.058826 | 0.153803 | 0.048279 | 0.117673 | 0.037774 | 0.155013 |
| 58.60 | 0.070829 | 0.173674 | 0.048764 | 0.125593 | 0.040470 | 0.173440 |
| 62.41 | 0.121785 | 0.210169 | 0.061526 | 0.153636 | 0.071345 | 0.205007 |
| 66.75 | 0.151067 | 0.259694 | 0.060059 | 0.158104 | 0.080254 | 0.237892 |
| 71.20 | 0.172699 | 0.309278 | 0.066849 | 0.178419 | 0.093853 | 0.269737 |

**Table 7.1**

Percentage Compression vs. Average $l_1$-Error

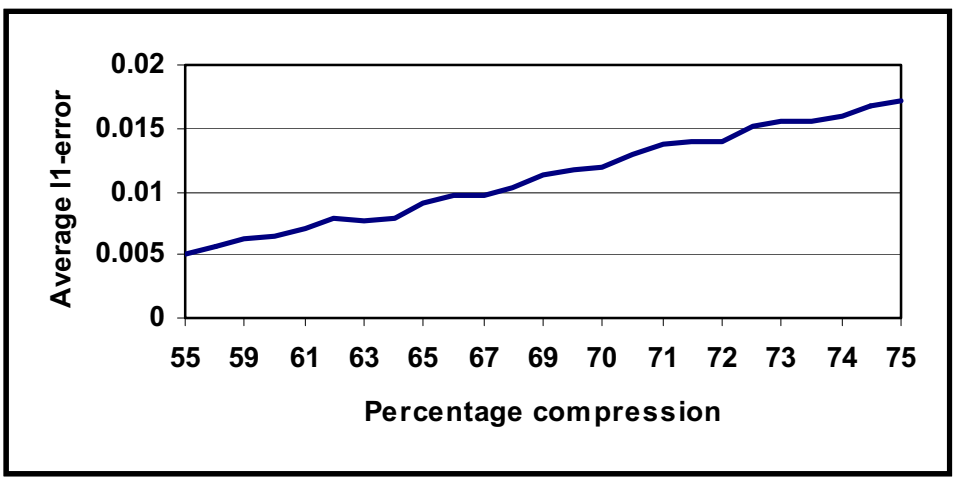


**(Compression of Raw data)**

**Graph 7.5**

*International Journal of Tomography & Statistics (IJTS),*
*June-July 2005, Vol. 3, No. JJ05, 81-88*
*ISSN 0972-9976;* 

# Statistical Modeling of Primary Ewing Tumours of the Bone

**Sreepurna Malakar[1], F. Smarandache[2], and S. Bhattacharya[3]**

[1]Department of Chemistry and Biochemistry
University of Alaska, U.S.A.

[2]Department of Mathematics
University of New Mexico, U.S.A.

[3]Department of Business Administration
Alaska Pacific University, U.S.A.
E-mail: sbhattacharya@alaskapacific.edu

**ABSTRACT**

*This short technical paper advocates a bootstrapping algorithm from which we can form a statistically reliable opinion based on limited clinically observed data, regarding whether an osteo-hyperplasia could actually be a case of Ewing's osteosarcoma. The basic premise underlying our methodology is that a primary bone tumour, if it is indeed Ewing's osteosarcoma, cannot increase in volume beyond some critical limit without showing metastasis. We propose a statistical method to extrapolate such critical limit to primary tumour volume. Our model does not involve any physiological variables but rather is entirely based on time series observations of increase in primary tumour volume from the point of initial detection to the actual detection of metastases.*

**KEY WORDS**

*Ewing's bone tumour, multi-cellular spheroids, linear difference equations*

## INTRODUCTION

To date, oncogenetic studies of *EWS/FLI-1*1 induced malignant transformation have largely relied upon experimental manipulation of Ewing's bone tumour cell lines and fibroblasts that have been induced to express the oncogene. It has been shown that the biology of Ewing's tumour cells *in vitro* is dramatically different

between cells grown as mono-layers and cells grown as anchorage-independent, multi-cellular spheroids (MCS). The latter is more representative of primary Ewing's tumour *in vivo* (Lawlor et. al, 2002). MCS are clusters of cancer cells, used in the laboratory to study the early stages of avascular tumour growth. Mature MCS possess a well-defined structure, comprising a central core of necrotic i.e. dead cells, surrounded by a layer of non-proliferating, quiescent cells, with proliferating cells restricted to the outer, nutrient-rich layer of the tumour. As such, they are often used to assess the efficacy of new anti-cancer drugs and treatment therapies. The majority of mathematical models focus on the growth of MCS or avascular tumour growth. Most recent works have focused on the evolution of MCS growing in response to a single, externally-supplied nutrient, such as oxygen or glucose, and usually two growth inhibitors (Marusic et. al., 1994).

Mathematical models of MCS growth typically consist of an *ordinary differential equation* (ODE) coupled to one or more *reaction-diffusion equations* (RDEs). The ODE is derived from mass conservation and describes the evolution of the outer tumour boundary, whereas the RDEs describe the distribution within the tumour of vital nutrients such as oxygen and glucose and growth inhibitors (Dorman and Deutsch, 2002). However studies of this type, no matter how mathematically refined, often fall short of direct clinical applicability because of rather rigorous restrictions imposed on the boundary conditions. Moreover, these models focus more on the structural evolution of a tumour that is already positively classified as cancerous rather than on the clinically pertinent question of whether an initially benign growth can at a subsequent stage become invasive and show metastases (De Vita et. al., 2001).

What we therefore aim to devise in our present paper is a bootstrapping algorithm from which we can form an educated opinion based on clinically observed data, regarding whether a bone growth initially diagnosed as benign can subsequently prove to be malignant (i.e. specifically, a case of Ewing's osteosarcoma) . The strength of our proposed algorithm lies mainly in its computational simplicity – our model does not involve any physiological variables but is entirely based on time series observations of progression in tumour volume from the first observation point till detection of metastases.

## LITERATURE SUPPORT

In a clinical study conducted by Hense et. al. (1999), restricted to patients with suspected Ewing's sarcoma, tumour volumes of more than 100 ml and the presence of primary metastases were identified as determinants of poor prognosis in patients with such tumours. Diagnoses of primary tumours were ascertained exclusively by biopsies. The diagnosis of primary metastases was based on *thoracic computed tomography* or on whole body bone scans. It was observed that of 559 of the patients (approx. 68% in a total sample size of 821) had a volume

above 100 ml with smaller tumours being more common in childhood than in late adolescence and early adulthood. Extensive volumes were observed in almost 90% of the tumours located in femur and pelvis while they were less common in other sites ($p < 0.001$). On average, 26% of all patients were detected with clinically apparent primary metastases.

The detection rate of metastases was markedly higher in patients diagnosed after 1991 ($p < 0.001$). Primary metastases were also significantly more common for tumours originating in the pelvis and for other tumours in the Ewing's family of tumours (EFT); mainly the peripheral neuro-ectodermal tumours (PNET); ($p < 0.01$). Tumours greater than 100 ml were positively associated with metastatic disease ($p < 0.001$). Multivariate analyses, which included simultaneously all univariate predictors in a *logistic regression model*, indicated the observed associations were mostly unconfounded. Further it has been found that the metastatic potential of human tumours is encoded in the bulk of a primary tumour, thus challenging the notion that metastases arise from sparse cells within a primary tumour that have the ability to metastasize (Sridhar Ramaswamy et. al., 2003). These studies lend credence to our fundamental premise about a critical primary tumour volume being used as a classification factor to distinguish between benign and potentially malignant bone growth.

## STATISTICAL MODELLING METHODOLOGY

Assuming that the temporal drift process governing the progression in size of a primary Ewing tumour of the bone to be linear (the computationally simplest process), we suggest a straightforward computational technique to generate a large family of possible tumour propagation paths based on clinically observed growth patterns under laboratory conditions. In case the governing process is decidedly non-linear, then our proposed scheme would not be applicable and in such a case one will have to rely on a completely non-parametric classification technique like e.g. an Artificial Neural Network (ANN).

Our proposed approach is a bootstrapping one, whereby a linear autoregression model is fitted through the origin to the observation data in the first stage. If one or more beta coefficients are found to be significant at least at a 95% level for the fitted model then, in the second stage, the autoregression equation is formulated and solved as a *linear difference equation* to extract the governing equation.

In the final stage, the governing equation obtained as above is plotted, for different values of the constant coefficients, as a family of possible temporal progression curves generated to explain the propagation property of that particular strain of tumour. The critical volume of the primary growth can thereafter be visually extrapolated from the observed cluster of points where the generated family of primary tumour progression curves shows a *definite uptrend* vis-à-vis the actual progression curve.

If no beta coefficient is found to be significant in the first stage, a non-linear temporal progression process is strongly suspected and the algorithm terminates without proceeding onto the subsequent stages, thereby implicitly recommending the problem to a non-parametric classification model.

The mathematical structure of our proposed model may be given as follows:

Progression in primary Ewing tumour size over time expressed as an n-step general autoregressive process through the origin:

$$S_t = \sum_{j=1}^{n} \beta_j S_{t-j} + \varepsilon \qquad \text{(I)}$$

Formulated as a linear, difference equation we can write:

$$-S_t + \beta_1 S_{t-1} + \beta_2 S_{t-2} + \ldots + \beta_n S_{t-n} = -\varepsilon \qquad \text{(II)}$$

Taking $S_t$ common and applying the *negative shift operator* throughout, we get:

$$[-1 + \beta_1 E^{-1} + \beta_2 E^{-2} + \ldots + \beta_n E^{-n}] S_t = -\varepsilon \qquad \text{(III)}$$

Now applying the *positive shift operator* throughout we get:

$$[-E^n + \beta_1 E^{n-1} + \beta_2 E^{n-2} + \ldots + \beta_n] S_t = -\varepsilon \qquad \text{(IV)}$$

The *characteristic equation* of the above form is then obtained as follows:

$$-r^n + \beta_1 r^{n-1} + \beta_2 r^{n-2} + \ldots + (\beta_n + \varepsilon) = 0 \qquad \text{(V)}$$

Here r is the root of the characteristic equation. After solving for r, the governing equation can be derived in accordance with the well-known analytical solution techniques for ordinary linear difference equations (Kelly and Peterson, 2000).

## SIMULATED CLINICAL STUDY

We set up a simulated clinical study applying our modeling methodology with the following hypothetical primary Ewing tumour progression data adapted from the clinical study of Hense et. al. (1999) as given in Table I below:

**Table I**

| Observation (t) | Primary Ewing tumour volume (in ml.) |
|---|---|
| (At point of first detection) 1 | 5 |
| 2 | 7 |
| 3 | 9 |
| 4 | 19 |
| 5 | 39 |
| 6 | 91 |
| 7 (At the point of detection of metastasis) | 102 |

**Figure I**

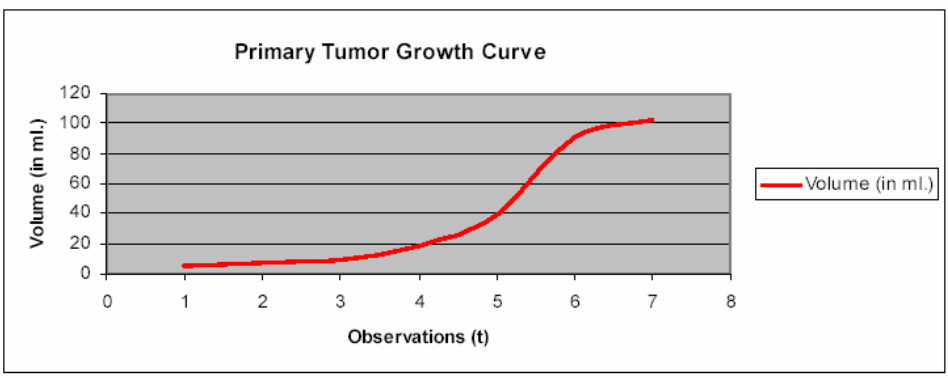


The temporal progression path of the primary growth from the point of first detection to the onset of metastasis is plotted above in Figure I.

We have fitted an AR (2) model to the primary tumour growth data as follows:

$$\mathbf{E\,(S_t) = -1.01081081S_{t-1} + 5.32365561S_{t-2}} \qquad \textbf{(VI)}$$

The $R^2$ of the fitted model is approximately 0.8311 and the *F*-statistic is 9.83832

with an associated p-value of approximately 0.04812. Therefore the fitted model definitely has an overall predictive utility at the 5% level of significance. The residuals of the above AR (2) fitted model are given in Table II as follows:

**Table II**

| *Observation* | *Predicted $S_t$* | *Residuals* |
|---|---|---|
| 1 | -5.05405405 | 12.05405405 |
| 2 | 19.5426024 | -10.5426024 |
| 3 | 28.168292 | -9.168292003 |
| 4 | 28.7074951 | 10.29250488 |
| 5 | 61.7278351 | 29.27216495 |
| 6 | 115.638785 | -13.63878518 |

The average of the residuals comes to 3.044841. Therefore the linear difference equation to be solved in this case is as follows:

$$X_t = -1.01081081X_{t-1} + 5.32365561X_{t-2} + 3.044841 \qquad \text{(VII)}$$

Applying usual solution techniques, the general solution to equation (VII) is obtained as follows:

$$X_t = c_1 (2.43124756)^t + c_2 (-3.44205837)^t \qquad \text{(VIII)}$$

Here $c_1$ and $c_2$ are the constant coefficients which may now be suitably varied to generate family of possible primary tumour progression curves as in Figure II below:

**Figure II**

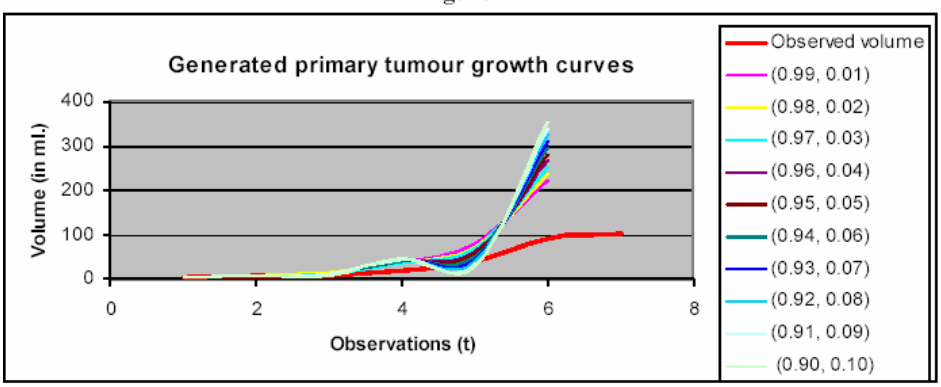

In the above plot, we have varied $c_2$ in the range 0.01 to 0.10 and imposed the condition $c_1 = 1 - c_2$. The other obvious condition is that choice of $c_1$ and $c_2$ would be such as to rule out any absurd case of negative volume. Of course the choice of the governing equation parameters would also depend on specific clinical considerations (King, 2000).

## CONCLUSION

From Figure II, it becomes visually apparent that continuing increase in the observed size of the primary growth beyond approximately 52 ml. in volume would be potentially malignant as this would imply that the tumour would possibly keep exhibiting uncontrolled progression till it shows metastasis. This could also be obtained arithmetically as the average volume for t = 5. Therefore the critical volume could be fixed around 2 ml. as per the computational results obtained in our illustrative example.

Though our computational study is intended to be purely illustrative as we have worked with hypothetical figures and hence cannot yield any clinical conclusion, we believe we have hereby aptly demonstrated the essential algorithm of our statistical approach and justified its practical usability under laboratory settings. This is not intended to be a clinical paper and in defense, it may be stated that given the immense potential of computer modeling and simulation in present times, a number of mathematical tumor growth studies are being conducted now that are essentially theoretical rather than clinical in nature (Swanson et. al. 2003; Tabatabai, Williams and Bursac, 2005).

We have used a difference equation model rather than a differential equation one because under practical laboratory settings, observations cannot be made continuously but only at discrete time intervals. However, as already stated previously, the numerical example we have provided is purely demonstrative - its purpose is illustrating the computational modeling technique rather than drawing clinically viable conclusions based on the model coefficients. Having said that, we definitely feel that there is an immediate scope of taking our line of research further forward by actually implementing an autoregressive process to model *in vitro* growth of MCS with clinically observed data.

## ACKNOWLEDGEMENT

*We sincerely thank all the referees for their valued comments and observations.*

## REFERENCES

DeVita, V., T., S. Hellman, and S.A. Rosenberg, 2001, *Cancer – Principles & Practice of Oncology*, 6th Ed., Lippincott Williams & Wilkins, Philadelphia, USA

Dormann, S. and A. Deutsch, 2003, *Modeling of self-organized, avascular tumour growth with a hybrid cellular automaton*, www.bioinfo.de/isb/2002/02/0035/main.html, (last accessed on 09/09/2003)

Hense, H.W., S. Ahrens, M. Paulussen, M. Lehnert and H. Jurgens, 1999, Factors *associated with tumor volume and primary metastases in Ewing tumors: results from the (EI) CESS studies*, Annals of Oncology, 10(9), 1073-1077

Kelly, Walter G. and Allan C. Peterson, 2000,. *Difference Equations – An Introduction with Applications*, 2nd Ed., Academic Press, Massachusetts, Burlington, USA

King, Roger J.B., 2000, *Cancer Biology*, 2nd Ed., Pearson Education Limited, Essex, UK

Lawlor E.R., C. Scheel, J. Irving, and P.H.B. Sorensen, 2002, *Anchorage-Independent multicellular spheroids as an in vitro model of growth signaling in Ewing tumors*, Oncogene, 21, 307-318

Marusic, M., Z. Bajzer, S. Vuk-Pavlovic, and J.P. Freyer, 1994, *Tumor growth in vivo and as multicellular spheroids compared by mathematical models*, Bulletin of Mathematical Biology, 56(4), 617-31

Ramaswamy, S., K.N. Ross, E.S. Lander and T.R. Golub, *Evidence for a Molecular Signature of Metastasis in Primary Solid Tumours*, www.genome.wi.mit.edu/cancer/solid_tumor_metastasis, (last accessed on 09/09/2003)

Swanson, K.R., C. Bridge, J.D. Murray, and E.C. Alvord Jr., 2003, Virtual and real brain tumors: using mathematical model to quantify glioma growth and invasion, Journal of the Neurological Sciences, 216, 1 -10

Tabatabai, M., D.K. Williams, and Z. Bursac, 2005, *Hyperbolastic growth models: theory and application*, Theoretical Biology and Medical Modelling, 2(14), (in print)

# Submission of Manuscripts

## International Journal of Tomography & Statistics

The authors should submit two complete hard copies of manuscript of their unpublished and original paper to *Executive Editor, International Journal of Tomography & Statistics, Indian Society for Development & Environment Research, Post Box No. 113, Roorkee-247667, INDIA*; **Email:** isder_*ceser@yahoo.com*. It will be assume that authors will keep a copy of their paper. We strongly encourage electronic submission of manuscript by email along with one hard copy.

**Format of Manuscripts:** should be in the following format-

| | |
|---|---|
| Page Size | 6.5 inch (W) x 9.4 inch (H) |
| Page Margin | Top=1.0 inch, Bottom=1.0 inch<br>Left=1.0 inch, Right=1.0 inch |
| Font Face | Arial |
| Font Size for Title | 16 pt. Bold & Title Case |
| Font Size for Headings | 10 pt. Bold & CAPITAL CASE |
| Font Size for Sub-Headings | 10 pt. Bold & Title Case |
| Alignment for Title & Headings | Center |
| Font size for Text | 10 pt. |
| Line Space | 1.3 line space |
| Paragraph | No Tab, and 10 pt. Space after paragraph & Alignment=Justify |
| Abstract & Keyword | Margin: Top=1.4", Left=1.4",<br>Font: size=9 pt.<br>Font Face =Arial & italic<br>Align= justify<br>Line Space=single |
| Reference | Align= justify<br>Line Space=single and 10 pt. space before the next reference. |
| Table and Figures | Should be separate and at the last of manuscript. |

A covering letter should identify the person (with address, telephone numbers and email address) responsible for correspondence concerning manuscripts.

Submission of a paper implies that the reported work is neither under consideration for a scientific journal nor already published. All manuscripts are subject to peer review. If revisions are required for acceptance of a manuscript, one copy of the revised manuscript should be submitted. Print copy of the journal will be dispatch to subscribers only. However, authors will get the electronic copy of journal without any payment. A copy of single issue of journal is available on a special

discount to the authors only. Furthermore, you are welcome to support the journal by requesting that your library to subscribe the journal, or by taking out an individual subscription.

**Preparation of the Manuscript**

Papers must be clearly written in English. All sections of the manuscript should be typed, double-spaced, on one side of the paper only. In addition to the full title of the paper, authors should supply a running title, of less than 40 characters, and up to five keywords.

Research papers should be accompanied by an abstract, which will appear in front of the main body of the text. It should be written in complete sentences and should summarize the aims, methods, results and conclusions in less than 250 words. The abstract should be comprehensible to readers before they read the paper, and abbreviations and citations should be avoided.

Authors are responsible for the accuracy of references. Within the text, references should be cited by author's name(s) and year of publication (where there are more than two authors please use et al.). Published articles and those in press (state the journal which has accepted them and enclose a copy of the manuscript) may be included. Citations should be typed at the end of the manuscript in alphabetical order, with authors' surnames and initials inverted. References should include, in the following order: authors' names, year, paper title, journal title, volume number, issue number, inclusive page numbers and (for books only) name and address of publishers. References should therefore be listed as follows:

> Natterer, F., 1986, *The Mathematics of Computerized Tomography,* John Wiley & Sons, New York.
>
> Herman, G.T., 1972, Two *Direct Methods for Reconstructing Pictures from their Projections: A Comparative Study,* Computer Graphics and Image Processing, 1, 123-144.
>
> Dasgupta. P., 2003, *Population, Poverty, and the Natural Environment.* in Mäler K.-G. and Vincent, J. (Eds.), Handbook of Environmental and Resource Economics, Amsterdam: North Holland.
>
> Levin, S.A., Grenfell, B., Hastings, A., and Perelson. A.S. 1997, *Mathematical and Computational Challenges in Population Biology and Ecosystem Science,* Science, 275, 334-343.

Tables should be self-explanatory and should include a brief descriptive title. Illustrations should be clearly lettered and of the highest quality. Acknowledgements and Footnotes should be included at the end of the text. Any footnote should be identified by superscripted numbers.

# SUBSCRIPTIONS

## International Journal of Tomography & Statistics

Followings are the Annual Subscription rate

*For India:*

Individual: Rs. 2500.00 Library: Rs. 3000.00

*For USA, Europe, Australia and Developed Countries:*

Individual: US$ 250.00 Library: US$ 300.00
(Please Add US$ 20 for Air Mail)

*For Developing Countries:*

Individual: US$ 200.00 Library: US$ 250.00
(Please Add US$ 20 for Air Mail)

**How to Pay Subscriptions?**

Subscriptions are payable in advance. Subscribers are requested to send payment with their order. Issues will only be sent on receipt of payment. Subscriptions are entered on an annual basis and may be paid in Rupees or US Dollars.

US Dollar rates apply to subscribers in all countries except the India where the Rupees rate is applicable.

Payment can be made by Bank Draft/ Bank Wire Transfers/ Bank Cheque (please add US $ 25 as cheque transfer charges, in case of cheque) only. *All payments should be send to "*Indian Society for Development & Environment Research"*, Post Box No. 113, Roorkee-247667, INDIA".* The bank draft should be drawn on a Roorkee, India.

**Claims and Cancellations**

Claims for issues not received should be made in writing within three months of the date of publication. Cancellations: no refunds will be made after the first issue of the journal for the year has been dispatched.

**Details about the journal also available on website**

**Http://www.geocities.com/isder_ceser/ijts1.html**